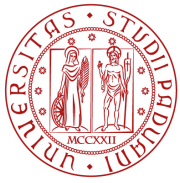

UNIVERSITÀ
DEGLI STUDI
DI PADOVA

Sede Amministrativa: Università degli Studi di Padova

Dipartimento di *Biologia*

SCUOLA DI DOTTORATO DI RICERCA IN BIOSCIENZE E BIOTECNOLOGIE

INDIRIZZO: GENETICA E BIOLOGIA MOLECOLARE DELLO SVILUPPO

CICLO XXVI

Investigating the role of Emilin3, an extracellular matrix protein of the Emilin/Multimerin family

Direttore della Scuola: Ch.mo Prof. Giuseppe Zanotti

Coordinatore d'indirizzo: Ch.mo Prof. Rodolfo Costa

Supervisore: Ch.mo Prof. Paolo Bonaldo

Dottoranda: Diana Corallo

Abstract

Emilin3 is an extracellular matrix molecule belonging to the EMILIN/Multimerin family. Emilin1, the founding member of this family, was originally identified as a glycoprotein particularly abundant in blood vessels, where it was found to be associated with elastic fibers. Whether Emilin3 is also associated with elastic fibers is still unknown. Differently from Emilin1 and all the other members of the family, Emilin3 is not expressed in the cardiovascular system, as shown by our studies both in mouse and zebrafish.

The main focus of my PhD study was to elucidate the function of Emilin3 during embryonic development, using zebrafish as a model. The two zebrafish Emilin3 paralog genes, *emilin3a* and *emilin3b,* are dynamically expressed in the tail bud, in the chordoneural hinge, and in the notochord during early zebrafish development. By using a novel specific antibody, I found that Emilin3 is deposited in the notochord sheath, a specialized extracellular matrix structure that surrounds the notochord. Morpholino-mediated knockdown of both Emilin3 paralogs led to a marked distortion of the notochord, as a consequence of structural defects of the notochord sheath. Besides its structural role, the notochord has also an important patterning activity, a process that is mainly mediated by the secretion of Hedgehog (Hh) ligands. Notably, the patterning activity of the notochord is also affected by Emilin3, as revealed by increased Hh signaling in Emilin3 depleted embryos and decreased Hh signaling in embryos overexpressing Emilin3 in notochord cells. Mechanistically, *in vitro* and *in vivo* experiments showed that Emilin3 modulates the availability of Hh ligands by interacting with the permissive factor Scube2. Altogether, these findings indicate that Emilin3 has an essential role for the proper structure and function of the developing notochord.

During my PhD, I also investigated the distribution pattern of Emilin3 in mouse tissues. Taking advantage of specific antibodies, I investigated and compared the distribution of different Emilin proteins in mouse tissues. The data show that, similarly to what I observed in zebrafish, Emilin3 has the most restricted

tissue distribution. The elucidation of Emilin3 distribution in embryonic and adult tissues was also crucial for starting, during the very last part of my PhD, the phenotypic characterization of Emilin3 knockout mice, which were previously generated in our lab. I found that Emilin3 knockout mice display a decreased body weight gain and an increased mortality during the first four weeks after birth. Microscope analysis revealed strong structural abnormalities of hair follicles within the first catagen/telogen transition. These findings point at a role for Emilin3 in hair follicle maturation, and are the basis for future studies aimed at the full understanding of the role of Emilin3 in embryonic and postnatal development and in tissue homeostasis.

Riassunto

Emilina3 è una proteina della matrice extracellulare appartenente alla famiglia delle Emiline/Multimerine. Emilina1, il membro fondatore della famiglia, è abbondantemente espressa nei vasi sanguigni, in associazione alle fibre elastiche. Al contrario, non è ancora noto se Emilina3 sia anch'essa associata a queste strutture. Inoltre, diversamente da Emilina1 e da tutti gli altri membri della famiglia, Emilina3 non è presente nel sistema cardiovascolare, come dimostrato dai nostri studi effettuati sia nel modello murino che in zebrafish.

L'obiettivo principale del mio percorso di dottorato è stato quello di chiarire la funzione di Emilina3 durante lo sviluppo embrionale di zebrafish. Durante le prime fasi di vita, i due geni paraloghi di Emilina3, *emilin3a* ed *emilin3b*, sono fortemente espressi nella parte posteriore del tronco, in particolare dalle cellule della cerniera cordo-neurale e della notocorda. Dalle 48 ore dopo la fecondazione, l'espressione a livello della notocorda si riduce fino a scomparire e i due trascritti iniziano ad essere espressi a livello degli elementi cartilaginei cranio-facciali in via di sviluppo. L'utilizzo di un anticorpo che riconosce specificatamente Emilina3 di zebrafish mi ha permesso di dimostrare che questa glicoproteina viene depositata nella membrana basale della notocorda, una struttura composta da diverse proteine della matrice extracellulare e che circonda le cellule della notocorda. Tramite la messa a punto di una strategia di *knockdown,* che prevede l'iniezione di oligonucleotidi morfolino diretti contro entrambi i geni paraloghi di Emilina3, si è osservata una significativa e macroscopica distorsione della notocorda, in seguito allo sviluppo di difetti strutturali della membrana basale della stessa. Oltre al suo ruolo strutturale, la notocorda ha anche un'importante attività di *signaling*, processo mediato pricipalmente dalla secrezione dei ligandi della via di segnale di Hedgehog (Hh). I dati da me ottenuti in questo lavoro di tesi dimostrano che Emilina3 è in grado di modulare l'attività di segnalazione della notocorda, come si evince

dall'aumento dell'attività della via di segnale di Hh in embrioni privi di Emilina3. Viceversa, embrioni che sovraesprimono Emilina3 murina nelle cellule della notocorda mostrano una ridotta attività della via di segnale di Hh. Esperimenti *in vivo* ed *in vitro* hanno rivelato che Emilina3 è in grado di modulare la disponibilità dei ligandi di Hh tramite l'interazione con Scube2, un fattore secreto con funzioni permissive nel regolare l'attività di Hh. Complessivamente, questi risultati indicano che Emilina3 ha un ruolo essenziale per il mantenimento della corretta struttura e funzione della notocorda.

Durante il mio percorso di dottorato, ho anche analizzato la distribuzione di Emilina3 nei tessuti di topo adulto, confrontandola con quella di Emilina1. I dati mostrano che Emilina3 ha una distribuzione tessutale più ristretta rispetto a quanto osservato per Emilina1. Queste analisi di localizzazione sono state fondamentali anche per l'avvio, durante l'ultima parte del mio dottorato di ricerca, della caratterizzazione fenotipica di topi *knockout* privi di Emilina3, precedentemente generati nel laboratorio del Prof. Paolo Bonaldo. I dati da me ottenuti dimostrano che l'assenza di Emilina3 porta ad una riduzione del peso corporeo e ad un aumento della mortalità dei topi *Emilin3 knockout* durante le prime quattro settimane di vita. Le successive analisi istologiche hanno rivelato marcate alterazioni nei follicoli piliferi, in particolare durante la prima transizione tra le fasi di regressione (catagen) e quiescenza (telogen) del follicolo pilifero. Questi risultati ottenuti nei topi *Emilin3 knockout* rappresentano una base importante per futuri studi volti a comprendere in dettaglio la funzione di Emilina3 nella regolazione dell'omeostasi tissutale nei mammiferi.

1. Introduction

1.1 The extracellular matrix

The extracellular matrix (ECM) is a key component of the cellular environment and it is composed of secreted proteins and polysaccharides that are assembled locally into an organised network to which cells adhere (Hay, 1981). The ECM is well known for its ability to provide structural support for organs and tissues, for cell layers in the form of basement membranes, and for individual cells as substrates for migration. The role of the ECM in cell adhesion and signaling through receptors such as integrins has received much attention (Hynes, 2002; Berrier and Yamada, 2007; Legate et al., 2009), and recently the biomechanical properties of the ECM, such as stiffness and deformability, have also been recognized to provide inputs for cell behavior (Discher et al., 2009; Dupont et al., 2011). Thus, ECM macromolecules and scaffolds play vital roles in the determination, differentiation, proliferation, survival, polarity and migration of cells. ECM signals are arguably at least as important as soluble signals in governing these processes.

In keeping with its various roles and functions, the ECM has a complex molecular composition. It is mainly composed of fibrous proteins embedded in a gel-like polysaccharide ground substance. In addition to fibrous structural proteins (e. g. collagens, elastin), glycosaminoglycans and proteoglycans, the ECM contains adhesion proteins (e. g. fibronectin, laminins, fibrillins) that link components of the matrix both to one another and to the cell surface. The differences between these three major types of ECM result from variations on this general theme.

Proteoglycans are a group of proteins bound to complex chains of polysaccharides, named glycosaminoglycans (GAG). Proteoglycans can contain up to several hundred GAG chains attached usually to serine residues of a core protein. A variety of core proteins (ranging from 10 to >500 kDa) have been

identified, so the proteoglycans are a complex and heterogeneous group of macromolecules (Poole, 1986; Ruoslahti, 1988; Kjellen and Lindahl, 1991; Silbert and Sugumaran, 1995). Because of their high content of charged polysaccharides, GAGs and proteoglycans bind positively charged ions and trap water molecules to form hydrated gels, providing mechanical support to the ECM. Besides acting in this way as structural components, both extracellular and cell-surface proteoglycans also bind several growth factors and other types of secreted proteins (e. g. proteases and protease inhibitors). Thus, proteoglycans can also contribute to the regulation of the metabolites and cell traffic (Scott, 2001; Hardingham et al., 1992).

Besides proteoglycans, the main component of the ECM consists of **collagens**, a class of secreted fibrous proteins. Collagens are found in all metazoa and provide structural strength to all forms of extracellular matrices, including the strong fibers of tendons, the organic matrices of bones and cartilages, the laminar sheets of basement membranes, the viscous matrix of the vitreous humor, and the interstitial ECMs of the dermis and of capsules around organs. Collagens are characterized by the presence of repeats of the triplet Gly-X-Y, where X is frequently proline and Y is frequently 4- hydroxyproline. This repeating structure forms stable, rodlike, trimeric, coiled coils, which can be of varying lengths. Based on the type of polymeric assemblies, the collagen superfamily can be divided into at least six families, with different three-dimensional structure and tissue distribution (Ricard-Blum S. 2011). Beside forming fibrils or network-like structures and thus providing the integrity of tissues, collagens fulfil a variety of other biological functions such as cell adhesion, growth, differentiation and motility.

In addition to collagens and proteoglycans that provide strength and space-filling functions (among others), there are around 200 complex **glycoproteins** in the mammalian matrisome (Naba et al. 2011). These proteins have many different functions, including structural organization of ECM and cell adhesion. Moreover, these proteins contain domains responsible for binding a variety of other matrix proteins, polysaccharides, cell-surface proteins, and

signaling molecules such as growth factors and hormones. The bound growth factors can serve as reservoirs that can be released (e.g., by proteolysis) or can be presented as solid-phase ligands by the ECM proteins (Hynes 2009). The best-studied ECM glycoproteins are the laminins (Yurchenco, 2011) and fibronectins (Schwarzbauer JE, DeSimone DW. 2011). The structures of these glycoproteins are well known and exemplify the typical multiple repeating domain structure and extended multimeric forms of ECM proteins. However, there are multiple other ECM glycoproteins about which much less or nothing is known.

1.2 Elastic fibers

In order to fulfill their proper functions, different organs need to be elastic and flexible. These physical characteristics have been essentially required among multicellular organisms and maintained during evolution.

Elastic fibers are ECM assemblies that give resiliency to the connective tissues, permitting long-range deformability and passive recoil without energy input. This elastic function complements collagen fibrils, which impart tensile strength and limit tissue stretching and damage. Genesis of elastic fibers in early development involves deposition of tropoelastin (the soluble precursor of mature elastin) on a preformed template of fibrillin-rich microfibrils (Mecham and Davis, 1994). Thus mature elastic fibers are a complex network formed by an outer microfibrillar mantle and an inner core of amorphous crosslinked elastin.

The main structural components of elastic-fiber-associated microfibrils are fibrillin-1 and -2 (Sakai et al., 1986, Zhang et al., 1994). Nevertheless, a large spectrum of different elastic-fibers-associated-molecules has been identified in the past years. They can be broadly categorized as *i)* molecules that co-localize with microfibrils, *ii)* molecules that occur at the elastin-microfibril interface or at the elastic-fiber-cell interface, and *iii)* molecules that are involved in the process of elastic fiber formation.

The first group includes proteins such as MFAP (Microfibril-Associated Protein) -1, -3 and -4 (Liu et al., 1997; Abrams et al., 1995; Lausen et al., 1999), MAGP (Microfibril-Associated GlycoProtein) -1 and -2 (Hatzinikolas and Gibson, 1998), LTBP (Latent TGF-β Binding Protein) -1, -2, -3 and -4 (Kanzaki et al., 1990; Gibson et al., 1995; Giltay et al., 1997). The second group includes Fibulin-1, -2, -3, -4 and -5 (Roark et al., 1995; Raughunath et al., 1999; Nakamura et al., 2002; Yanagisawa et al., 2002), MP78/70 (Gibson et al., 1997), and Emilins (described below). Finally, the third group of proteins includes molecules involved in elastic fiber formation, such as LOX (Lysil Oxydase), LOXL (Lysil-Oxidase-Like Protein), LOXL-2, LOXL-3 and LOXC (Borel et al., 2001).

1.3 The Emilin/Multimerin family

Several molecules localize to the elastin-microfibril interface or to the cell-surface–elastic-fibre interface. These molecules could regulate tropoelastin deposition on microfibrils and link elastic fibers to the cell surface. One of these proteins is Emilin1, a 136 kDa glycoprotein, that localises to the elastin microfibril interface (Bressan et al., 1993; Doliana et al., 1999). Emilin1 belongs to the Emilin/Multimerin family that includes five proteins, namely Emilin1, Emilin2, Emilin3, Multimerin1 and Multimerin2. The primary structure of these ECM proteins is composed by an N-terminal EMI domain, followed by a long central region with a high probability of forming coiled-coil structures and a C-terminal region homologous to the globular domain of C1q (gC1q domain). Emilin3 is the only protein of the family that lacks the gC1q domain in its C-terminal region. Moreover, the EMI domain is always located in a single copy at the N- terminal portion of the mature protein and it encodes for seven cysteine residues, while the majority of cysteine-rich domains contains either six or eight cysteine residues.

It has been demonstrated that the EMI domain of Emilin1 binds proTGF-β1, thereby preventing its proteolytic processing into the mature and active cytokine (Zacchigna et al., 2006). The gC1q domain was shown to be essential

for the cell adhesion properties of Emilin1, and it was proposed that this domain is involved in the supramolecular organization and assembly of Emilin1 into multimers (Mongiat et al., 2000; Spessotto et al., 2003). Since it has been found that Emilin1 interacts with both elastin and Fibulin-5 (Zanetti et al., 2004), it could be possible that Emilin1 can stabilize interactions among different components of the elastic fiber and by enabling the proper attachment of elastic fibers to cells.

The biological roles of the Emilin/Multimerin proteins are far from clear. Only Emilin1 has been well characterized, by taking advantage of the knockout mouse model: these animals show subtle structural alterations of the elastic fibers and of the cells in the wall of large blood vessels (Zanetti et al., 2004). Moreover, it has been demonstrated that Emilin1 knockout mice are affected by arterial hypertension due to increased TGF-β signaling in the vascular wall, consistent with the finding that Emilin1 is a regulator of TGF-β processing and activation (Zacchigna et al., 2006). In addition, Emilin1 knockout mice display defects in the lymphatic system and skin (Danussi et al., 2008; Danussi 2011).
In vitro and *in vivo* studies pointed out that Emilin2 is an extracellular pro-apoptotic factor, a role that is exerted through a direct binding to death receptors (Mongiat et al., 2007). More recently, a significant antitumoral effect of this ECM protein *in vivo* has been reported (Mongiat et al., 2010).

1.4 In vitro characterization of the biochemical properties of Emilin3

During my PhD, I was engaged in a project aimed at investigating the expression and the biochemical properties of Emilin3 in mouse. *In situ* hybridization data and immunofluorescence showed that during mouse development Emilin3 has a dynamic expression pattern, which only partially overlaps with that of other Emilin/Multimerin genes (Braghetta et al., 2004). In contrast to other Emilin/Multimerin genes, we found that Emilin3 is not expressed in the cardiovascular system and during postnatal life its deposition becomes

restricted to only few tissues (e.g. testis, uterus and ovaries, pericondrium of the external ear, myenteric plexus of the gastrointestinal tract and skeletal muscle) and does not overlap with that of any other Emilin/Multimerin proteins.

To elucidate the biochemical properties of Emilin3, we carried out transfection experiments with recombinant constructs and we found that Emilin3 is able to form disulfide-bonded homotrimers and higher-order oligomers, despite the absence of the gC1q domain nor the EMI domain. These data suggest that the coiled-coil regions with their flanking cysteine residues are important for this process. In particular, the EMI domain contributes to the formation of higher-order oligomers but is not dispensable for the homotrimers assembly. Moreover, a new function of the EMI domain has been elucidated, since we found that it binds heparin with high affinity. Finally, we carried out luciferase assays to evaluate whether Emilin3 could acts as a TGF- β antagonist, as already demonstrated for Emilin1. These sets of *in vitro* data indicate that EMILIN-3 works as an extracellular regulator of TGF-β signaling, and this function is exerted through the EMI domain.

I contributed to this work by carrying out the immunoprecipitation of endogenous Emilin3 from adult mouse tissues and whole embryo extracts and by measuring the TGF-β activity in HEK293T transfected cells (Schiavinato et al., 2012).

EMILIN-3, a peculiar member of the EMILIN/Multimerin family, has a distinct expression pattern, forms oligomeric assemblies and serves as a pro TGF-β antagonist.

Glycobiology and Extracellular Matrices:

EMILIN-3, Peculiar Member of Elastin Microfibril Interface-located Protein (EMILIN) Family, Has Distinct Expression Pattern, Forms Oligomeric Assemblies, and Serves as Transforming Growth Factor β (TGF-β) Antagonist

Alvise Schiavinato, Ann-Kathrin A. Becker, Miriam Zanetti, Diana Corallo, Martina Milanetto, Dario Bizzotto, Giorgio Bressan, Marija Guljelmovic, Mats Paulsson, Raimund Wagener, Paola Braghetta and Paolo Bonaldo

J. Biol. Chem. 2012, 287:11498-11515.
doi: 10.1074/jbc.M111.303578 originally published online February 10, 2012

THE JOURNAL OF BIOLOGICAL CHEMISTRY VOL. 287, NO. 14, pp. 11498–11515, March 30, 2012

EMILIN-3, Peculiar Member of Elastin Microfibril Interface-located Protein (EMILIN) Family, Has Distinct Expression Pattern, Forms Oligomeric Assemblies, and Serves as Transforming Growth Factor β (TGF-β) Antagonist*[S]

Received for publication, September 12, 2011, and in revised form, January 23, 2012 Published, JBC Papers in Press, February 10, 2012, DOI 10.1074/jbc.M111.303578

Alvise Schiavinato[‡], Ann-Kathrin A. Becker[§], Miriam Zanetti[‡], Diana Corallo[‡], Martina Milanetto[‡], Dario Bizzotto[‡], Giorgio Bressan[‡], Marija Guljelmovic[‡], Mats Paulsson[§¶‖], Raimund Wagener[§¶], Paola Braghetta[‡], and Paolo Bonaldo[‡1]

From the [‡]Department of Biomedical Sciences, University of Padova, I-35121 Padova, Italy and [§]Center for Biochemistry, Medical Faculty, [¶]Center for Molecular Medicine Cologne (CMMC), and [‖]Cologne Excellence Cluster on Cellular Stress Responses in Aging-Associated Diseases (CECAD), University of Cologne, D-50931 Cologne, Germany

Background: EMILIN-3 is the least characterized member of the EMILIN/Multimerin family.
Results: EMILIN-3 forms homotrimers and higher order oligomers, binds heparin, has a dynamic expression during development and a restricted distribution in adult tissues, and serves as a pro-TGF-β antagonist.
Conclusion: The structure and expression of EMILIN-3 are different from other EMILINs/Multimerins.
Significance: EMILIN-3, a TGF-β antagonist, is likely to be an important regulator during development of several tissues.

EMILIN-3 is a glycoprotein of the extracellular matrix belonging to a family that contains a characteristic N-terminal cysteine-rich EMI domain. Currently, EMILIN-3 is the least characterized member of the elastin microfibril interface-located protein (EMILIN)/Multimerin family. Using RNA, immunohistochemical, and protein chemistry approaches, we carried out a detailed characterization of the expression and biochemical properties of EMILIN-3 in mouse. During embryonic and postnatal development, EMILIN-3 showed a peculiar and dynamic pattern of gene expression and protein distribution. EMILIN-3 mRNA was first detected at E8.5–E9.5 in the tail bud and in the primitive gut, and at later stages it became abundant in the developing gonads and osteogenic mesenchyme. Interestingly and in contrast to other EMILIN/Multimerin genes, EMILIN-3 was not found in the cardiovascular system. Despite the absence of the globular C1q domain, immunoprecipitation and Western blot analyses demonstrated that EMILIN-3 forms disulfide-bonded homotrimers and higher order oligomers. Circular dichroism spectroscopy indicated that the most C-terminal part of EMILIN-3 has a substantial α-helical content and forms coiled coil structures involved in EMILIN-3 homo-oligomerization. Transfection experiments with recombinant constructs showed that the EMI domain contributes to the higher order self-assembly but was dispensable for homotrimer formation. EMILIN-3 was found to bind heparin with high affinity, a property mediated by the EMI domain, thus revealing a new function for this domain that may contribute to the interaction of EMILIN-3 with other extracellular matrix and/or cell surface molecules. Finally, *in vitro* experiments showed that EMILIN-3 is able to function as an extracellular regulator of the activity of TGF-β ligands.

EMILINs[2] belong to a family of secreted glycoproteins sharing some structural features and a unique N-terminal cysteine-rich region, the EMI domain. The term EMILIN was first coined to describe an elastin microfibril interface-located protein (1) (now called EMILIN-1). In mammals, the "EMILIN/Multimerin" family includes five genes coding for EMILIN-1, EMILIN-2, EMILIN-3, Multimerin-1, and Multimerin-2 (2).[3] Besides the common presence of the EMI domain, these proteins contain a long region predicted to form coiled coil structures and a globular C1q (gC1q) domain at their C-terminal end (3–6). EMILIN-3 is the only protein of the family that lacks the gC1q domain in its C-terminal region (see also Fig. 1*A*) (2, 7, 8).

The EMI domain spans ~80 amino acids and is characterized by the presence of highly conserved cysteine residues located at regular positions (9). This domain is rather unique as (i) it is always located in a single copy at the N-terminal portion of the mature protein and (ii) it encodes for seven cysteine residues, whereas the majority of cysteine-rich domains contain either six or eight cysteine residues. It has been demonstrated that the EMI domain of EMILIN-1 binds pro-TGF-β1, thereby preventing its proteolytic processing into the mature and active cytokine (10). The gC1q domain was shown to be essential for the cell adhesion properties of EMILIN-1, and it was proposed that

* This work was supported by the University of Padova (Grant CPDA075559), the Italian Ministry of University and Research (Progetti di Ricerca di Interesse Nazionale), and the German Research Council (Deutsche Forschungsgemeinschaft Grants WA1338/2-6 and SFB 829).
[S] This article contains supplemental Figs. S1–S8.
[1] To whom correspondence should be addressed: Dept. of Biomedical Sciences, University of Padova, Viale G. Colombo 3, I-35121 Padova, Italy. Tel.: 39-049-827-6084; Fax: 39-049-827-6079; E-mail: bonaldo@bio.unipd.it.

[2] The abbreviations used are: EMILIN, elastin microfibril interface-located protein; ECM, extracellular matrix; GdnHCl, guanidine hydrochloride; gC1q, globular C1q; RIPA, radioimmune precipitation assay.
[3] Several names are used for the members of the EMILIN/Multimerin family in the literature. In this study, we adopted the current approved nomenclature (see also HUGO Gene Nomenclature Committee). Previous names include gp115 and EMILIN (for EMILIN-1), Basilin and FOAP-10 (for EMILIN-2), EMILIN-5 and EMILIN-T (for EMILIN-3), EMILIN-4 and Multimerin (for Multimerin-1), and EndoGlyx-1 and EMILIN-3 (for Multimerin-2).

this domain is involved in the supramolecular organization and assembly of EMILIN-1 into multimers (11, 12). EMILIN-1 and Multimerin-1 were shown to multimerize, forming disulfide-linked trimers and larger complexes reaching a size of several million daltons (11, 13). EMILINs/Multimerins contain various regions endowed with oligomerization capability, such as the gC1q and EMI domains, collagen repeats, and long regions potentially forming coiled coil structures. Although the effective formation of coiled coil structures in these proteins was never demonstrated until now, it was suggested that coiled coil stretches and the gC1q domain may be implicated in the oligomerization of EMILINs/Multimerins into higher order structures.

Previous studies have provided information on the expression pattern of some EMILIN/Multimerin genes during mouse development (2, 7, 14). As a general feature, different members of the EMILIN/Multimerin family show both overlapping and complementary expression patterns. Among them, EMILIN-1 displays the most abundant and broad expression (14). A common hallmark of mammalian EMILIN-1, EMILIN-2, Multimerin-1, and Multimerin-2 is their abundance throughout the cardiovascular system during both embryonic development and postnatal life (2, 7, 14). A study carried out in *Danio rerio* yielded information on the expression of EMILIN/Multimerin genes during fish development, confirming that the zebrafish orthologs coding for EMILIN-1, EMILIN-2, and Multimerin-2 are abundantly expressed in the cardiovascular system (15). Interestingly, zebrafish EMILIN-3 orthologs are not expressed in heart and vessels, and they display a peculiar expression in the developing notochord and in craniofacial cartilage primordia (15).

The *in vivo* biological functions of EMILINs/Multimerins are largely unknown, and thus far only the phenotype of EMILIN-1 knock-out mice has been characterized in detail. Mice deficient for EMILIN-1 show subtle structural alterations of the elastic fibers and of the cells in the wall of large blood vessels (16). Further studies revealed that EMILIN-1 knock-out mice are affected by arterial hypertension due to increased TGF-β signaling in the vascular wall, which is consistent with the finding that EMILIN-1 is a regulator of TGF-β processing and activation (10). Moreover, EMILIN-1 knock-out mice display defects in skin and in the lymphatic system (17, 18). *In vitro* and *in vivo* studies pointed at a role for EMILIN-2 as an extracellular regulator of apoptosis through binding of the tumor necrosis factor-related apoptosis-inducing ligand (TRAIL) receptors (19).

Thus far only a few data are available on EMILIN-3 expression and distribution, and the biochemical properties of this protein have not been investigated.[3] In a previous study aimed at identifying human genes associated with skeletal development, a gene designated "*EMILIN-5*" and coding for a deduced protein corresponding to EMILIN-3 was found to be expressed in some mesenchymal cells during *in vitro* induction of osteogenesis and in the perichondrium of developing limbs (8). Another study suggested that the gene for EMILIN-3 is expressed at sites of mesenchymal condensations during cartilage and bone formation (7). Here we present a detailed study of the expression of EMILIN-3 during mouse embryonic and postnatal development together with a characterization of the biochemical properties of the endogenous protein and its recombinant products.

EXPERIMENTAL PROCEDURES

RT-PCR—Total RNA was extracted from different organs of newborn and adult mice, mouse embryos, and cultured cells using TRIzol Reagent (Invitrogen) as recommended by the manufacturer. First strand cDNA synthesis was performed with 0.8 μg of total RNA using random hexanucleotides and SuperScript reverse transcriptase (Invitrogen). Amplification was carried out in 50-μl reaction mixtures containing 0.1–0.3 μg of cDNA, 10 mM Tris-HCl, pH 9.0, 50 mM KCl, 1.5 mM $MgCl_2$, 0.1% Triton X-100, 0.2 mM dNTPs, 25 pmol of each primer, and 2 units of *Taq* I polymerase (Promega). The optimal annealing conditions and number of cycles were determined to allow amplification of samples within the exponential phase of the PCR. After 25–35 amplification cycles, the reaction products were separated in 1% agarose gels. The following primers were used: murine EMILIN-3: 5′-ACA GCC CAG TGC CTC CCG TTA CA-3′ (forward) and 5′-CAG GGT GCC ATA TGC TTG CGA CA-3′ (reverse); reaction product, 487 bp; murine EMILIN-3L and -3S: 5′-CCC GTT ACA GCC TCT ACA CCA CC-3′ (forward) and 5′-CAG CCC ACG CAC CTC ATC TAA CA-3′ (reverse); reaction products, 696 (EMILIN-3L) or 555 bp (EMILIN-3S); murine eIF1A: 5′-AAG AAG TCT GAA GGC CTA TG-3′ (forward) and 5′-CAG AGA ACT TGG AAT GTA GC-3′ (reverse); reaction product, 170 bp; human EMILIN-3: 5′-CCA GGA CAC AGC CCA GAA ACT T-3′ (forward) and 5′-GGT GAT GTT CCC CGA GTT GG TG-3′ (reverse); reaction product, 330 bp; and human GAPDH: 5′-ACC CAC TCC TCC ACC TTT GAC G-3′ (forward) and 5′-CTC TCT TCC TCT TGT GCT CTT GC-3′ (reverse); reaction product, 186 bp.

Northern Blotting—Total RNA (15 μg) was extracted from newborn murine tissues with TRIzol Reagent, separated in 1% formaldehyde gels, transferred to nylon membranes (Hybond N, Amersham Biosciences), and hybridized at 42 °C with a ^{32}P-labeled 1.1-kb cDNA probe spanning the 3′-region of murine EMILIN-3 cDNA.

In Situ Hybridization—*In situ* hybridization on whole mouse embryos and sections was performed as described previously (14) using a digoxigenin-labeled antisense 2.3-kb riboprobe synthesized from murine EMILIN-3 full-length cDNA. Nonspecific hybridization was evaluated with the respective sense riboprobe.

Preparation of Recombinant Murine EMILIN-3 C-terminal Region—A cDNA construct coding for the C-terminal region of murine EMILIN-3 (EMILIN-CTR; amino acids 171–758) was generated by RT-PCR and cloned with 5′-terminal NheI and 3′-terminal BamHI restriction sites using oligonucleotide primers 5′-CAA TGC TAG CTG GAA GAA AAG GCC AAG GG-3′ (forward) and 5′-CAA TGG ATC CGT CAG CTC GCC CTG GCC G-3′ (reverse). The amplified PCR product was inserted into a modified pCEP-Pu vector containing an N-terminal BM-40 signal peptide (20) and a C-terminal One-STrEP-tag (IBA GmbH) downstream of the restriction sites. The recombinant plasmids were introduced into HEK293-EBNA cells (Invitrogen) using FuGENE 6 transfection reagents (Roche

Applied Science). Cells were selected with puromycin (1 mg/ml), and the recombinant protein was purified from serum-containing culture medium. After filtration and centrifugation for 1 h at 10,000 × *g*, the cell culture supernatants were applied to a Streptactin column (1.5 ml; IBA GmbH) and eluted with 2.5 mM desthiobiotin, 10 mM Tris-HCl, pH 8.0.

Preparation of Antibodies against Murine EMILIN-3—Purified recombinant EMILIN-3CTR was used for rabbit and guinea pig immunization. The obtained antisera were purified by affinity chromatography on a column with antigen coupled to CNBr-activated Sepharose (GE Healthcare). Specific antibodies were eluted with 0.1 M glycine, pH 2.5, and the eluate was neutralized with 1 M Tris-HCl, pH 8.8.

Immunohistochemistry—Frozen sections (7 μm) were prepared from 2-month-old mice, washed in PBS, and saturated with 10% goat serum (Sigma). Sections were incubated overnight with EMILIN-3 antibodies diluted 1:1000 in PBS supplemented with 5% goat serum. Reactions were developed by incubation with DyLight 488-conjugated donkey anti-guinea pig IgG or Cy3-conjugated goat anti-rabbit IgG (Jackson ImmunoResearch Laboratories; 1:800 dilution).

cDNA Constructs—Constructs used in cell culture experiments were cloned into the pCS2 expression vector. Murine FLAG-EMILIN-1 and FLAG-EMILIN-1ΔEMI cDNAs were described previously (10). Full-length EMILIN-3L and EMILIN-3S cDNAs were obtained from mouse embryo RNA by PCR amplification with the following primers: 5′-AAA GAA TTC CGA GGG ACA GAG TGA CGA C-3′ (forward) and 5′-TTT TCT AGA GTT GGT GGG ATC TGC ACT TT-3′ (reverse). The amplified products were inserted as EcoRI-XbaI fragments in pCS2 vector. For the generation of a FLAG-EMILIN-3 construct, a fragment corresponding to amino acids 32–758 of EMILIN-3 was amplified from full-length EMILIN-3L cDNA by PCR using a forward primer (5′-AAA CTC GAG CAG CCC AGT GCC TCC CGT TAC AG-3′) with an XhoI site at the 5′-end of the cDNA and the same reverse primers as above. The amplified product was cloned into a pCS2 expression construct containing sequences coding for the mouse chordin signal peptide followed by a FLAG epitope tag (Chordin-FLAG-pCS2) (21). The EMILIN-3ΔEMI construct, containing a deletion of amino acid residues 54–189, was generated as follows. A fragment coding for amino acids 1–54 was amplified from full-length EMILIN-3L and FLAG-EMILIN-3 constructs by PCR using SP6 primer (5′-TAC GAT TTA GGT GAC ACT ATA G-3′) and a reverse primer carrying an NdeI restriction site (5′-TTT CAT ATG CTG GCC CCG GGC GCA GC-3′), and the amplified products were cloned as EcoRI-NdeI fragments in the EMILIN-3L or FLAG-EMILIN-3L plasmid, respectively, generating the deleted constructs. The FLAG-EMILIN-1ΔgC1q construct, containing sequences coding for amino acid residues 32–860 of murine EMILIN-1, was obtained from FLAG-EMILIN-1 by PCR amplification with SP6 primer and a specific reverse primer (5′-TTT TCC CTG CTC CCC TTG AGG AC-3′), and the amplified product was cloned into the Chordin-FLAG-pCS2 vector as an XhoI-XbaI fragment. The HA-EMILIN-3 and HA-EMILIN-3ΔEMI were obtained by subcloning the respective XhoI-XbaI fragments into a Chordin-HA-pCS2 vector containing the HA epitope tag. The EMI3-FLAG construct, containing amino acids 1–190 of EMILIN-3L, was obtained by PCR amplification of the full-length EMILIN-3 using the SP6 primer and a reverse primer (5′-CTA CTT ATC GTC GTC ATC CTT GTA ATC ATA TGC TTG CGA CAG GCG CT-3′) carrying the FLAG coding sequence before the stop codon. Mouse constitutively active pro-TGF-β2 (C226S/C228S/C229S) and pro-TGF-β3 (C228S/C230S) were generated by site-directed mutagenesis by overlap extension of cysteine residues essential for latency and located in conserved positions of latency-associated peptide. Two sets of primers, containing the mutation site together with upstream or downstream sequences, respectively, were used in two separate reactions to amplify overlapping DNA fragments. Cysteines 226, 228, and 229 of mouse pro-TGF-β2 were mutated to serines using full-length mouse pro-TGF-β2 cloned in pCMV-SPORT6 plasmid (RZPD) as a template. A fragment spanning from the Eco47III site to the BamHI site of pro-TGF-β2 cDNA was mutated using the following two sets of oligonucleotide primers: 5′-CCA AAG ACT TAA CAT CTC CCA CC-3′ (forward) and 5′-CGA AGG TAC **T**GC **T**GG GGC **T**GT-3′ (reverse with mutations in bold letters) and 5′-AC**A** GCC CC**A** GC**A** GTA CCT TCG-3′ (forward with mutations in bold letters) and 5′-ATG CCC CAG CAC AGA AGT TAG C-3′ (reverse). The mutated DNA was cloned in pGEM-T Easy vector (Promega), sequenced, and subcloned into full-length pro-TGF-β2 by BamHI and Eco47III digestion. The mutated TGF-β2 cDNA was finally subcloned into pCS2 to produce pro-TGF-β2 (C226S/C228S/C229S). Cysteines 228 and 230 of TGF-β3 were mutated using full-length mouse pro-TGF-β3 cloned in pCMV-SPORT6 plasmid as a template. To produce a mutated fragment of pro-TGF-β3 comprising the region between the two BglII sites of the cDNA sequence, three fragments were generated by PCR using the following sets of primers: 5′-CGT TGG ACT TCG GCC ACA TC-3′ (forward) and 5′-CCT ATG TAG CGC TGC TTG GC-3′ (reverse), 5′-CAG CTC CAA GCG CAC AGA AC-3′ (forward) and 5′-GTG TGA C**T**T GGA C**T**G TGG ATG-3′ (reverse with mutations in bold face letters), 5′-CAT CCA C**A**G TCC A**A**G TCA CAC-3′ (forward with mutations in bold letters) and 5′-CCA CCT CTG CCT GCA CCA C-3′ (reverse), and 5′-GAG GCC TGG AGC CCA GAA G-3′ (forward) and 5′-CCA GGG GAC TTT GGC TTG GT-3′ (reverse). Fragments were inserted into pGEM-T easy vector (Promega), sequenced, and subcloned in BglII-restricted full-length pro-TGF-β3. The mutated pro-TGF-β3 cDNA was finally subcloned into pCS2 to produce pro-TGF-β3 (C228S/C230S). Full-length cDNA for human pro-TGFβ1 was a gift from Jorma Keski-Oja (University of Helsinki, Helsinki, Finland). The porcine constitutively active pro-TGF-β1 (C223S/C225S) expression plasmid was obtained from Jeffrey M. Davidson (Vanderbilt University, Nashville, TN). All plasmids were sequenced prior to use.

Cell Transfection, Protein Extracts, and Luciferase Assay—HEK293T cells were cultured in Dulbecco's modified Eagle's medium containing 4.5 g/liter glucose, 25 mM HEPES, 2 mM L-glutamine, and 10% fetal bovine serum (Invitrogen) and maintained at 37 °C in a humidified 5% CO_2 atmosphere. Subconfluent HEK293T cultures were transfected overnight with the indicated plasmids using the calcium phosphate procedure

(22). Cells were washed with phosphate-buffered saline and fed with serum-free medium, and cell lysate and conditioned medium were collected after 48 h. The conditioned media were supplemented with a protease inhibitors mixture (Roche Applied Science). The cell extracts were prepared by lysis in an ice-cold buffer containing 25 mM Tris, pH 7.5, 150 mM NaCl, 2.5 mM EDTA, 10% glycerol, 1% Nonidet P-40, and protease inhibitors. For the preparation of ECM extracts, cells were lysed in culture dishes at 4 °C with RIPA buffer (50 mM NaCl, 25 mM Tris-HCI, pH 7.5, 0.5% Nonidet P-40, 0.5% sodium deoxycholate, 0.1% SDS) supplemented with protease inhibitors. The dishes were then rinsed three times with cold RIPA buffer, and the extracellular material attached to the dish was extracted by scraping at 90 °C in 2× Laemmli sample buffer. Where indicated, cells were treated with 50 μg/ml soluble heparin (Sigma). Glycosylation was assessed by treatment of samples using an Enzymatic Protein Deglycosylation kit (Sigma) following manufacturer's instructions. For luciferase assays, 6×10^4 cells were plated in each well of 24-well plates. The CAGA12-lux reporter (a gift from Peter ten Djike) and the pCMV-LacZ plasmids were used together with the indicated constructs. Cell layers were harvested with luciferase lysis buffer (25 mM Tris-HCl, pH 7.8, 2.5 mM EDTA, 10% glycerol, 1% Nonidet P-40, 2 mM DTT). Luciferase and β-galactosidase activities were measured in each sample, and values of luciferase activity were normalized to β-galactosidase activity to account for differences in transfection efficiencies. Every sample was transfected in triplicate, and every experiment was repeated at least two times.

Immunoprecipitation—For the immunoprecipitation of endogenous EMILIN-3, adult mouse tissues or whole embryos were snap frozen in liquid nitrogen, pulverized by pestle and mortar, and lysed for 30 min at 4 °C in a solution containing 50 mM Tris-HCl, pH 7.5, 150 mM NaCl, 2 mM EDTA, 1% Triton X-100, and protease inhibitors. Tissue extracts were then centrifuged for 90 min at 4 °C, and the supernatants were recovered. Samples were first precleared by incubation for 5 h at 4 °C with 50 μl of protein A-Sepharose (Amersham Biosciences), 2% bovine serum albumin, and 10 μl of preimmune serum. The samples were centrifuged for 2 min at 500 × *g*, and the supernatants were incubated overnight at 4 °C with 10 μl of rabbit EMILIN-3 antiserum and 50 μl of protein A-Sepharose. After centrifugation at 500 × *g*, the precipitates were washed three times with PBS containing 1.5 mM $MgCl_2$ and 0.05% CHAPS (Roche Applied Science), eluted in 2× Laemmli sample buffer, boiled for 3 min, and analyzed by gel electrophoresis. For co-immunoprecipitation of transfected FLAG-EMILIN-3 and HA-EMILIN-3, transfected HEK293T cells were harvested in cold RIPA buffer, and cell lysates were immunoprecipitated by overnight incubation at 4 °C with an anti-FLAG resin (Sigma). After three washes in cold RIPA buffer, precipitated material was eluted in 2× Laemmli sample buffer, boiled for 3 min, separated by gel electrophoresis, and analyzed by Western blot with an anti-HA antibody (Sigma; 1:1000 dilution).

Gel Electrophoresis and Western Blot—Unreduced samples were subjected to SDS-PAGE on 3–8% (w/v) gradient polyacrylamide gels or composite 2.4% acrylamide, 0.5% agarose gels. Where indicated, samples were reduced by addition of 200 mM DTT and subjected to SDS-PAGE on 4–12% (w/v) gradient polyacrylamide gels. For Western blot, proteins were electrophoretically transferred to nitrocellulose membranes. The membrane was saturated with 5% nonfat milk in Tris-buffered saline with 0.1% Tween 20 and incubated in the same buffer with rabbit and guinea pig affinity-purified anti-EMILIN-3 (1:1000–1:3000 dilution), rabbit polyclonal anti-FLAG (Sigma; 1:3000 dilution), or mouse monoclonal anti-HA (Sigma; 1:1000 dilution) antibody. Membranes were incubated with the appropriate horseradish peroxidase-conjugated secondary antibody (Amersham Biosciences), and reacting bands were revealed by chemiluminescence with SuperSignal West Pico or SuperSignal West Dura (Pierce). For gel electrophoresis after partial reduction, protein samples were reduced with DTT at final concentrations of 0–10 mM at 37 °C for 45 min. Subsequent alkylation of the samples was done by adding iodoacetamide to a final concentration of 25 mM and incubation for 30 min at room temperature in the dark. The samples were then subjected to SDS-PAGE on a 4–10% (w/v) gradient polyacrylamide gel, and proteins were visualized by staining with Coomassie Brilliant Blue G-250.

Circular Dichroism Spectroscopy—Circular dichroism spectra were recorded in a Jasco J-715 spectropolarimeter using a thermostated 1-mm-path length quartz cell (Hellma). Proteins were dissolved in 10 mM Tris, 150 mM NaCl, pH 7.4 at a concentration of 0.3 mg/ml. Samples were reduced by adding DTT to a final concentration of 10 mM and incubating the sample for 45 min at 37 °C. The far-ultraviolet spectra (195–250 nm) were measured at 20 °C. After subtraction of the buffer contribution, data were converted to mean molar residue ellipticity. Secondary structures were calculated with the online server DICHROWEB (23) using the K2D algorithm (24). Melting curves were recorded at a fixed wavelength of 220 nm while the sample was heated up to 90 °C at a rate of 12 °C/h. The reversibility of the unfolding was tested by gradual cooling to 20 °C.

RESULTS

Structure and Domain Organization of Mouse EMILIN-3—The murine *Emilin3* gene (Mouse Genome Informatics Database MGI:2389142) spans about 6.4 kb and contains four exons separated by three relatively small introns. Mouse *Emilin3* cDNA (GenBank™ accession number NM_182840) contains an open reading frame of 2277 bp and encodes for a protein of 758 amino acids including a signal peptide of 21 residues (Fig. 1, *A* and *B*). The mature secreted protein has a calculated molecular mass of 82.5 kDa. At its N-terminal end, EMILIN-3 contains an EMI domain of 79 amino acid residues with an identity of 52.6 and 53.9% when compared with the EMI domain of EMILIN-1 and EMILIN-2, respectively, whereas the overall identity with these two proteins is about 20%. Database comparisons did not identify any other known domain within EMILIN-3. mRNA analysis (see also below) revealed that murine EMILIN-3 has two splicing isoforms, hereafter referred to as EMILIN-3L and -3S with the shorter one lacking the first 141 bp of the fourth exon (Fig. 1*B*).

Sequence analysis with the COILS program (25) predicted several regions with a high probability of forming coiled coil structures at the C-terminal end of the protein (Fig. 1*C*). Coiled coil regions contain only α-helices as secondary structure ele-

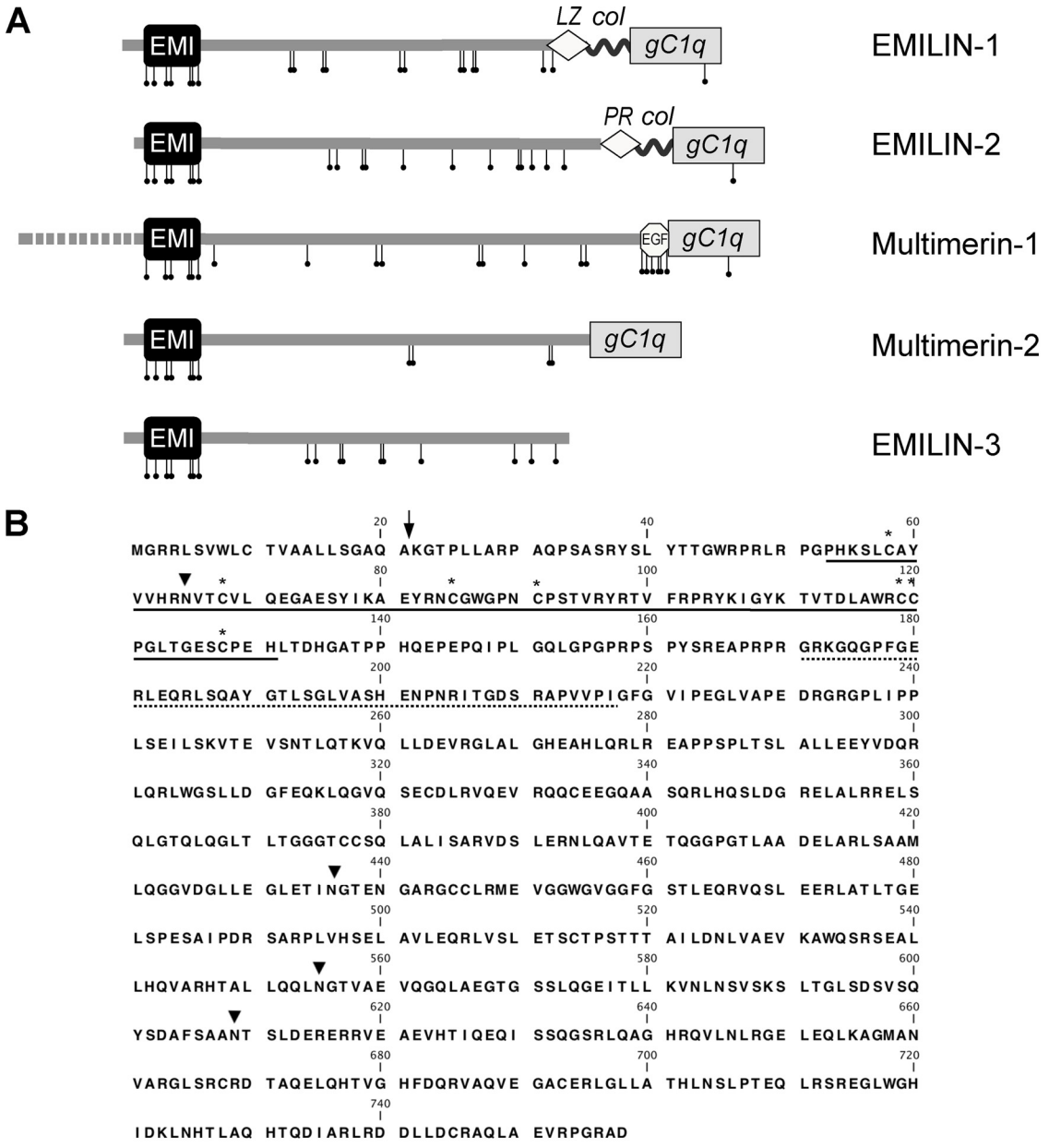

TABLE 1
Secondary structure content of EMILIN-3CTR
Values were calculated using the DICHROWEB program (23).

	NRMSD[a]	α-Helix	β-Sheet	Random coil
EMILIN-3CTR	0.072	0.31	0.14	0.56
EMILIN-3CTR + 10 mM DTT	0.107	0.26	0.14	0.60
EMILIN-3CTR + 2 M GdnHCl	0.106	0.31	0.12	0.58

[a] Normalized root mean square deviation.

ments, and the α-helix conformation can be stabilized by oxidized cysteine residues (26, 27). To verify coiled coil formation, a recombinant fragment of EMILIN-3 corresponding to the C-terminal region of the protein (EMILIN-3CTR; amino acid residues 171–758) was generated and analyzed by circular dichroism spectroscopy to determine the α-helix content (Fig. 1*D*). The far-ultraviolet spectrum of the oxidized EMILIN-3CTR showed slight minima at 208 and 222 nm, indicating that parts of the protein have an α-helical conformation. The secondary structure analysis algorithm K2D gave a good fit with a normalized root mean square deviation of 0.072 and yielded an α-helical content of about 31% (Table 1). This value is in agreement with the fact that only the C-terminal third of EMILIN-3CTR is predicted to form coiled coil structures (Fig. 1*C*). The N-terminal part of EMILIN-3CTR is likely to form random coils and other secondary structures as circular dichroism spectroscopy indicated that EMILIN-3CTR contains about 50% random coil. After reduction of EMILIN-3CTR with 10 mM DTT, the α-helical content decreased slightly to about 26%, suggesting that disulfide bonds stabilize the coiled coil region. This could also be shown after addition of the denaturing agent guanidine hydrochloride (GdnHCl). All ordered structures of oxidized EMILIN-3CTR were lost when the protein was treated with 4 M GdnHCl. In the presence of 2 M GdnHCl, 30% α-helix was detected, whereas reduced EMILIN-3CTR lost all secondary structure after the addition of 2 M GdnHCl (Fig. 1*D*). Both GdnHCl and DTT disturbed the spectra at wavelengths below 210 nm, but assessment of α-helical content was still possible.

To monitor the thermal transition from coiled coil α-helix to random coil, oxidized EMILIN-3CTR and reduced EMILIN-3CTR were analyzed by circular dichroism at 220 nm while samples were heated to 90 °C (supplemental Fig. S1A). As only parts of EMILIN-3CTR appear to form coiled coil structures, it was not surprising that the thermal denaturation curves were complex, not allowing the calculation of distinct melting points. However, for both the oxidized EMILIN-3CTR and reduced EMILIN-3CTR, heat denaturation was partially reversible after cooling the sample to 20 °C. After complete denaturation in the presence of 4 M GdnHCl or 2 M GdnHCl and 10 mM DTT, no refolding was observed (supplemental Fig. S1B).

Expression of EMILIN-3 during Mouse Embryonic and Postnatal Development—We first investigated EMILIN-3 expression by RT-PCR analysis. EMILIN-3 mRNA was detected in preimplantation mouse blastocysts and in a few human and murine cell lines (Fig. 2*A* and supplemental Fig. S2). During mouse postimplantation development, EMILIN-3 transcripts were present at all studied stages with stronger expression during midgestation (Fig. 2*B*). RT-PCR analysis of various tissues derived from neonatal and adult mice showed that, similar to other EMILIN/Multimerin genes, EMILIN-3 expression decreases after birth. In adult mice, EMILIN-3 transcripts were found only in a few of the examined tissues, namely testis, eye, and brain (Fig. 2*C*). When using oligonucleotide primers for the two EMILIN-3 isoforms, both fragments corresponding to EMILIN-3L and -3S were detected in mouse embryos and postnatal tissues, confirming that these are *bona fide* mRNA splicing isoforms (Fig. 2, *B* and *C*). Northern blot analysis of newborn mouse tissues showed that EMILIN-3 mRNA migrates at about 3.8 kb and confirmed expression in postnatal testis, uterus, and intestine (Fig. 2*D*).

We further analyzed EMILIN-3 mRNA expression by *in situ* hybridization of whole-mount E8.5 and E9.5 embryos and serial sections derived from E10.5–E14.5 embryos. At E8.5, EMILIN-3 mRNA was detected at low levels in the tail bud, whereas at E9.5, expression became more abundant in the tail bud region with also a faint labeling in the primitive hindgut (supplemental Fig. S3). At E10.5, strong expression was detected in the esophageal bud, the mesenchyme of branchial arches, the tail bud, and a small region of the developing midbrain (data not shown). Expression in the midbrain, now confined to the ventricular zone of the third ventricle, was still present at both E11.5 and E12.5 and disappeared at E13.5 (Fig. 3, *A–C*, and data not shown). During organogenesis, EMILIN-3 was strongly expressed throughout the gastrointestinal tract. At earlier stages (E10.5–E12.5), EMILIN-3 mRNA was diffusely present in the wall of the gastrointestinal system from the esophagus to the hindgut (Fig. 3, *A* and *D*). Starting from E13.5, EMILIN-3 transcripts became restricted to a thin layer corresponding to the myenteric plexus, showing a craniocaudal gradient with strongest signal in the esophagus (Fig. 3, *E–H*). At E13.5, expression became abundant in the subepidermal mes-

FIGURE 1. **Amino acid sequence of murine EMILIN-3 and evidence for coiled coil α-helical region.** *A*, schematic diagram of the structure of mouse EMILIN/Multimerin proteins. *CoI*, short collagenous region; *EGF*, EGF-like domain; *EMI*, EMI domain; *gC1q*, globular C1q domain; *LZ*, leucine zipper motif; *PR*, proline-rich region. Cysteine residues are marked by *vertical bars*. The *dashed line* in Multimerin-1 indicates a cleaved propeptide region. *B*, murine EMILIN-3 amino acid sequence as derived from the full-length cDNA. An *arrow* marks the putative signal peptide cleavage site. The EMI domain is *underlined*, and the seven conserved cysteine residues are marked by *asterisks*. *Arrowheads* indicate four sites predicted to be *N*-glycosylated. The *dotted underline* indicates the sequence that can be removed by alternative splicing. *C*, prediction of coiled coil formation as deduced by analysis with the COILS program. Three regions with high probability of forming coiled coil structures are predicted in the C-terminal part of murine EMILIN-3 sequence. *D*, circular dichroism spectra revealing the presence of about 31% α-helix in the EMILIN-3CTR recombinant fragment (amino acid residues 171–758). The α-helical structure was lost upon treatment with 4 M GdnHCl (*GuHCl*) or 2 M GdnHCl together with 10 mM DTT. *θ*, mean molar residual ellipticity; *deg*, degrees.

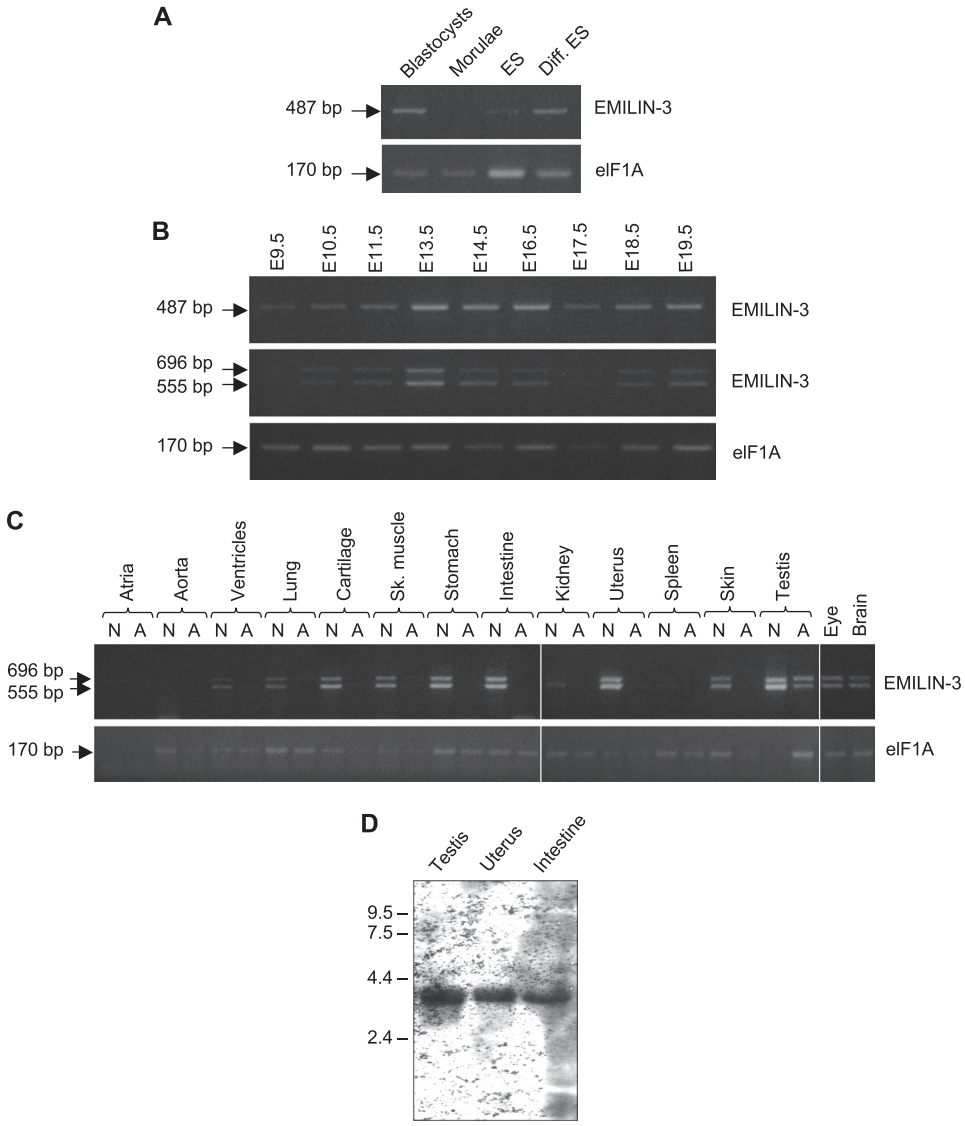

FIGURE 2. **Detection of EMILIN-3 mRNA transcripts during mouse development and in postnatal and adult mouse tissues.** *A–C*, RT-PCR analysis of total RNA derived from whole mouse embryos at the indicated developmental stages (*A* and *B*) or from postnatal and adult mouse tissues (*C*). Semiquantitative RT-PCR was carried out using oligonucleotide primers able to detect either all EMILIN-3 transcripts or the two splicing variants differing by 141 base pairs. Amplification of eIF1A was used as an RNA loading control. *D*, Northern blotting identification of EMILIN-3 mRNA in newborn mouse tissues. The migration of molecular weight markers is indicated in kb on the *left*. *A*, adult; *Diff. ES*, differentiated mouse embryonic stem cells; *ES*, undifferentiated mouse embryonic stem cells; *N*, neonatal; *Sk.*, skeletal.

enchyme (Fig. 3*I*). Genital ridges were strongly labeled throughout their development, whereas metanephric tissues and kidney were negative (Fig. 3, *J–L*). Expression of EMILIN-3 was also found in the intervertebral discs, the region surrounding the main branches of alveoli, the mesenchymal tissue around vibrissae, the diaphragm, and the cephalic mesenchyme (Fig. 3, *M–Q*). A strong expression was also detected in the perichondrium around sites of bone and cartilage formation in trunk, skull, and limbs (Fig. 3, *R* and *S*). In contrast to other EMILIN/Multimerin genes, EMILIN-3 expression was not detected in the cardiovascular system at any developmental stage (Fig. 3, *A* and *M*, and supplemental Fig. S3).

EMILIN-3 Has Restricted Distribution in Adult Mouse Tissues—As specific antibodies for EMILIN-3 were not available, guinea pigs and rabbits were immunized with recombinant EMILIN-3CTR. After affinity purification, both guinea pig and rabbit antibodies detected EMILIN-3, and their specificity was confirmed by Western blot and immunofluorescence (supplemental Figs. S4–S6).

To investigate EMILIN-3 protein distribution, we carried out immunofluorescence on frozen sections from adult mouse tissues. EMILIN-3 antisera raised in guinea pig and rabbit gave very similar results, and immunofluorescence data obtained with the guinea pig antibody are shown here. EMILIN-3 displayed a restricted protein distribution in adult tissues (Fig. 4). In agreement with the mRNA expression, a conspicuous labeling was detected in testis where EMILIN-3 was abundantly deposited in the collagenous structure of the tunica albuginea and the basement membrane surrounding each seminiferous tubule (Fig. 4, *A–C*). Conversely, EMILIN-3 distribution in ovary was confined to the tunica albuginea, and no labeling was found in cortical and medullary regions or around follicles (Fig.

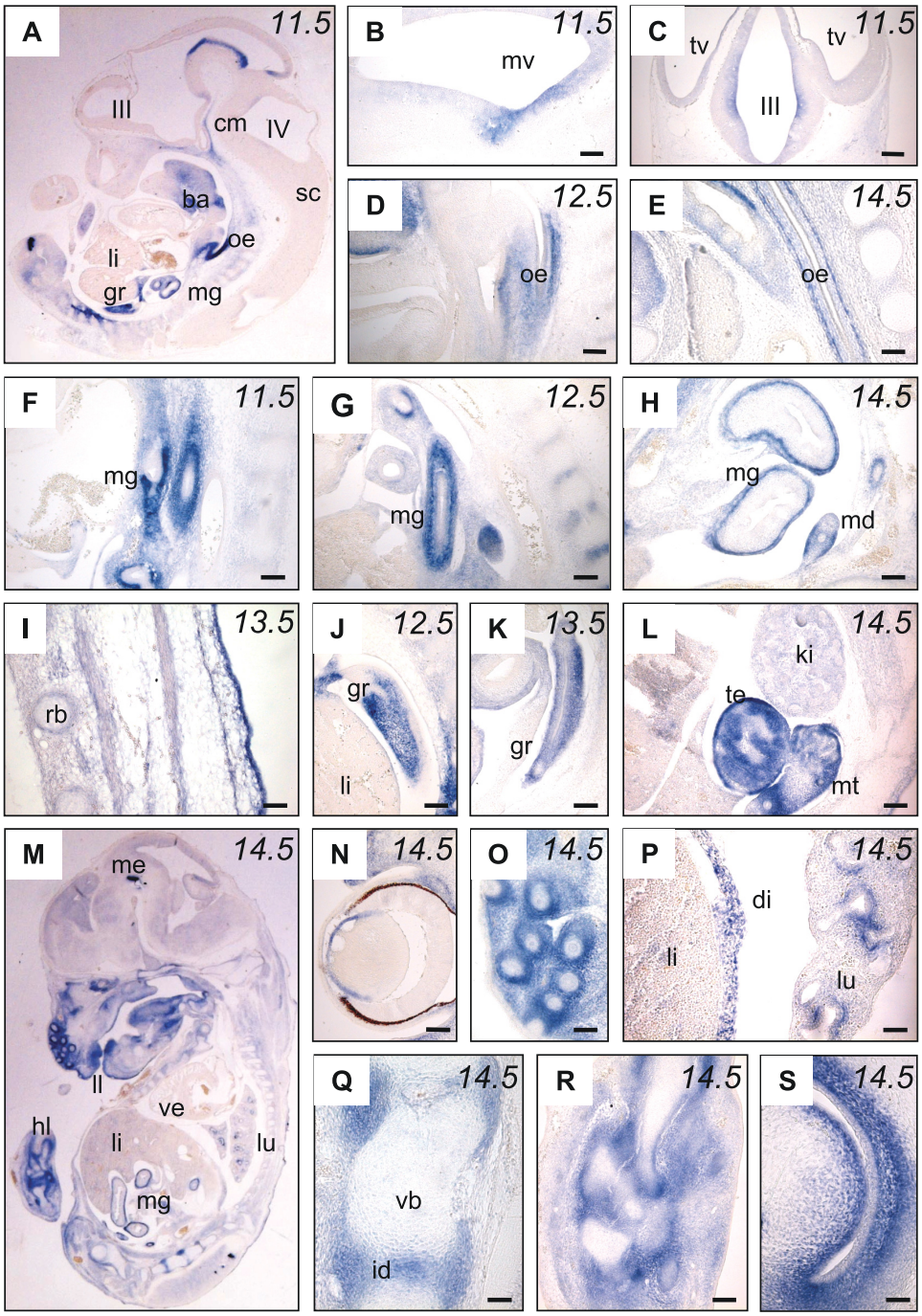

FIGURE 3. ***In situ* hybridization analysis of EMILIN-3 mRNA expression during mouse embryonic development.** Mouse embryos at different developmental stages (E11.5–E14.5) were processed and analyzed by *in situ* hybridization on paraffin sections with an EMILIN-3 antisense probe. *A*, parasagittal section of whole E11.5 embryo. *B* and *C*, sagittal and transverse sections, respectively, at E11.5 showing EMILIN-3 expression in the ventricular zone of ventral midbrain. *D–H*, expression in the gastrointestinal tract was detected at all stages starting from E11.5; esophagus (*D* and *E*) and midgut (*F–H*) are shown. *I–L*, expression in the subepidermal mesenchyme of trunk (*I*), genital ridges (*J* and *K*), and mesonephric tissue (*L*). *M*, parasagittal section of whole E14.5 embryo. *N–S*, details of E14.5 sections showing EMILIN-3 expression in the developing eye (*N*), vibrissae (*O*), diaphragm and main bronchi (*P*), intervertebral discs (*Q*), perichondrium of the hind limbs (*R*), and inner ear (*S*). *III*, third ventricle; *IV*, fourth ventricle; *ba*, branchial arches; *cm*, cephalic mesenchyme; *di*, diaphragm; *gr*, genital ridge; *hl*, hind limb; *id*, intervertebral discs; *ki*, kidney; *li*, liver; *ll*, lower lip; *lu*, lung; *md*, mesonephric duct; *me*, mesencephalon; *mg*, midgut; *mt*, mesonephric tissue; *mv*, mesencephalic vesicle; *oe*; esophagus; *rb*, rib primordia; *sc*, spinal cord; *te*, testis; *tv*, telencephalic vesicle; *vb*, vertebral bodies; *ve*, ventricle. *Scale bar*, 50 (*I*, *P*, and *Q*) or 100 μm (other panels).

4*D*). A diffuse staining was detected in the wall of the uterus (Fig. 4*E*). Strong labeling for EMILIN-3 was found in the external ear where the protein localizes in the perichondrium of the elastic cartilage (Fig. 4*F*). EMILIN-3 was also detected in skeletal muscles, but the distribution was variable among different muscles. For example, in quadriceps, the endomysium of many (but not all) myofibers was labeled, and in tibialis anterior, staining was restricted to the epimysium, whereas the diaphragm was negative (Fig. 4, *G* and *H*, and data not shown). EMILIN-3 showed a peculiar distribution throughout the gas-

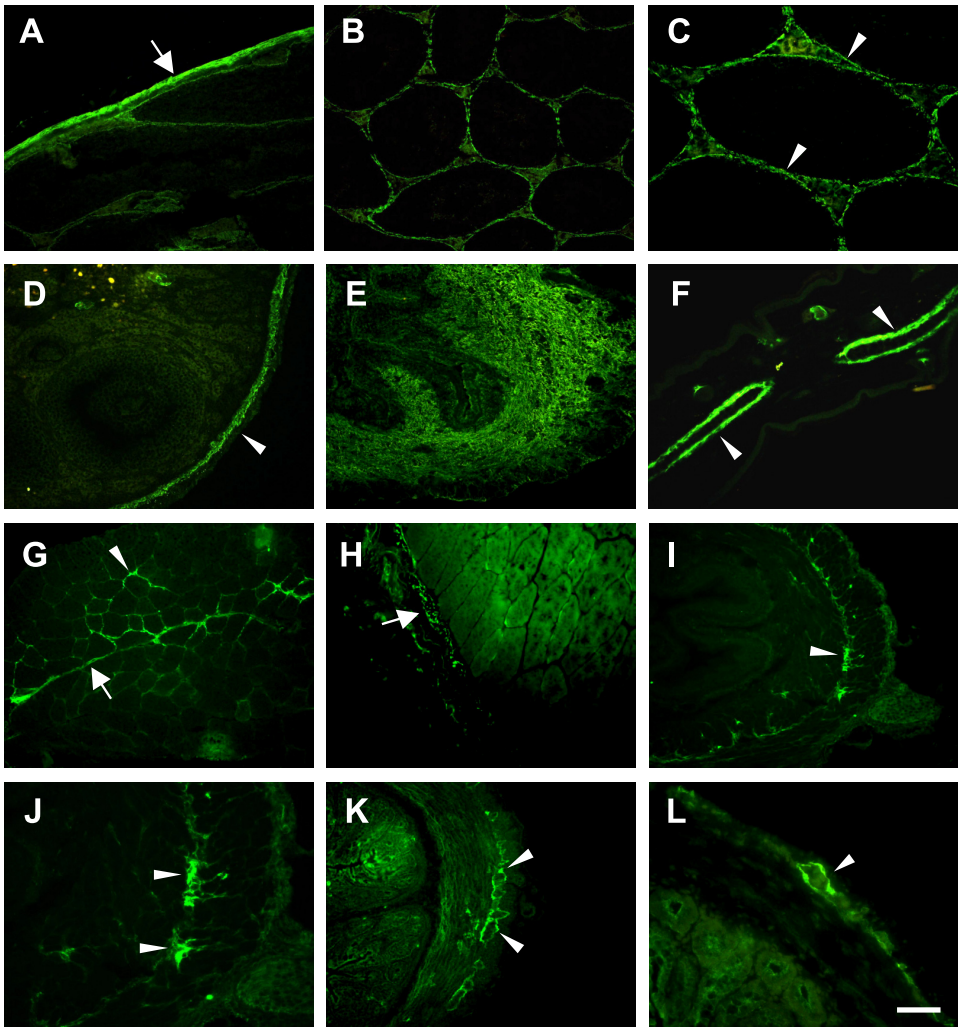

FIGURE 4. **EMILIN-3 has restricted protein distribution in adult tissues.** Adult mouse tissues were processed and analyzed by immunofluorescence with the affinity-purified guinea pig EMILIN-3 antibody. *A–C*, sections from adult testis with abundant EMILIN-3 deposition in the tunica albuginea (*arrow*) and at the level of basement membranes of seminiferous tubules (*arrowheads*). *D*, in ovary, staining is detectable only in the tunica albuginea (*arrowhead*). *E*, section of uterus wall showing a diffuse labeling for EMILIN-3. *F*, transverse section of the external ear showing strong EMILIN-3 deposition in the perichondrium surrounding elastic cartilage (*arrowheads*). *G*, section of quadriceps muscle where labeling is found in the perimysium (*arrow*) and endomysium (*arrowheads*) of several myofibers. *H*, section of tibialis anterior muscle showing staining of the epimysium (*arrow*). *I–L*, transverse sections of esophagus (*I* and *J*) and colon (*K* and *L*) revealing strong labeling at the level of the myenteric plexus (*arrowheads*). *Scale bar*, 50 (*C*, *H*, *J*, and *L*) or 100 μm (other panels).

trointestinal tract from esophagus to colon where immunofluorescence was found in a thin region between the longitudinal and transverse smooth muscle layers corresponding to the myenteric plexus (Fig. 4, *I–L*). In contrast to other EMILINs/Multimerins, EMILIN-3 was totally absent in the cardiovascular system, and parenchymatous organs, such as heart, blood vessels, kidneys, spleen, and liver, were completely negative for EMILIN-3 immunostaining (supplemental Fig. S7 and data not shown).

EMILIN-3 Forms Disulfide-bonded Homotrimers and High Molecular Weight Multimers and Carries N-Glycans—Immunoprecipitation and Western blotting of adult mouse tissue extracts with the two EMILIN-3 antisera showed a major band migrating at about 105 kDa, which is consistent with the expected molecular mass of the protein (Fig. 5*A*). Interestingly, even under strong reducing conditions, a fraction of the protein migrated as discrete bands with lower mobility; their calculated molecular masses (210 and 315 kDa) are in agreement with the potential formation of dimers and trimers. Some protein was also detected at the gel origin, suggesting a strong tendency of EMILIN-3 to form high molecular weight aggregates. Western blot analysis under reducing conditions of immunoprecipitated EMILIN-3 extracts from whole E14.5 embryos resulted in a doublet of bands at about 95 and 105 kDa (Fig. 5*B*), which may correspond to the two splicing isoforms detected by RT-PCR experiments. When analyzed by SDS-PAGE under non-reducing conditions, immunoprecipitated EMILIN-3 material migrated in two distinct regions of the gel with a lower band at about 105 kDa, corresponding to the size of the monomeric protein, and a broad band migrating between the 268 and 460 kDa size markers, suggesting that *in vivo* EMILIN-3 largely exists as cysteine-bound oligomers (Fig. 5*B*).

To further explore the biochemical properties of EMILIN-3, we carried out transient transfection experiments of HEK293T cells with full-length expression constructs coding for EMILIN-3L and EMILIN-3S. Cell lysates and conditioned media were collected and analyzed by Western blotting. Under

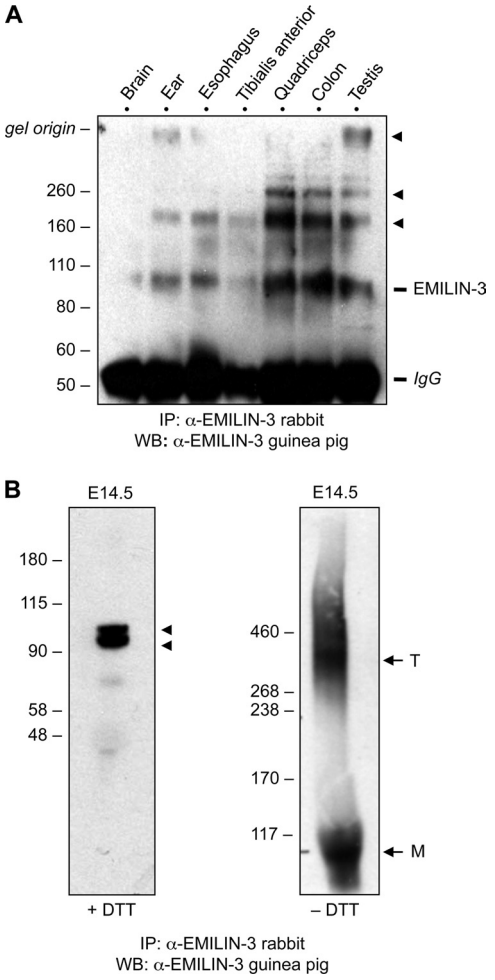

FIGURE 5. **Immunoprecipitation of EMILIN-3 from adult mouse tissues and whole embryo extracts.** *A*, immunoprecipitation of protein extracts from different adult tissues with affinity-purified rabbit EMILIN-3 antiserum followed by SDS-PAGE on a 4–12% gradient gel under reducing conditions and Western blot with affinity-purified guinea pig EMILIN-3 antibodies. A major band migrating at about 105 kDa and corresponding to the EMILIN-3 monomeric form is present in most tissues together with a ladder of slower migrating bands above 200 kDa (*arrowheads*) probably representing partially unreduced EMILIN-3 dimers and multimers. The abundant band migrating at about 55 kDa corresponds to IgG. *B*, immunoprecipitation from whole E14.5 embryo extracts followed by SDS-PAGE on a 4–12% gradient gel under reducing conditions (+ *DTT*; *left panel*) or on a 3–8% gradient gel under non-reducing conditions (− *DTT*; *right panel*) and Western blot for EMILIN-3. Two distinct EMILIN-3 bands migrating at about 95 and 105 kDa (*arrowheads*) are present in reduced E14.5 extracts. Under non-reducing conditions, EMILIN-3 migrates as a broad band at about 100 kDa and a larger diffuse product at about 300 kDa, a molecular mass compatible with homotrimer formation. Migration of protein size markers is indicated in kDa on the *left* of each panel. *IP*, immunoprecipitation; *M*, monomers; *T*, trimers; *WB*, Western blot.

reducing conditions, EMILIN-3L and EMILIN-3S migrated at about 105 and 95 kDa, respectively. Conversely, under non-reducing conditions, the two transfected proteins migrated at about 300 and 270 kDa (Fig. 6*A*), which is consistent with the formation of trimers as observed *in vivo* for the endogenous EMILIN-3. To investigate the nature of these higher molecular weight products and assess whether EMILIN-3 may form homo-oligomers, we generated FLAG- and HA-tagged constructs of full-length EMILIN-3 or EMILIN-3 lacking the EMI domain (EMILIN-3ΔEMI where amino acids 54–189 were missing). After cotransfection of these constructs in HEK293T cells, we immunoprecipitated cell lysates with an anti-FLAG antibody and found that HA-tagged proteins were coprecipitated, strongly suggesting that EMILIN-3 complexes are composed of disulfide-linked homo-oligomers. EMILIN-3ΔEMI coprecipitated with full-length EMILIN-3, indicating that the EMI domain is not required for EMILIN-3 homo-oligomerization (Fig. 6*B*). To further confirm these results, we studied the oligomerization of the EMILIN-3CTR recombinant protein by SDS-PAGE after treatment with increasing concentrations of the reducing agent DTT. In the absence of DTT, the major band migrated at 270–300 kDa in agreement with the calculated mass of trimeric EMILIN-3CTR. With increasing reduction, the trimer band became weaker, and a doublet at about 160 kDa and a band at 80 kDa appeared, indicating that reduction of the trimer in the presence of SDS led to the formation of dimeric and monomeric forms of EMILIN-3CTR. Apparently two dimer forms occur that are presumably connected by different disulfide bonds after partial reduction (Fig. 6*C*).

It has been proposed that the C-terminal gC1q domain of EMILIN-1 plays a role in multimer formation (11). Because EMILIN-3 is able to form disulfide-bonded homotrimers even in the absence of a gC1q domain, we investigated whether the cysteine-rich EMI domain plays any role in the formation of the higher order multimers of EMILIN-3 and EMILIN-1. Toward this aim, FLAG-tagged EMILIN-1 constructs lacking either the EMI domain (EMILIN-1ΔEMI) or the gC1q domain (EMILIN-1Δg1q) were produced and transfected into HEK293T cells in parallel with FLAG-tagged EMILIN-3 and EMILIN-3ΔEMI constructs. Extracts from transfected cells were analyzed by electrophoresis and Western blot under reducing and non-reducing conditions. Under non-reducing conditions, all the recombinant proteins were able to form homotrimers, suggesting that neither the gC1q domain nor the EMI domain is necessary for this process (Fig. 7*A*). Further assembly into higher order multimers was studied by electrophoresis in composite acrylamide-agarose gels under non-reducing conditions. EMILIN-1, EMILIN-1ΔgC1q, and EMILIN-3 were found almost exclusively as large aggregates reaching a size of about 1000–2000 kDa. Conversely, EMILIN-1ΔEMI and EMILIN-3ΔEMI aggregated with a lower efficiency. In particular, almost no high molecular weight aggregates of EMILIN-1ΔEMI could be detected (Fig. 7*B*). Altogether, these data indicate that the gCq1 domain is not strictly required for trimer and multimer formation and suggest a role for the EMI domain in the formation of higher order multimers.

Because the amino acid sequence of EMILIN-3 gives a predicted molecular mass of 82.5 kDa and contains four putative *N*-glycosylation sites, we investigated whether the migration of full-length EMILIN-3 at 105 kDa as detected by SDS-PAGE under reducing conditions was the result of post-translational modifications. Cell lysates and concentrated conditioned media of EMILIN-3-transfected cells were treated with different deglycosylating enzymes and subjected to SDS-PAGE and immunoblotting. This analysis showed that EMILIN-3 undergoes extensive *N*-glycosylation because treatment with endoglycosidase F shifted EMILIN-3 migration to its predicted molecular weight (Fig. 7*C*).

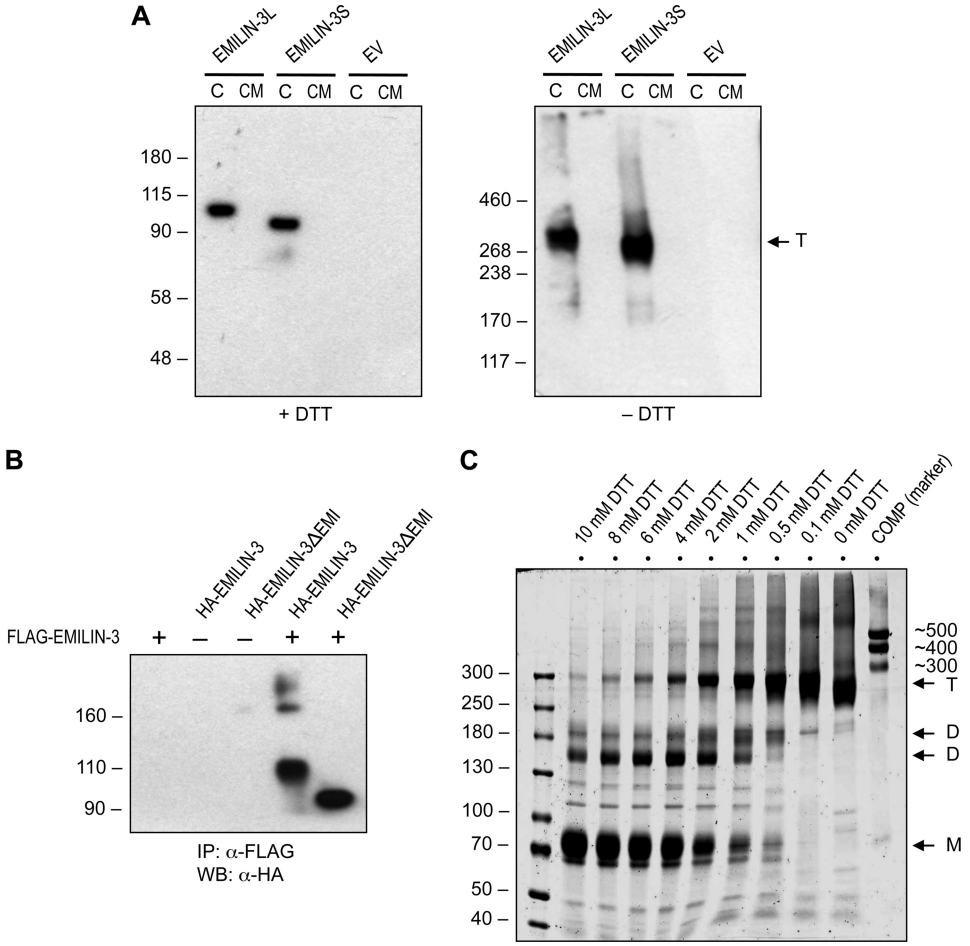

FIGURE 6. **EMILIN-3 forms disulfide-bonded homotrimers.** *A*, HEK293T cells were transfected with the indicated expression constructs. The cell layer and conditioned medium were separated by 4–12% gradient SDS-PAGE under reducing conditions (+ *DTT*; *left panel*) or by 3–8% gradient SDS-PAGE under non-reducing conditions (− *DTT*; *right panel*) and analyzed by Western blot with rabbit EMILIN-3 antiserum. Both transfected EMILIN-3L and -3S proteins were readily detected in the cell extracts but not in the conditioned media. The mobility of transfected EMILIN-3 proteins under non-reducing conditions suggests trimer (*T*) formation. Transfection with the empty vector was used as a control. *B*, HEK293T cells were transfected with HA-tagged EMILIN-3 or HA-tagged EMILIN-3ΔEMI in the presence (+) or in the absence (−) of FLAG-tagged EMILIN-3. Anti-FLAG immunoprecipitation was performed on cell lysates, and samples were separated by 4–12% gradient SDS-PAGE under reducing conditions and analyzed by Western blot with anti-HA antibody. *C*, SDS-PAGE of partially reduced EMILIN-3CTR on a 4–10% polyacrylamide gel. Although oxidized EMILIN-3CTR migrates only as a trimer (*T*) and higher aggregates, reduction releases dimeric (*D*) and monomeric (*M*) protein fragments. Non-reduced cartilage oligomeric matrix protein (COMP) was used as a marker. Migration of protein size markers is indicated in kDa on the *left* of each panel. *C*, cell layer; *CM*, conditioned medium; *EV*, empty vector; *IP*, immunoprecipitation; *WB*, Western blot.

EMILIN-3 Binds Heparin through Its EMI Domain and Is Associated with ECM via Heparin or Heparan Sulfate Proteoglycans—Despite the relatively high levels of transfected EMILIN-3 observed in cell extracts, the protein was barely detectable in conditioned media (see Fig. 6*A*). To further investigate this finding, HEK293T cells were transfected with expression constructs coding for either EMILIN-1, EMILIN-2, or EMILIN-3 protein fused to a FLAG epitope and a heterologous chordin signal peptide, and cell lysates and conditioned media were analyzed by Western blot under reducing conditions with an anti-FLAG antibody. Although EMILIN-1 and EMILIN-2 proteins were detected in both samples, EMILIN-3 could not be detected in the conditioned medium (supplemental Fig. S8A). Therefore, the absence of EMILIN-3 in conditioned media was not dependent on its own signal peptide. Immunofluorescence analysis of cells following cotransfection of EMILIN-3 with a cDNA coding for an endoplasmic reticulum probe revealed that EMILIN-3 colocalized with endoplasmic reticulum, indicating that transfected EMILIN-3 was in the cell secretory pathway. Moreover, some immunolabeling was also found outside the cells, confirming that EMILIN-3 is indeed secreted by transfected cells and that the protein can be found in the extracellular space (supplemental Fig. S8B).

The lack of EMILIN-3 in the conditioned media of transfected cells despite its presence in the secretory pathway and on culture coverslips suggested that the protein might become readily bound to the ECM once secreted. Therefore, we examined the insoluble material that remained associated with the culture dish of HEK293T cells transfected with EMILIN-3 constructs. Protein extracts were prepared by lysing cells in the culture dish with RIPA buffer at 4 °C. After removal of the cell lysate, culture dishes were washed three times with RIPA buffer, and the extracellular material still bound to the dish was extracted with Laemmli buffer at 90 °C. Western blot analysis revealed that the insoluble ECM fraction contained a noticeable amount of EMILIN-3 (Fig. 8*A*). Interestingly, ECM-associated EMILIN-3 migrated slightly more slowly than the protein associated with the cell layer, sug-

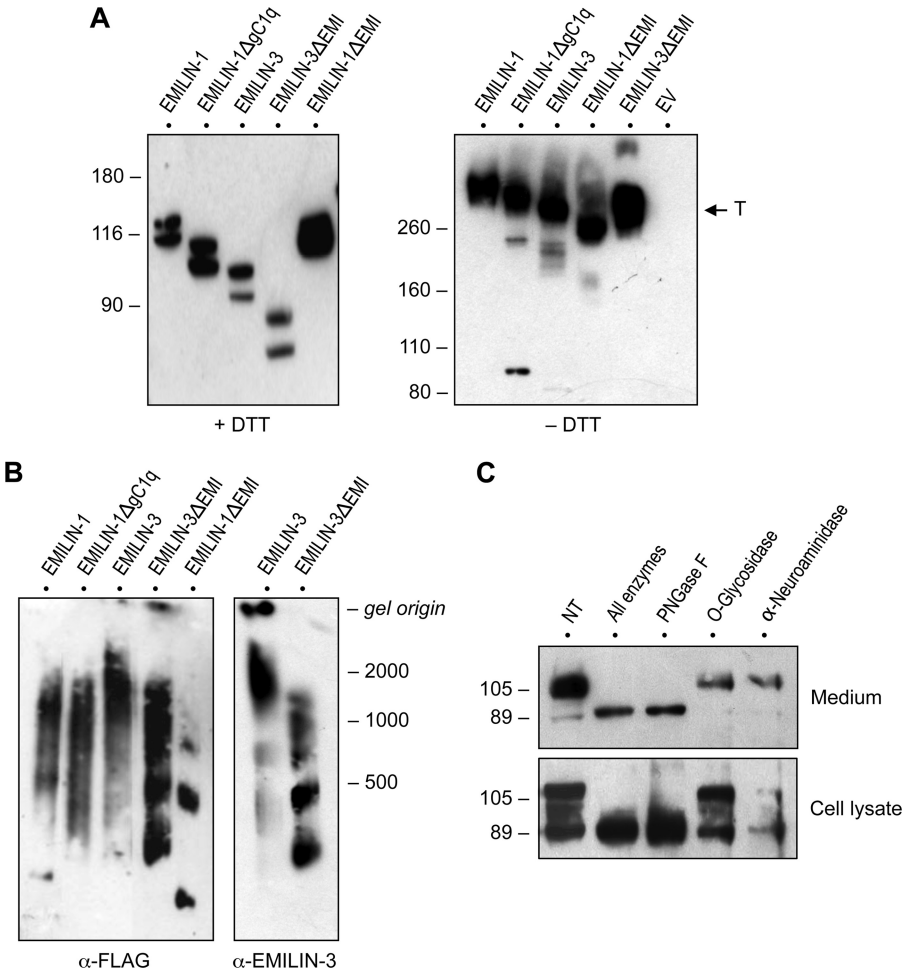

FIGURE 7. **EMILIN-3 undergoes oligomerization and is *N*-glycosylated.** *A*, lysates of HEK293T cells transfected with the indicated plasmids were separated by 4–12% gradient SDS-PAGE under reducing conditions (+ *DTT*; *left panel*) or by 3–8% gradient SDS-PAGE under non-reducing conditions (− *DDT*; *right panel*) followed by Western blot with anti-FLAG antibody. All the tested recombinant proteins migrated at the expected sizes and formed disulfide-linked homotrimers under non-reducing conditions. *B*, lysates of HEK293T cells transfected with the indicated plasmids were separated by electrophoresis on composite 2.4% acrylamide, 0.5% agarose gels under non-reducing conditions and analyzed by Western blot with anti-FLAG or anti-EMILIN-3 antibodies. *C*, HEK293T cells were transfected with the FLAG-tagged EMILIN-3 construct. Cell lysate and acetone-precipitated conditioned medium were treated with the indicated enzymes and analyzed by 3–8% gradient SDS-PAGE under reducing conditions followed by Western blot with anti-FLAG antibody. Migration of protein size markers is indicated in kDa on the *left* (*A* and *C*) or on the right (*B*). *EV*, empty vector; *NT*, no treatment; *T*, trimers.

gesting that further post-translational modifications occur during EMILIN-3 secretion.

A number of growth factors and other secreted proteins are thought to associate with the ECM because of their affinity for heparin and heparan sulfate proteoglycans (28, 29). Therefore, we investigated the possibility that EMILIN-3 might be endowed with heparin binding properties. Toward this aim, soluble heparin was added to the culture medium of transfected HEK293T cells. Whereas little or no EMILIN-3 was present in the conditioned media of cells grown under standard conditions, the protein could be readily detected in the medium fraction when transfected cells were grown in the presence of 50 μg/ml soluble heparin (Fig. 8*A*). To evaluate whether this effect was specific for heparin, we treated transfected HEK293T cells with the same concentrations of soluble chondroitin 4-sulfate and hyaluronic acid and analyzed the amount of EMILIN-3 released in the conditioned media. Although EMILIN-3 was abundant in heparin-treated medium, almost no protein was detected in media treated with the other glycosaminoglycans (Fig. 8*B*). Several potential interpretations can be put forward for these results including the possibility that soluble heparin in the medium may compete with the binding of EMILIN-3 to the ECM or that EMILIN-3 could bind directly to the heparin moiety. To investigate whether EMILIN-3 binds heparin, lysates of cells transfected with EMILIN-3L and -3S constructs were incubated with heparin-conjugated agarose beads, and the material bound to the beads was eluted with buffers at different salt concentrations and analyzed by Western blot. EMILIN-3L displayed efficient binding to the heparin-conjugated beads, and most of the protein eluted at high salt (0.6–1.0 M NaCl) concentrations. This association was specifically dependent on the heparin moiety because EMILIN-3L did not bind to unconjugated agarose beads (Fig. 8*C*). Similar results were also obtained for EMILIN-3S. To determine which fragment of EMILIN-3 is required for heparin binding, cells were transfected with the EMILIN-3ΔEMI construct. Interestingly, the EMILIN-3ΔEMI recombinant protein did not bind to heparin-conjugated beads, suggesting that the presence of the EMI domain is necessary for the association with heparin (Fig. 8*C*). In agreement with this, the EMILIN-3ΔEMI protein could be

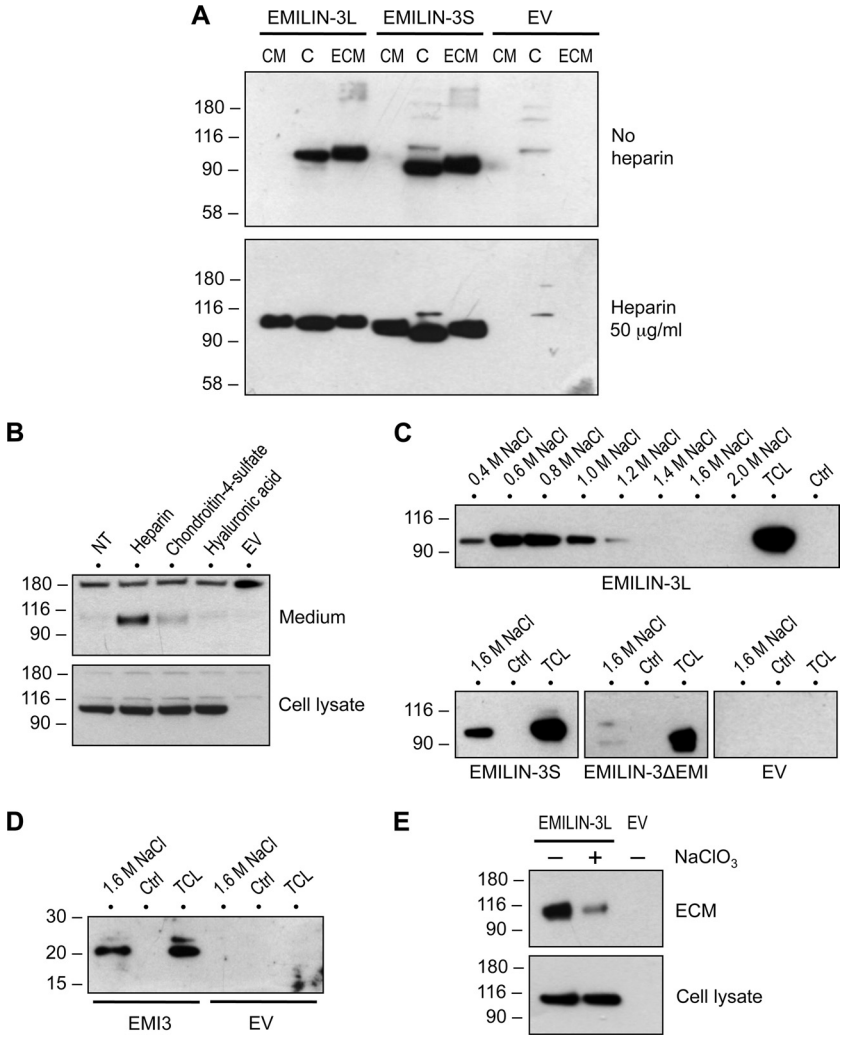

FIGURE 8. **EMILIN-3 is associated with ECM and binds to heparin.** *A*, after transfection with the indicated constructs, HEK293T cells were cultured in the absence or presence of 50 μg/ml soluble heparin. Cells were lysed at 4 °C in RIPA buffer, and the ECM material remaining on the culture dishes was extracted in Laemmli sample buffer at 90 °C. Cell lysate, conditioned medium, and ECM extract were analyzed by 4–12% gradient SDS-PAGE under reducing conditions followed by Western blot with rabbit EMILIN-3 antiserum. *B*, HEK293T transfected with EMILIN-3L were treated with the indicated glycosaminoglycans at 50 μg/ml, and cell lysates and conditioned media were subjected to SDS-PAGE on a 4–12% gel under reducing conditions and immunoblotted for EMILIN-3. *C* and *D*, cell lysates from HEK293T cells transfected with the indicated constructs were precipitated with heparin-conjugated agarose beads. After extensive washes, bound proteins were eluted with buffers containing increasing concentrations of NaCl from 0.4 to 2.0 M and separated by 4–12% gradient SDS-PAGE under reducing conditions, and transfected proteins were detected by Western blot with rabbit EMILIN-3 antiserum (*C*) or anti-FLAG antibody (*D*). *E*, HEK293T cells transfected with EMILIN-3L were left untreated (−) or treated with 30 μM sodium chlorate (+), and cell lysate and ECM extracts were prepared as above and analyzed by Western blot with rabbit EMILIN-3 antiserum. Migration of protein size markers is indicated in kDa on the *left* of each panel. *C*, cell layer; *CM*, conditioned medium; *Ctrl*, samples precipitated with unconjugated beads; *ECM*, insoluble ECM extract; *EV*, empty vector; *NT*, no treatment; *TCL*, total cell lysate.

readily detected in the conditioned medium of transfected cells (supplemental Fig. S8C).

To directly verify that the EMI domain is the heparin binding region of EMILIN-3, we prepared an expression construct (hereafter referred to as EMI3) encompassing the EMI domain and including amino acids 1–190 of EMILIN-3 with a FLAG tag at the C terminus. We then transfected HEK293T cells with the EMI3 construct and incubated the cell lysate with heparin-conjugated beads. In agreement with the above data, the recombinant EMI3 fragment did not bind to unconjugated beads but was efficiently precipitated by the heparin-conjugated beads, thus demonstrating that the EMI domain is directly responsible for the heparin binding properties of EMILIN-3 (Fig. 8*D*). To assess whether the strong association of EMILIN-3 to the ECM was mediated at least in part by the binding to endogenous heparan sulfate groups, we treated transfected HEK293T cells with the sulfotransferase inhibitor sodium chlorate and analyzed the insoluble ECM fraction. Interestingly, treatment with sodium chlorate strongly decreased the amount of transfected EMILIN-3 that could be extracted from the ECM, thus confirming that sulfated glycosaminoglycans markedly contribute to the association of EMILIN-3 with ECM (Fig. 8*E*).

EMILIN-3 Acts in Vitro as Pro-TGF-β Antagonist—A previous study demonstrated that EMILIN-1 is an extracellular antagonist of TGF-β signaling (10). To investigate whether EMILIN-3 has a similar function, we used the CAGA12-lux reporter plasmid as a direct readout for TGF-β activity. Initially, we transfected HEK293T cells with the reporter plasmid either in the presence or absence of the EMILIN-3L construct and treated the transfected cells with mature TGF-β1. In these

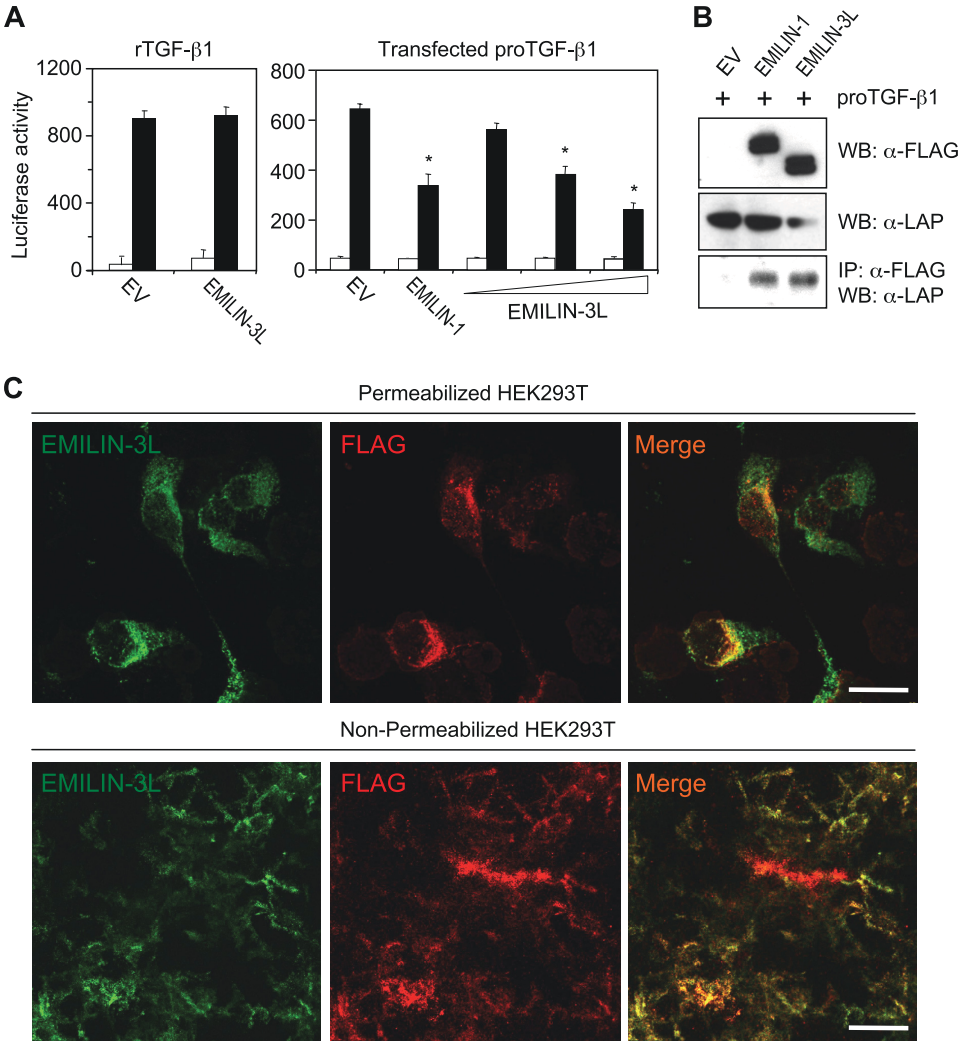

FIGURE 9. **EMILIN-3 is pro-TGF-β antagonist in HEK293T cells.** *A*, HEK293T cells were transfected in 24-well plates with the CAGA12-lux reporter plasmid (100 ng) alone or in combination with EMILIN-1 and EMILIN-3L expression constructs (300 ng). Transfected cells were left untreated (*open bars*) or treated overnight with 2.5 ng of recombinant mature human TGF-β1 (*rTGF-β1*) (*left panel*). Alternatively, cells were cotransfected with EMILIN-1 (300 ng), EMILIN-3 (100, 200, or 300 ng), and pro-TGF-β1 (C223S/C225S) variant plasmid (40 ng) (*right panel*). Luciferase activity was measured 24 h after the transfection. Data are shown as mean ± S.D. of at least three independent replicates. *, $p < 0.05$ compared with control (empty vector). *B*, HEK293T cells were transfected in 6-well plates with a pro-TGF-β1 expression plasmid (200 ng) together with FLAG-EMILIN-1, FLAG-EMILIN-3, or the empty vector (all 1 μg). The cell lysates were then subjected to immunoprecipitation with anti-FLAG antibody and Western blot with anti-latency-associated peptide (*LAP*) antibody. *C*, HEK293T were transfected with EMILIN-3L and a FLAG-tagged pro-TGF-β1 plasmid. Cells were then processed for immunofluorescence with or without permeabilization using rabbit EMILIN-3 antiserum and anti-FLAG antibody. For intracellular labeling, cells were permeabilized in methanol for 3 min at 20 °C. *Scale bar*, 25 (*upper panels*) or 50 μm (*lower panels*). *EV*, empty vector; *IP*, immunoprecipitation; *WB*, Western blot.

experimental conditions, EMILIN-3 had no effect on the luciferase reporter signal (Fig. 9*A*). We then tested the system by transfecting cells with a plasmid coding for the bioactive pro-TGF-β1 (C223S/C225S), a variant recombinant form that ensures that TGF-β1 is secreted as a biologically active molecule (30). We also used the EMILIN-1 construct as a positive control. When we cotransfected this pro-TGF-β1 plasmid with EMILIN-1 or with increasing concentrations of EMILIN-3, we detected a strong and dose-dependent inhibition of the reporter signal (Fig. 9*A*). Immunoprecipitation experiments on cell lysates of transfected HEK293T cells showed that pro-TGF-β1 was coprecipitated by both EMILIN-1 and EMILIN-3 (Fig. 9*B*). Further evidence for the interaction of EMILIN-3 with TGF-β1 was obtained upon subcellular colocalization by immunofluorescence. HEK293T cells were plated onto glass coverslips and cotransfected with the EMILIN-3L construct and a plasmid coding for pro-TGF-β1 with a FLAG tag inserted in the sequence of the mature cytokine (10). Under permeabilizing conditions, EMILIN-3 and pro-TGF-β1 colocalized in the endoplasmic reticulum compartment. Under non-permeabilizing conditions, the two proteins also partially colocalized in the ECM (Fig. 9*C*).

Next, we assessed whether EMILIN-3 could inhibit pro-TGF-β2 and -β3 activity as well. Toward this aim, we transfected cells with plasmids coding for the constitutively active forms of murine pro-TGF-β2 (C226S/C228S/C229S) and pro-TGF-β3 (C228S/C230S). Using a setup similar to that described above, we found that both EMILIN-3 and EMILIN-1 are very effective in inhibiting the signal induced by these two ligands (Fig. 10, *A* and *B*). It has been shown that EMILIN-1 can inhibit the pro-TGF-β-mediated signaling in the extracellular space through its EMI domain (10). To evaluate whether EMILIN-3

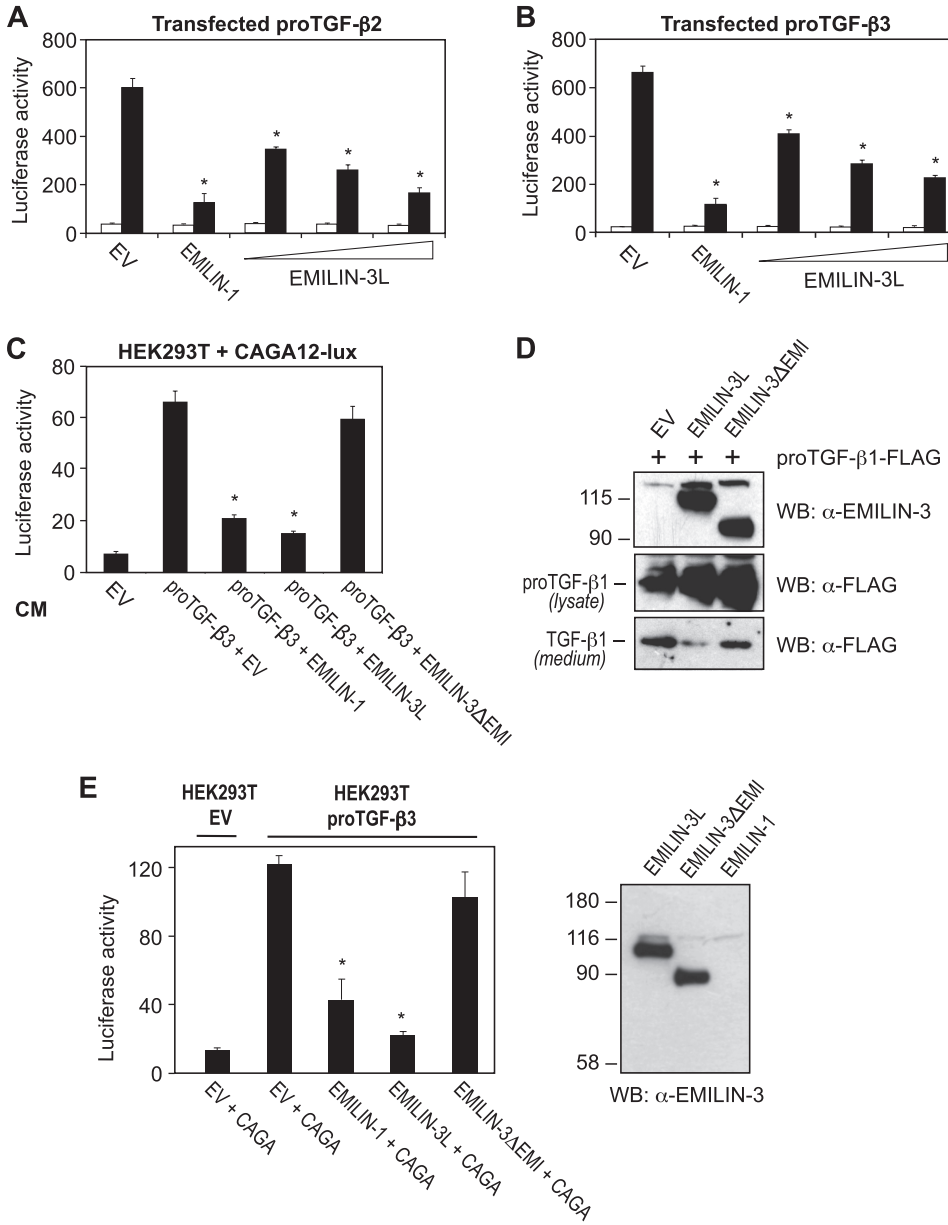

FIGURE 10. **EMILIN-3 is active in inhibiting pro-TGF-β2 and pro-TGF-β3 non-cell autonomously.** *A* and *B*, HEK293T cells were cotransfected with the CAGA12-lux reporter plasmid with plasmids coding for mutated bioactive forms of pro-TGF-β2 (*A*) or pro-TGF-β3 (*B*) and with EMILIN-1 (300 ng) or EMILIN-3L (100, 200, or 300 ng) expression constructs. Luciferase activity was measured 24 h after the transfection. Data are shown as mean ± S.D. of at least three independent replicates. *, $p < 0.05$ compared with control (empty vector). *C*, plasmid coding for the mutated bioactive pro-TGF-β3 (200 ng) was cotransfected with EMILIN-1, EMILIN-3L, or EMILIN-3ΔEMI expression constructs (all 2 μg) in a 6-well plate. After 48 h, the conditioned media were collected and used to treat HEK293T cells transfected with the CAGA12-lux reporter plasmid. Luciferase activity was measured 24 h after the treatment. Data are shown as mean ± S.D. of at least three independent replicates. *, $p < 0.05$ compared with control (empty vector). *D*, HEK293T cells were transfected with the indicated plasmids. Cell lysates and conditioned media were separated by 4–12% gradient SDS-PAGE under reducing conditions and immunoblotted with rabbit EMILIN-3 antiserum and anti-FLAG antibody. *E*, HEK293T cells were cotransfected with the CAGA12-lux reporter plasmid and the indicated expression constructs. Transfected cells were then mixed with cells transfected with the empty vector (*HEK293T EV*) or with the mutated bioactive pro-TGF-β3 plasmid (*HEK293T pro-TGF-β3*). After 24 h, mixed cells were lysed, and luciferase activity was measured (*left panel*). EMILIN-3 protein levels in the transfected cell lysates were assessed by Western blot with rabbit EMILIN-3 antiserum. Data are shown as mean ± S.D. of at least three independent replicates. *, $p < 0.05$ compared with control (empty vector). *CAGA*, CAGA12-lux; *CM*, conditioned medium; *EV*, empty vector; *WB*, Western blot.

can also act non-cell autonomously via its EMI domain, we carried out different experiments. First, we transfected pro-TGF-β3 alone or together with EMILIN constructs and then used the corresponding conditioned media to treat CAGA12-lux-transfected HEK293T cells. Strikingly, EMILIN-3L was able to inhibit almost completely the induction of the reporter plasmid, whereas EMILIN-3ΔEMI was much less efficient (Fig. 10*C*). In agreement with this, cotransfection of the FLAG-tagged pro-TGF-β1 with EMILIN-3 constructs showed that EMILIN-3L could prevent the release of the mature cytokine in the conditioned medium, whereas EMILIN-3ΔEMI could not (Fig. 10*D*). Finally, we performed cell mixing experiments to verify whether EMILIN-3 can act as a negative regulator of TGF-β signaling in the extracellular environment. Toward this aim, we prepared "responding" HEK293T cells transfected with the CAGA12-lux reporter plasmid in the presence or absence of

EMILIN constructs and "stimulatory" cells producing pro-TGF-β3. As expected, only when responding cells were mixed with stimulatory cells, the luciferase signal was induced. Remarkably, transfection of either EMILIN-1 or EMILIN-3 in responding cells led to a strong inhibition of the TGF-β response, whereas EMILIN-3ΔEMI was ineffective (Fig. 10*E*). Altogether, these latter sets of *in vitro* data indicate that EMILIN-3 works as an extracellular regulator of TGF-β signaling through its EMI domain.

DISCUSSION

Our data represent the first thorough characterization of the expression and biochemical properties of EMILIN-3. Two major features make EMILIN-3 a peculiar member within the EMILIN/Multimerin family of secreted proteins. First, as revealed by data presented in this work for the mouse and by our previous studies in zebrafish (15), EMILIN-3 is not expressed in any region of the cardiovascular system where all the other EMILINs/Multimerins are abundant. Second, despite a high degree of conservation of global protein organization with the other EMILINs/Multimerins (*i.e.* the presence of one EMI domain at the N-terminal end and a large region with high propensity for forming coiled coil structures), EMILIN-3 is lacking the C-terminal gC1q domain that is present in all other members of the family (2).

Our *in situ* hybridization data show that during mouse development EMILIN-3 has a dynamic pattern of expression, which only partially overlaps with the expression patterns of other EMILIN/Multimerin genes (2, 14). Expression of EMILIN-3 is first detected at E8.5–E.9.5 in the tail bud region, a structure known to contain a multipotent stem cell population (31). This peculiar expression during early embryogenesis was never observed for other EMILIN/Multimerin genes and is in full agreement with what we observed in early zebrafish embryos for EMILIN-3 ortholog genes (15). Subsequently and similar to EMILIN-1 (14), expression of EMILIN-3 becomes prominent in mesenchymal condensations where differentiation is taking place, such as branchial arches and limb buds. As the development proceeds, EMILIN-3 becomes restricted to more specific sites or disappears. For instance, EMILIN-3 is strongly expressed in the skeletal primordia, but when differentiation proceeds, the expression becomes confined to the perichondrium. The conspicuous expression of EMILIN-3 in the developing mouse skeleton is in agreement with previous reports (7) and with our studies in zebrafish where expression of EMILIN-3 orthologs was found in the cartilage primordia of the developing craniofacial skeleton (15). In another example, at early developmental stages, EMILIN-3 is strongly expressed in the esophageal buds, whereas at later stages, the expression is confined to myenteric cells. A further example is the central nervous system where EMILIN-3 is transiently expressed from E10.5 to E12.5 at the level of the ventricular zone midbrain where neuronal differentiation takes place (32). Interestingly, besides EMILIN-3, thus far only EMILIN-2 among the EMILIN/Multimerin proteins was found to be expressed in the nervous system (2). As reported for other EMILIN genes, during postnatal life, the levels of EMILIN-3 transcripts in different organs decrease with age, and in the adult, only a few tissues still express the mRNA. Immunofluorescence of adult tissues confirmed that EMILIN-3 has a restricted protein distribution, which does not overlap with that of any other EMILIN/Multimerin protein. As stated above, the most remarkable difference between EMILIN-3 and the other members of the EMILIN/Multimerin family is its absence from the cardiovascular system. Indeed, no mRNA expression was found throughout the development in blood vessels, heart, or kidneys, and no EMILIN-3 could be detected in these tissues even in adult mice.

As noted above, EMILIN-3 is the only protein of the EMILIN/Multimerin family that lacks the C-terminal gC1q domain. Because it has been proposed that this domain is involved in multimeric assembly of EMILIN-1 (11), the finding that EMILIN-3 exists *in vivo* as high molecular weight aggregates was unexpected. Further biochemical studies on transfected cells confirmed that EMILIN-3 is able to form disulfide-linked oligomers as reported previously for EMILIN-1, Multimerin-1, and Multimerin-2 (5, 11, 13, 33) and for the more distantly related Emu1 and Emu2 proteins (7). Our data indicate that the smallest EMILIN-3 oligomers have a mobility consistent with homotrimer formation and that EMILIN-3 predominantly exists as higher order oligomers. Transfection experiments with deletion constructs indicate that neither the gC1q domain nor the EMI domain is strictly necessary for the assembly of EMILIN-3, thus suggesting that the coiled coil regions with their flanking cysteine residues must be important for this process. Indeed, when the EMILIN-3CTR fragment corresponding to these regions was generated, it could be shown that this polypeptide formed disulfide bond-stabilized trimers with a substantial α-helical content. On the other hand, we found that EMILIN-1 is able to form higher order oligomers in the absence of the gC1q domain, but the process is impaired when the EMI domain is lacking, suggesting that the cysteine residues of the EMI domain contribute to the higher order self-assembly of EMILIN-1 and EMILIN-3. Although we did not investigate in detail which specific cysteines are required for EMILIN-3 self-assembly, the finding that EMILIN-3ΔEMI is able to associate with the full-length protein implies that the coiled coil regions are mediating this process.

Our biochemical studies on EMILIN-3 revealed another interesting property of this protein. We found that EMILIN-3 binds heparin with high affinity and that this binding is mediated by the EMI domain. It is not known whether other EMILINs/Multimerins or other EMI domains may have the same property, but the observation that Emu1 and Emu2 proteins are not detected in the conditioned medium of transfected cells (7) suggests that these two proteins may bind heparin as well. The cysteine-rich EMI domain was already found to work as a self-interacting module (9) and as a protein-protein interaction domain as in the case of the binding to pro-TGFβ-1 (10). Our results reveal a new function of the EMI domain that may be responsible for the interaction of EMILIN-3 with the heparan sulfate moiety of specific ECM and cell surface proteoglycans, such as perlecan, syndecans, and glypican, and/or secreted growth factors. Protein binding to heparin usually requires clusters of basic amino acid residues interspersed with one or two non-basic amino acid residues in the protein sequence (34). Although no typical heparin-binding consensus

sequences are found in EMILIN-3, our data clearly indicate that the EMI domain alone is sufficient to bind heparin. Notably, among the extracellular proteins known to bind heparin/heparan sulfate chains, there are several elastic fiber-associated proteins, such as tropoelastin (35), fibrillin-1 (36), latent TGF-β binding proteins (37, 38), and various members of the TGF-β superfamily (39).

TGF-β ligands are usually secreted as large latent complexes covalently bound to latent TGF-β-binding proteins and incorporated into the ECM in association with microfibrils (40). Although it is not known yet whether EMILIN-3, like EMILIN-1 (1), associates with elastic fiber components, our data indicate that EMILIN-3 could participate in the extracellular regulation of the bioavailability of TGF-β ligands. In our assays, EMILIN-3 appears ineffective in inhibiting the activity of the mature cytokine, whereas it is very effective in inhibiting the activity of pro-TGF-β1 as well as pro-TGF-β2 and -β3. Interestingly, our *in vitro* luciferase assay experiments showed that EMILIN-1 has a similar inhibitory activity for all three pro-TGF-β molecules, a function that was previously investigated only for pro-TGF-β1 (10). Although this activity largely relies upon the EMI domain, the precise molecular mechanisms involved in the *in vivo* regulation of TGF-β activity by EMILIN proteins remain to be understood. In this respect, it will be interesting to investigate whether EMILIN proteins contribute to the regulation of the bioavailability of mature TGF-β ligands by also interacting with the large ECM functional complex composed by latent TGF-β-binding proteins, fibrillin-1 and -2, and other microfibril-associated proteins, such as MAGP-1 and fibulin-4 (40, 41). Moreover, the finding that EMILIN-3 binds heparin suggests that this protein may participate in the modulation in the extracellular space of the availability and distribution of other secreted factors known to be regulated by heparan sulfate proteoglycans, such as Wnt, Hedgehog, or bone morphogenetic protein ligands (42).

Altogether, the data reported in this work represent the first detailed characterization of the distribution and biochemical properties of EMILIN-3. Given the unique primary structure and the peculiar expression of this member of the EMILIN/Multimerin family, future work aimed at elucidating its *in vivo* functional properties will allow a full understanding of the biological role of EMILIN-3 in embryonic development and tissue homeostasis.

Acknowledgments—We thank Birgit Kobbe for the generation of EMILIN-3 antibodies and Tullio Pozzan for the D1ER plasmid.

REFERENCES

1. Bressan, G. M., Daga-Gordini, D., Colombatti, A., Castellani, I., Marigo V, and Volpin, D. (1993) Emilin, a component of elastic fibers preferentially located at the elastin-microfibrils interface. *J. Cell Biol.* **121,** 201–212
2. Braghetta, P., Ferrari, A., De Gemmis, P., Zanetti, M., Volpin, D., Bonaldo, P., and Bressan, G. M. (2004) Overlapping, complementary and site-specific expression pattern of genes of the EMILIN/Multimerin family. *Matrix Biol.* **22,** 549–556
3. Hayward, C. P., Hassell, J. A., Denomme, G. A., Rachubinski, R. A., Brown, C., and Kelton, J. G. (1995) The cDNA sequence of human endothelial cell multimerin. A unique protein with RGDS, coiled-coil, and epidermal growth factor-like domains and a carboxyl terminus similar to the globular domain of complement C1q and collagens type VIII and X. *J. Biol. Chem.* **270,** 18246–18251
4. Doliana, R., Canton, A., Bucciotti, F., Mongiat, M., Bonaldo, P., and Colombatti, A. (2000) Structure, chromosomal localization, and promoter analysis of the human elastin microfibril interface located protein (EMILIN) gene. *J. Biol. Chem.* **275,** 785–792
5. Christian, S., Ahorn, H., Novatchkova, M., Garin-Chesa, P., Park, J. E., Weber, G., Eisenhaber, F., Rettig, W. J., and Lenter, M. C. (2001) Molecular cloning and characterization of EndoGlyx-1, an EMILIN-like multisubunit glycoprotein of vascular endothelium. *J. Biol. Chem.* **276,** 48588–48595
6. Doliana, R., Bot, S., Mungiguerra, G., Canton, A., Cilli, S. P., and Colombatti, A. (2001) Isolation and characterization of EMILIN-2, a new component of the growing EMILINs family and a member of the EMI domain-containing superfamily. *J. Biol. Chem.* **276,** 12003–12011
7. Leimeister, C., Steidl, C., Schumacher, N., Erhard, S., and Gessler, M. (2002) Developmental expression and biochemical characterization of Emu family members. *Dev. Biol.* **249,** 204–218
8. Doi, M., Nagano, A., and Nakamura, Y. (2004) Molecular cloning and characterization of a novel gene, EMILIN-5, and its possible involvement in skeletal development. *Biochem. Biophys. Res. Commun.* **313,** 888–893
9. Doliana, R., Bot, S., Bonaldo, P., and Colombatti, A. (2000) EMI, a novel cysteine-rich domain of EMILINs and other extracellular proteins, interacts with the gC1q domains and participates in multimerization. *FEBS Lett.* **484,** 164–168
10. Zacchigna, L., Vecchione, C., Notte, A., Cordenonsi, M., Dupont, S., Maretto, S., Cifelli, G., Ferrari, A., Maffei, A., Fabbro, C., Braghetta, P., Marino, G., Selvetella, G., Aretini, A., Colonnese, C., Bettarini, U., Russo, G., Soligo, S., Adorno, M., Bonaldo, P., Volpin, D., Piccolo, S., Lembo, G., and Bressan, G. M. (2006) Emilin1 links TGF-β maturation to blood pressure homeostasis. *Cell* **124,** 929–942
11. Mongiat, M., Mungiguerra, G., Bot, S., Mucignat, M. T., Giacomello, E., Doliana, R., and Colombatti, A. (2000) Self-assembly and supramolecular organization of EMILIN. *J. Biol. Chem.* **275,** 25471–25480
12. Spessotto, P., Cervi, M., Mucignat, M. T., Mungiguerra, G., Sartoretto, I., Doliana, R., and Colombatti, A. (2003) β1 integrin-dependent cell adhesion to EMILIN-1 is mediated by the gC1q domain. *J. Biol. Chem.* **278,** 6160–6167
13. Hayward, C. P., Warkentin, T. E., Horsewood, P., and Kelton, J. G. (1991) Multimerin: a series of large disulfide-linked multimeric proteins within platelets. *Blood* **77,** 2556–2560
14. Braghetta, P., Ferrari, A., de Gemmis, P., Zanetti, M., Volpin, D., Bonaldo, P., and Bressan, G. M. (2002) Expression of the EMILIN-1 gene during mouse development. *Matrix Biol.* **21,** 603–609
15. Milanetto, M., Tiso, N., Braghetta, P., Volpin, D., Argenton, F., and Bonaldo, P. (2008) Emilin genes are duplicated and dynamically expressed during zebrafish embryonic development. *Dev. Dyn.* **237,** 222–232
16. Zanetti, M., Braghetta, P., Sabatelli, P., Mura, I., Doliana, R., Colombatti, A., Volpin, D., Bonaldo, P., and Bressan, G. M. (2004) EMILIN-1 deficiency induces elastogenesis and vascular cell defects. *Mol. Cell. Biol.* **24,** 638–650
17. Danussi, C., Spessotto, P., Petrucco, A., Wassermann, B., Sabatelli, P., Montesi, M., Doliana, R., Bressan, G. M., and Colombatti, A. (2008) Emilin1 deficiency causes structural and functional defects of lymphatic vasculature. *Mol. Cell. Biol.* **28,** 4026–4039
18. Danussi, C., Petrucco, A., Wassermann, B., Pivetta, E., Modica, T. M., Belluz Ldel, B., Colombatti, A., and Spessotto, P. (2011) EMILIN1-α4/α9 integrin interaction inhibits dermal fibroblast and keratinocyte proliferation. *J. Cell Biol.* **195,** 131–145
19. Mongiat, M., Ligresti, G., Marastoni, S., Lorenzon, E., Doliana, R., and Colombatti, A. (2007) Regulation of the extrinsic apoptotic pathway by the extracellular matrix glycoprotein EMILIN2. *Mol. Cell. Biol.* **27,** 7176–7187
20. Kohfeldt, E., Maurer, P., Vannahme, C., and Timpl, R. (1997) Properties of the extracellular calcium binding module of the proteoglycan testican.

FEBS Lett. **414,** 557–561
21. Larraín, J., Bachiller, D., Lu, B., Agius, E., Piccolo, S., and De Robertis, E. M. (2000) BMP-binding modules in chordin: a model for signalling regulation in the extracellular space. *Development* **127,** 821–830
22. Sambrook, J., and Russell, D. W. (2001) *Molecular Cloning: A Laboratory Manual*, 3rd Ed., pp. 16.1–16.28, Cold Spring Harbor Laboratory Press, Cold Spring Harbor, NY
23. Whitmore, L., and Wallace, B. A. (2004) DICHROWEB, an online server for protein secondary structure analyses from circular dichroism spectroscopic data. *Nucleic Acids Res.* **32,** W668–W673
24. Andrade, M. A., Chacón, P., Merelo, J. J., and Morán, F. (1993) Evaluation of secondary structure of proteins from UV circular dichroism spectra using an unsupervised learning neural network. *Protein Eng.* **6,** 383–390
25. Lupas, A., Van Dyke, M., and Stock, J. (1991) Predicting coiled coils from protein sequences. *Science* **252,** 1162–1164
26. Hodges, R. S., Zhou, N. E., Kay, C. M., and Semchuk, P. D. (1990) Synthetic model proteins: contribution of hydrophobic residues and disulfide bonds to protein stability. *Pept. Res.* **3,** 123–137
27. Greenfield, N. J., and Hitchcock-DeGregori, S. E. (1993) Conformational intermediates in the folding of a coiled-coil model peptide of the N-terminus of tropomyosin and α α-tropomyosin. *Protein Sci.* **2,** 1263–1273
28. Bernfield, M., Götte, M., Park, P. W., Reizes, O., Fitzgerald, M. L., Lincecum, J., and Zako, M. (1999) Functions of cell surface heparan sulfate proteoglycans. *Annu. Rev. Biochem.* **68,** 729–777
29. Lin, X. (2004) Functions of heparan sulfate proteoglycans in cell signaling during development. *Development* **131,** 6009–60021
30. Brunner, A. M., Marquardt, H., Malacko, A. R., Lioubin, M. N., and Purchio, A. F. (1989) Site-directed mutagenesis of cysteine residues in the pro region of the transforming growth factor β1 precursor. Expression and characterization of mutant proteins. *J. Biol. Chem.* **264,** 13660–13664
31. Wilson, V., Olivera-Martinez, I., and Storey, K. G. (2009) Stem cells, signals and vertebrate body axis extension. *Development* **136,** 1591–1604
32. Corbin, J. G., Gaiano, N., Juliano, S. L., Poluch, S., Stancik, E., and Haydar, T. F. (2008) Regulation of neural progenitor cell development in the nervous system. *J. Neurochem.* **106,** 2272–2287
33. Colombatti, A., Bonaldo, P., Volpin, D., and Bressan, G. M. (1988) The elastin associated glycoprotein gp115. Synthesis and secretion by chick cells in culture. *J. Biol. Chem.* **263,** 17534–17540
34. Fromm, J. R., Hileman, R. E., Caldwell, E. E., Weiler, J. M., and Linhardt, R. J. (1997) Pattern and spacing of basic amino acids in heparin binding sites. *Arch. Biochem. Biophys.* **343,** 92–100
35. Broekelmann, T. J., Kozel, B. A., Ishibashi, H., Werneck, C. C., Keeley, F. W., Zhang, L., and Mecham, R. P. (2005) Tropoelastin interacts with cell-surface glycosaminoglycans via its COOH-terminal domain. *J. Biol. Chem.* **280,** 40939–40947
36. Cain, S. A., Baldock, C., Gallagher, J., Morgan, A., Bax, D. V., Weiss, A. S., Shuttleworth, C. A., and Kielty, C. M. (2005) Fibrillin-1 interactions with heparin. Implications for microfibril and elastic fiber assembly. *J. Biol. Chem.* **280,** 30526–30537
37. Kantola, A. K., Keski-Oja, J., and Koli, K. (2008) Fibronectin and heparin binding domains of latent TGF-β binding protein (LTBP)-4 mediate matrix targeting and cell adhesion. *Exp. Cell Res.* **314,** 2488–2500
38. Parsi, M. K., Adams, J. R., Whitelock, J., and Gibson, M. A. (2010) LTBP-2 has multiple heparin/heparan sulfate binding sites. *Matrix Biol.* **29,** 393–401
39. Rider, C. C. (2006) Heparin/heparan sulphate binding in the TGF-β cytokine superfamily. *Biochem. Soc. Trans.* **34,** 458–460
40. Annes, J. P., Munger, J. S., and Rifkin, D. B. (2003) Making sense of latent TGFβ activation. *J. Cell Sci.* **116,** 217–224
41. Massam-Wu, T., Chiu, M., Choudhury, R., Chaudhry, S. S., Baldwin, A. K., McGovern, A., Baldock, C., Shuttleworth, C. A., and Kielty, C. M. (2010) Assembly of fibrillin microfibrils governs extracellular deposition of latent TGFβ. *J. Cell Sci.* **123,** 3006–3018
42. Häcker, U., Nybakken, K., and Perrimon, N. (2005) Heparan sulphate proteoglycans: the sweet side of development. *Nat. Rev. Mol. Cell Biol.* **6,** 530–541

EMILIN-3, a peculiar member of the EMILIN/Multimerin protein family, has a distinct expression pattern, forms oligomeric assemblies and serves as a pro TGF-β antagonist*

Alvise Schiavinato[1], Ann-Kathrin A. Becker[2], Miriam Zanetti[1], Diana Corallo[1], Martina Milanetto[1], Dario Bizzotto[1], Giorgio Bressan[1], Marija Guljelmovic[1], Mats Paulsson[2,3,4], Raimund Wagener[2,3], Paola Braghetta[1], and Paolo Bonaldo[1]

[1]From the Department of Biomedical Sciences, University of Padova, I-35121 Padova, Italy; [2]Center for Biochemistry, Medical Faculty, [3]Center for Molecular Medicine Cologne (CMMC), [4]Cologne Excellence Cluster on Cellular Stress Responses in Aging-Associated Diseases (CECAD), University of Cologne, D-50931 Cologne, Germany.

Address correspondence to: Paolo Bonaldo, Department of Biomedical Sciences, University of Padova, Viale G. Colombo 3, I-35121 Padova, Italy; Tel.: (+39) 049 827 6084; Fax: (+39) 049 827 6079; E-mail: bonaldo@bio.unipd.it

This file contains:

- **Supplementary figure legends**
- **Supplementary Figures S1 to S8**

SUPPLEMENTAL FIGURE LEGENDS

Supplemental Figure S1. Thermal denaturation (A) and renaturation (B) of the EMILIN-3CTR fragment. Temperature-induced changes between 20°C and 90°C were monitored by circular dichroism following the mean molar residue ellipticity at 220 nm (θ_{220nm}) under different solvent conditions. (**A**) 4 M GuHCl or 2 M GuHCl and 10 mM DTT completely unfolded the proteins already at room temperature, whereas heating of the native protein, reduced protein or protein treated with 2M GuHCl gave thermal denaturation curves that did not show distinct transitions. (**B**) The denaturation of untreated, reduced or 2 M GuHCl treated EMILIN-3CTR fragment was partially reversible upon gradual cooling to 20°C.

Supplemental Figure S2. RT-PCR analysis of EMILIN-3 transcripts in murine and human cell lines. Total RNA was collected from the indicated murine (**A**) and human (**B**) cultured cells and analyzed by semi-quantitative RT-PCR with specific oligonucleotide primers able to detect either murine or human EMILIN-3 transcripts. Amplifications of eIF1A and GAPDH were used as RNA loading controls. The following cell lines or primary cells were used: A204, human rhabdomyosarcoma; BC3H1, murine smooth muscle cells; C2C12, murine undifferentiated C2C12 myoblast cell line; Diff. C2C12, murine C2C12 cells following differentiation and fusion into myotubes; ES, undifferentiated murine embryonic stem cells; HeLa, human carcinoma; hEND, murine endothelial cells; HepG2, human hepatocellular carcinoma; Jurkat, human lymphoblasts; HUVEC, human umbilical vein endothelial cells; MC615, murine chondrocytes; MDA, human breast cancer cells; MEF, murine embryonic fibroblasts; MG63, human osteosarcoma cells; mSM3, murine aorta smooth muscle cells; NIH/3T3, murine fibroblasts; RD, human rhabdomyosarcoma cells; SaOS-2, human osteosarcoma cells; TDM, murine trophoblast stem cells.

Supplemental Figure S3. *In situ* hybridization for EMILIN-3 during mouse embryonic development. (**A**) Whole-mount preparations of E8.5 and E9.5 mouse embryos, showing EMILIN-3 expression in the tail bud (black arrowheads) and in the primitive gut (white arrowhead). (**B**) Parasagittal sections of E11.5 and E14.5 embryos hybridized with either antisense probe (AS) or sense probe (S). The sense probe displays no staining, confirming the specificity of the signals obtained with the antisense probe. (**C**) Higher magnification of parasagittal sections of E14.5 embryos, confirming lack of EMILIN-3 expression in the heart and in blood vessels during

development. AS, antisense EMILIN-3 probe; cv, caudal vein; he, heart; S, sense EMILIN-3 probe. Scale bar, 50 μm.

Supplemental Figure S4. Documentation of the purity of the recombinant EMILIN-CTR antigen used for antibody generation. SDS-PAGE of reduced (+SH) and non-reduced (-SH) EMILIN-3CTR on a 4-12% Coomassie stained polyacrylamide gel. Under reducing conditions, a single band of the expected molecular mass was seen. The two lanes show the fractions with the highest concentrations from the Streptactin column, which were used for immunization.

Supplemental Figure S5. Documentation of the specificity of the EMILIN-3 antibodies by western blot of tissue extracts. Different tissue extracts were submitted to SDS-PAGE on a 4-12 % polyacrylamide gel and after blotting the affinity purified antibodies against EMILIN-3 were applied. Sample load was documented by Ponceau staining. Calvaria was sequentially extracted as described by Ko et al. (*Mol. Cell Biol.* 24, 1691-1699, 2004). Samples in lanes 4-9 were extracted with 100 mM NaCl, 1% sucrose, 1% Triton X-100, 1 mM PMSF, 20 mM Tris, pH 7.5, while samples in lanes 10-12 were extracted with 150 mM NaCl, 2 mM EDTA, 1% Nonidet P-40, 50 mM Tris, pH 7.5. With the exception of lung, no signals were obtained. The smear in the lanes with lung extracts is an artifact, most likely due to the binding of antibodies to Fc receptors of macrophages that are abundant in lung tissue. The supernatant of HEK293-EBNA cells expressing EMILIN-3CTR (supernatant) revealed a strong signal only for the recombinant protein, indicating that no major reactivity against serum proteins was present. The lack of signals in other tissue extracts points to the low abundance of EMILIN-3 and the lack of antibody cross-reactivity with unrelated proteins.

Supplemental Figure S6. Documentation of the specificity of the EMILIN-3 antibody by double immunofluorescence staining with EMILIN-1 antiserum. Immunofluorescence microscopy of E13.5 mouse embryo forelimb labeled with EMILIN-1 rabbit antiserum (**A**, **C**, **D**, **F**, red) and the guinea pig EMILIN-3 antibody (**B**, **C**, **E**, **F**, green). The staining pattern for EMILIN-3 showed only a partial overlap (**C**, **F**) with that for EMILIN-1, confirming the specificity of the EMILIN-3 antibody. Scale bar, 100 μM (panels A-C) or 50 μM (panels D-F).

Supplemental Figure S7. Immunofluorescence analysis of EMILIN-3 in adult mouse tissues. Immunofluorescence shows the absence of EMILIN-3 labeling in the cardiovascular system,

including thoracic aorta (**A**) and heart (**B**), and in parenchymatous organs such as kidneys (**C**) and spleen (**D**). Asterisk marks the lumen of aorta in A and a trabecular vein of the spleen in D. The fluorescent layer present in the aorta sections is due to autofluorescence of the elastic fiber layers. Scale bar, 100 μM.

Supplemental Figure S8. EMILIN-3 is associated with the ECM and binds to heparin. (**A**) HEK293T cells were transfected with plasmids coding for FLAG-tagged EMILIN-1, EMILIN-2, and EMILIN-3 constructs. Cell lysates and conditioned media were separated by 4-12% gradient SDS-PAGE under reducing conditions and analyzed by western blotting with an anti-FLAG antibody. Efficient synthesis of the transfected EMILIN-1, -2 and -3 proteins was confirmed by detection of bands migrating at the respective expected sizes in cell extract samples. While EMILIN-1 and EMILIN-2 were efficiently secreted, no EMILIN-3 was detected in the conditioned medium. Transfection with the empty vector was used as a control. Migration of protein size markers is indicated in kDa on the left. (**B**) HEK293T cells were co-transfected with the EMILIN-3 construct and a plasmid coding for fluorescent D1ER, an endoplasmic reticulum-targeted Ca^{2+}-indicator protein, and analyzed by immunofluorescence with antibodies against either EMILIN-3 or D1ER. The majority of EMILIN-3 protein co-localized with D1ER in the endoplasmic reticulum, while some EMILIN-3 was detected outside the cells and deposited onto the coverslip (arrowheads), indicating that EMILIN-3 is secreted by transfected cells. Scale bar, 10 μm. (**C**) HEK293T cells were transfected with a plasmid coding for an EMILIN-3 construct lacking the EMI domain (EMILIN-3ΔEMI). Cell lysates and conditioned media were separated by 4-12% gradient SDS-PAGE under reducing conditions and analyzed by western blotting with rabbit EMILIN-3 antiserum. In contrast to full-length EMILIN-3, EMILIN-3ΔEMI was found in the conditioned medium. Migration of protein size markers is indicated in kDa on the left. C, cell layer; ECM, insoluble ECM extract; EV, empty vector; M, conditioned medium.

Supplemental Figure S1

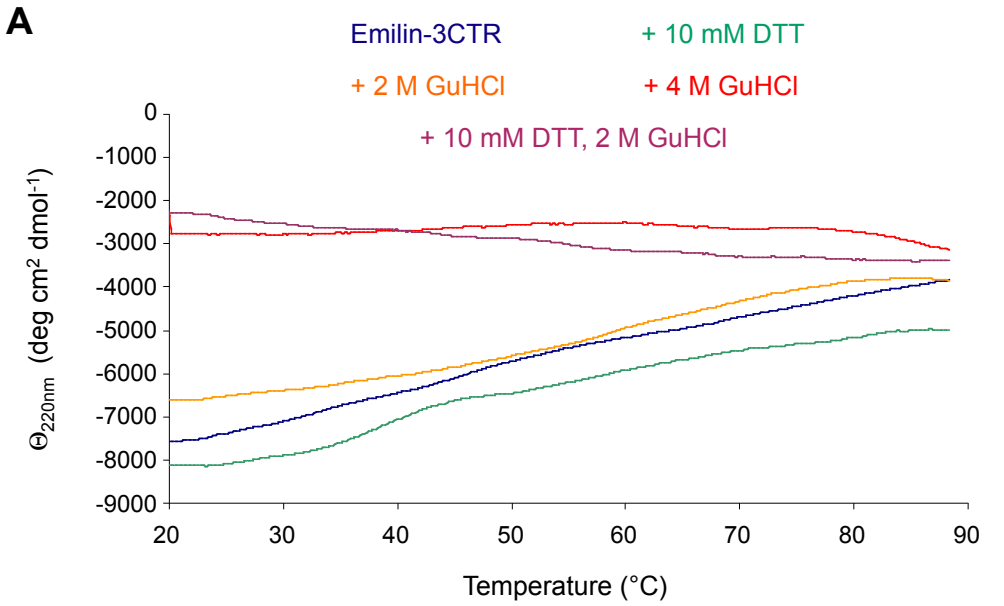

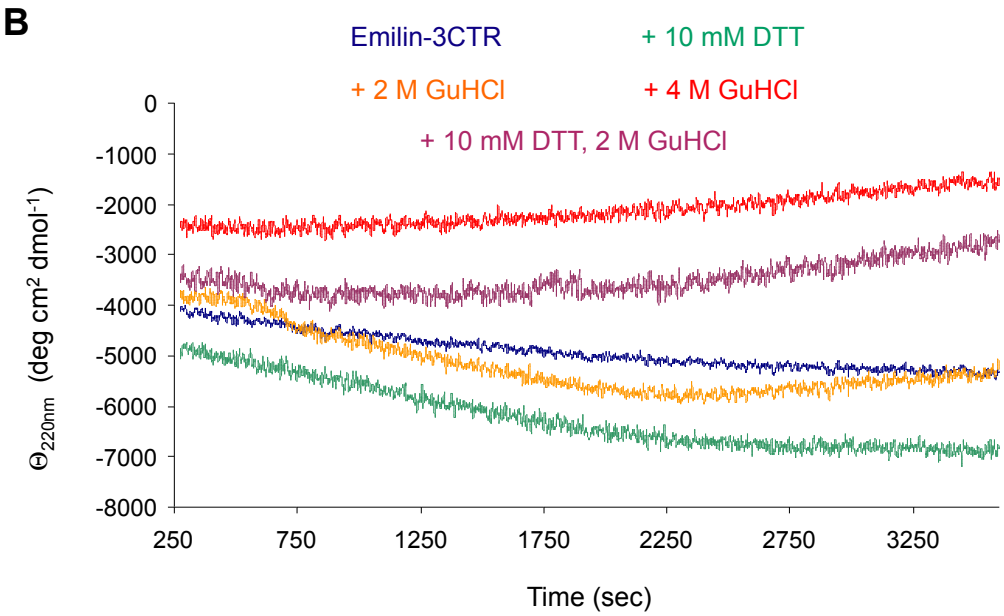

Supplemental Figure S2

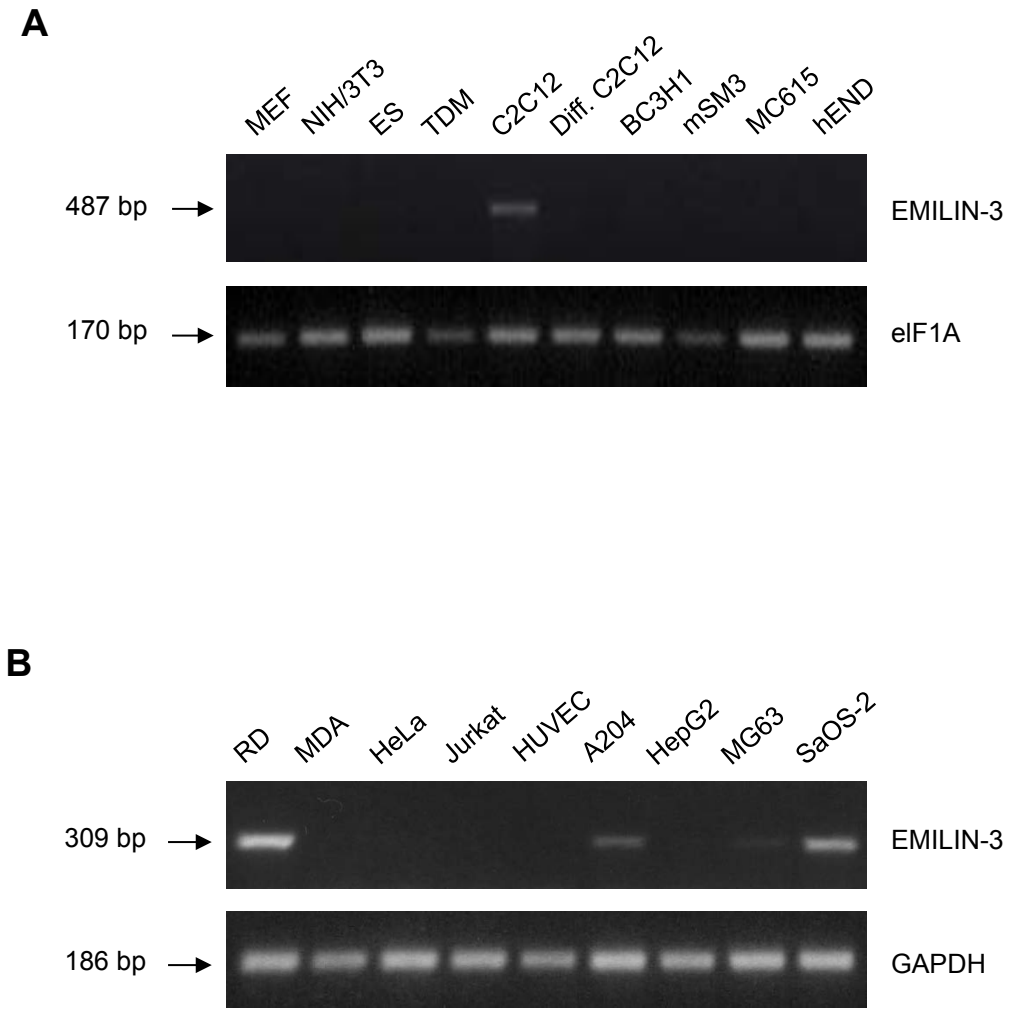

Supplemental Figure S3

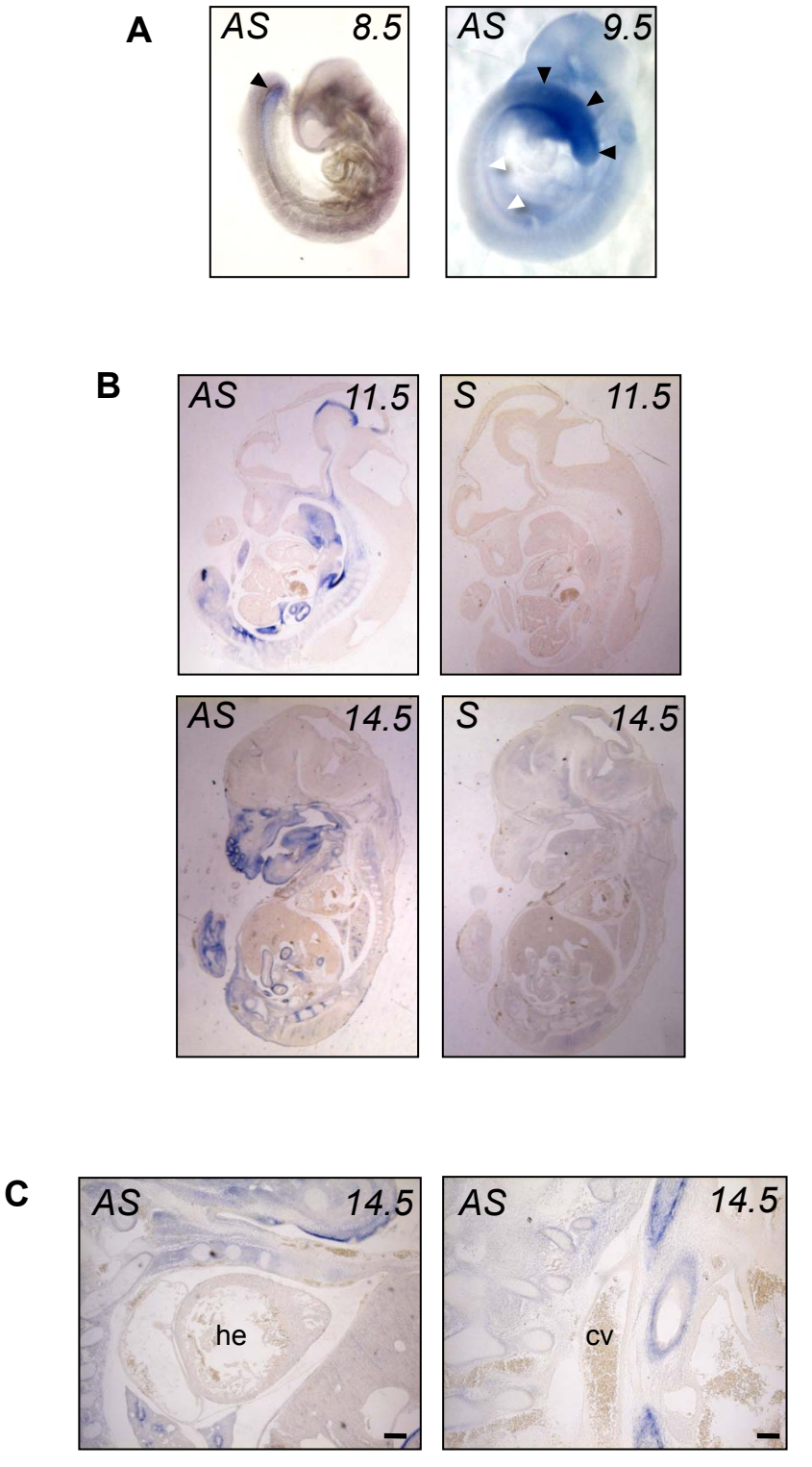

Supplemental Figure S4

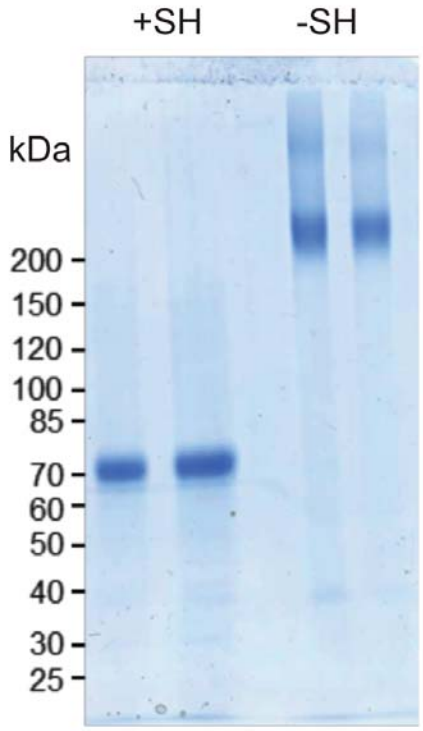

Supplemental Figure S5

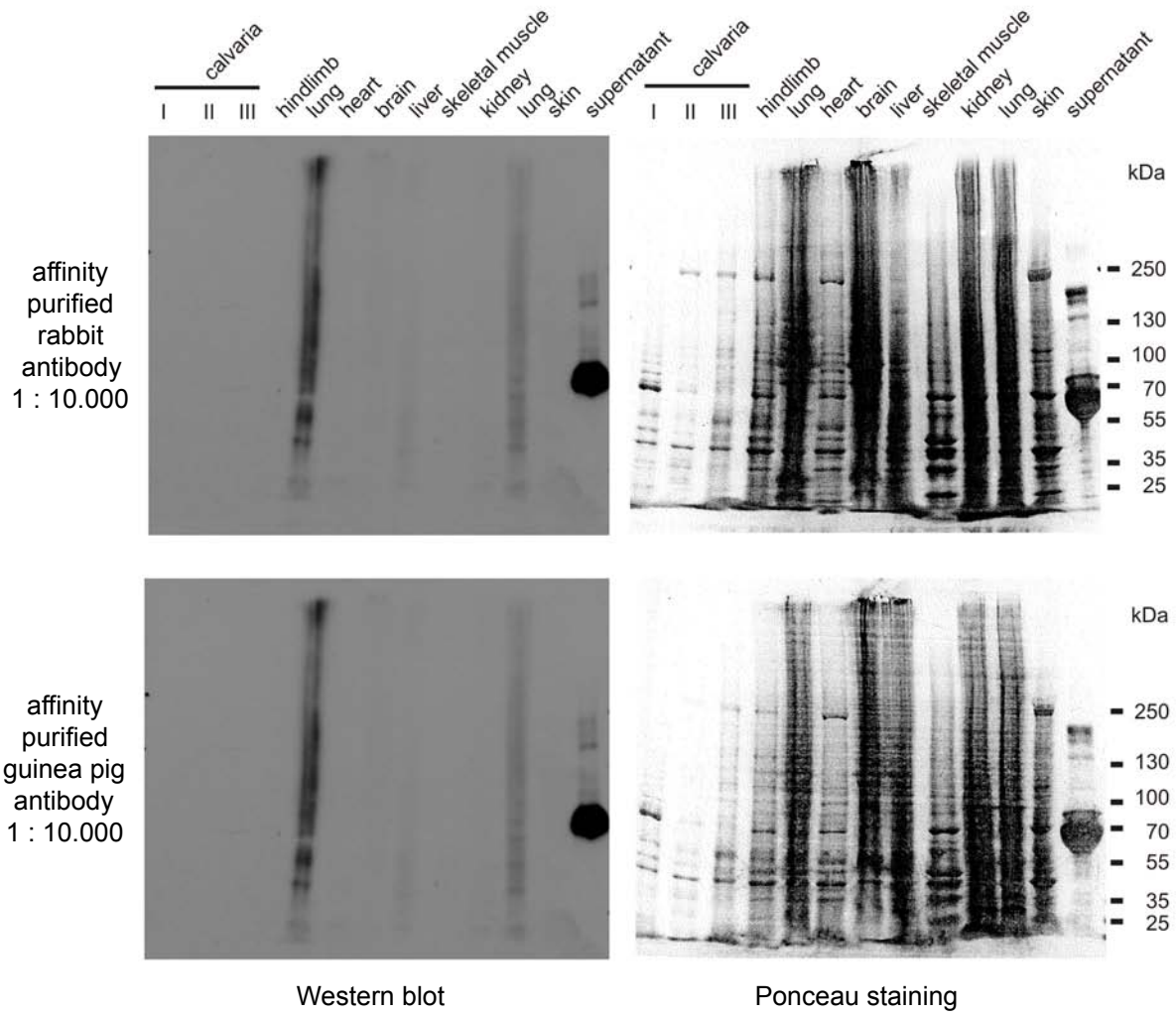

Supplemental Figure S6

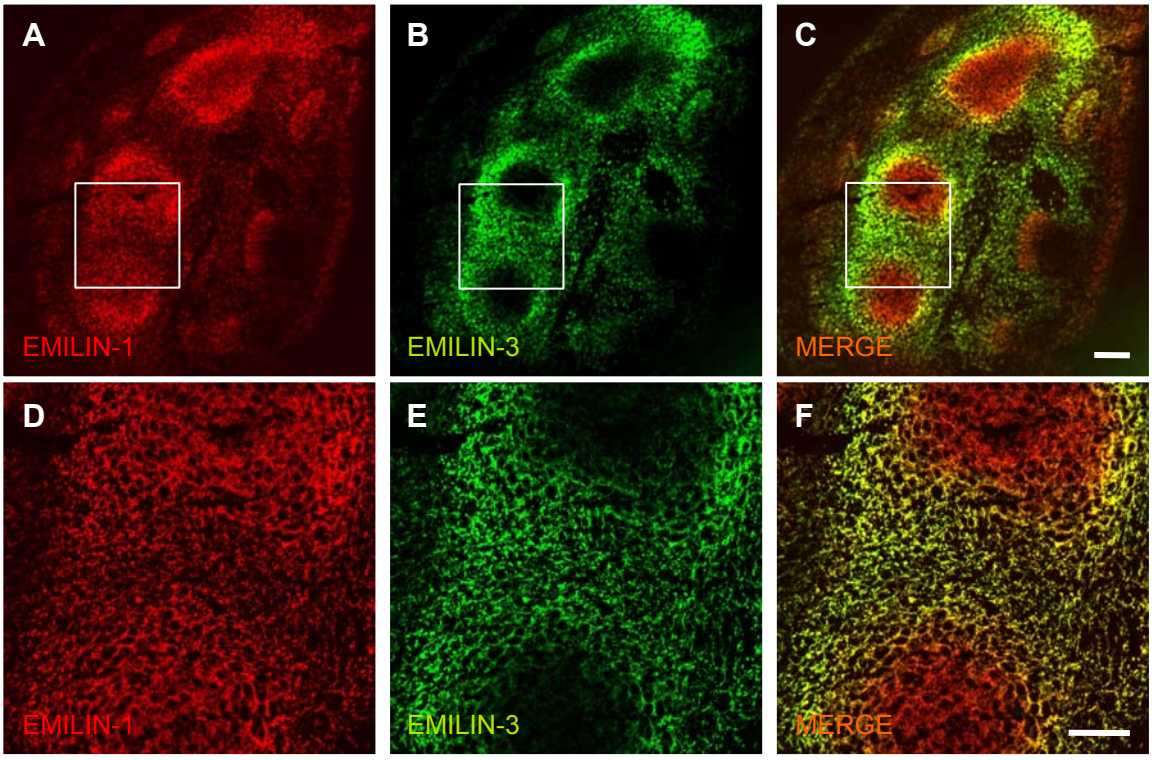

Supplemental Figure S7

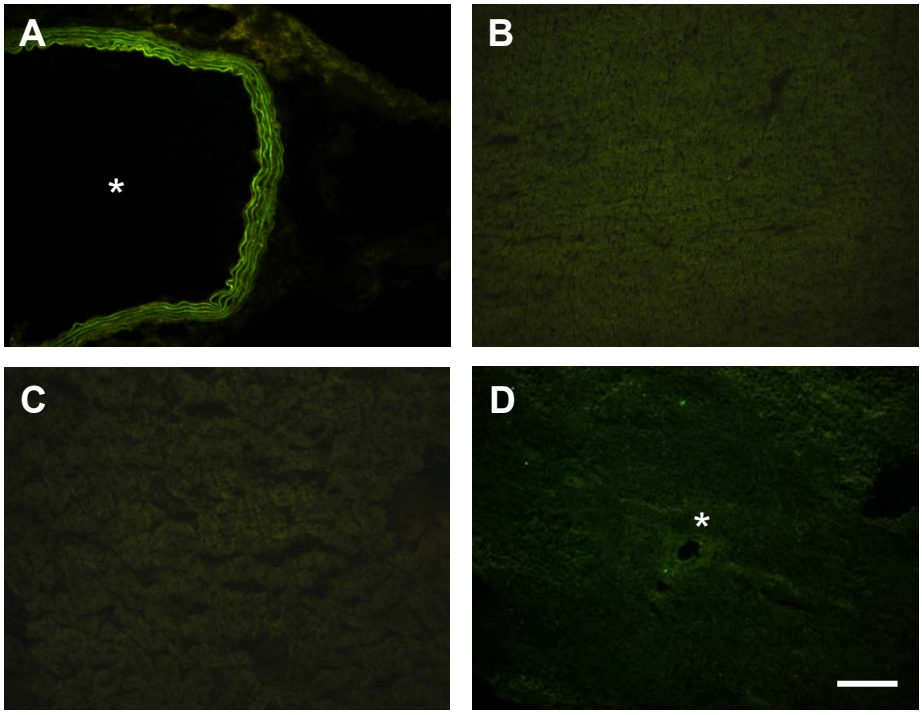

Supplemental Figure S8

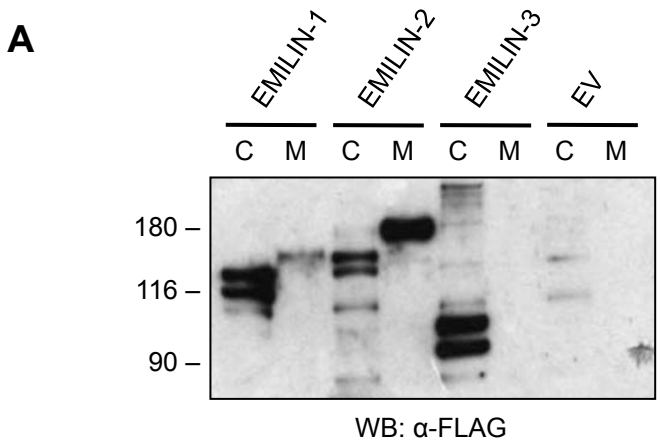

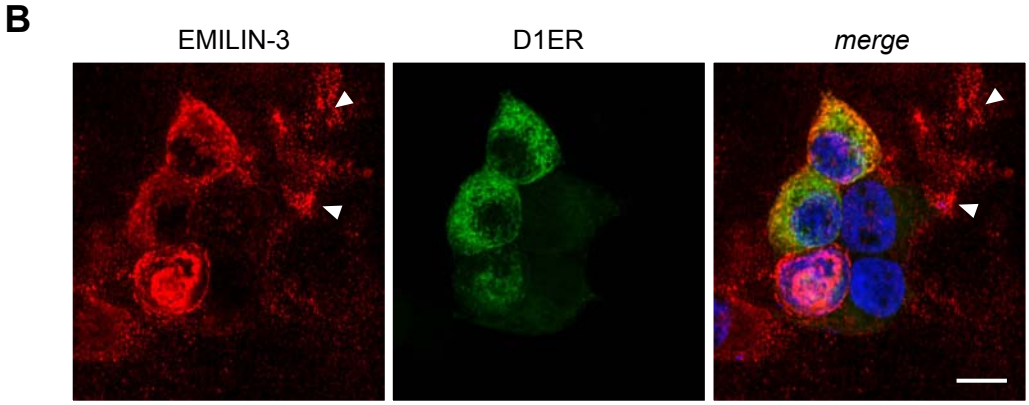

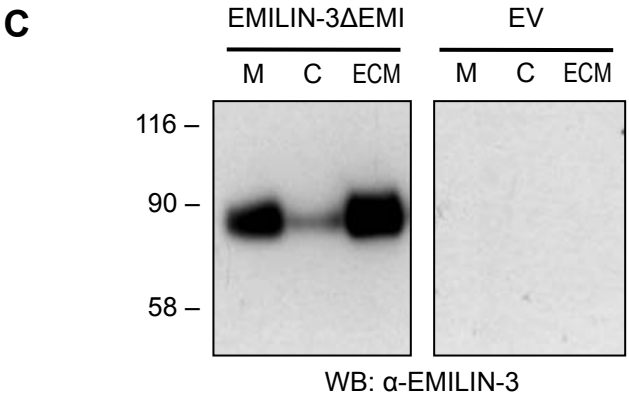

1. Introduction

1.1 The Emilin/ Multimerin family in *Danio rerio.*

The zebrafish genome contains eight Emilin/Multimerin genes that are the orthologs of mammalian genes coding for Emilin1, Emilin2, Multimerin2, and Emilin3. Each gene is present in two duplicated paralogs, in agreement with the proposed genomic duplication occurred in teleosts during evolution (Christoffels et al., 2004). The only mammalian Emilin/Multimerin gene for which no ortholog was found in *Danio rerio* is the one coding for Multimerin1 (Milanetto et al., 2008).

Bioinformatic analysis revealed that the predicted structural features of zebrafish Emilin/Multimerin proteins are highly conserved with those of their mammalian orthologs, showing similar domain structures and sequences. They all possess an EMI domain at the N-terminal portion and a long central region with high capability to form coiled coil structures. In particular, the EMI domain of all the zebrafish Emilin/Multimerin proteins contains the seven conserved cysteines, except for Emilin3a which lacks the second cysteine. Moreover, zebrafish Emilin/Multimerin proteins end with a globular C1q domain, which is missing in Emilin3a and Emilin3b, in agreement with their mammalian counterparts.

emilin1a and *emilin1b* are expressed with a pattern that is similar but not completely overlapping. At early developmental stages (5- to 25-somite) the expression of both zebrafish *emilin1* genes is restricted to distinct territories of the central nervous system, whereas at late somitogenesis (24 hpf) expression in the nervous system decreases and the two transcripts are mostly expressed by blood vessels, heart, and mesenchymal cells of various organs.

At all stages of zebrafish development, the expression of both zebrafish *emilin2* genes is mainly found in the heart and in the developing blood vessels of head and trunk. In particular, *emilin2a* is first detected in the lateral plate mesoderm,

in clusters of macrophages within the yolk and subsequently in the circulatory system. At 48 hpf, *emilin2a* transcript become restricted to the atrium of the developing heart. Besides its expression in the cardiovascular system, at 15 somites *emilin2b* is also detectable in few areas of the central nervous system. This particular expression of *emilin2b* in the central nervous system is no longer detectable after 24 hpf, when the labeling becomes restricted only in vascular structures such as the heart, the dorsal aorta, the cephalic blood vessels, the primordial hindbrain channel, the intersegmental blood vessels, and the caudal vein.

At 24 hpf, *mmrn2a* is expressed in the heart, in the caudal vein, in the posterior retina, in the most anterior part of the floor plate, and in the fin buds. At this stage, *mmrn2a* transcript is also detected in a region of the anterior gut where the intestinal bulb will form. At 48 hpf, *mmrn2a* is expressed in the circulatory system of the head, in the heart, in the anterior floor plate, and in the prospective intestinal bulb. Starting from 15 somites, *mmrn2b* is expressed in the dorsal region of the tail, and later in the heart, in the inner side of the otic vesicle, in the most posterior somites and in the ependymal cells lining the ventricles of midbrain and hindbrain.

The two zebrafish *emilin3* genes display the most peculiar expression pattern during zebrafish development, in agreement with the distinct protein structure. First of all, the labeling of *emilin3a* and *emilin3b* transcripts is very similar and mostly overlapping at all developmental stages. Moreover, this expression pattern never includes cardiovascular structures, differently from the other Emilin/Multimerin genes. Starting from 5-15 somites, both transcripts are found in the tail bud, in the notochord, and in the chordoneural hinge, a structure containing multipotent stem cell population. In embryos at 20 somites, the expression pattern in the notochord becomes more intense, with a characteristic postero-anterior gradient. At 24 hpf this expression decreases and becomes restricted to the more distal region, where the floorplate, the chordoneural hinge and the hypocord are also stained. At 48 hpf, expression in these regions disappears while becomes evident in the cartilage elements of branchial arches and craniofacial developing skeleton (Milanetto et al., 2008).

The pattern of expression of the zebrafish *emilin3* genes is in full agreement with that of their murine ortholog. In fact, during mouse embryogenesis Emilin3 mRNA is first detected in the tail bud and in the primitive gut, and at later stages it becomes abundant in the developing gonads and in the osteogenic mesenchyme. Moreover, murine Emilin3 is never expressed in the cardiovascular system (Schiavinato et al, 2012).

1.2 The notochord: structure and functions

The notochord is an embryonic midline structure common to all members of the *phylum* Chordata, providing both mechanical and signaling cues to the developing embryo. In vertebrates, the notochord arises from the dorsal organizer, also known as the embryonic shield in zebrafish, and is critical for proper vertebrate development (Shih and Fraser, 1996; Saúde et al., 2000).
In zebrafish, the notochord is one of the earliest distinguishable features in the embryo. It forms as chordamesoderm cells converge at the midline, creating a rod of stacked cells that then differentiate into two distinct cell populations in a Notch-dependent manner (Yamamoto et al., 2010) - the outer sheath layer, and an inner vacuolated cell layer. The outer cells secrete a thick extracellular peri-notochordal basement membrane, which is composed of several ECM proteins, whereas inner cells form large fluid-filled intracellular vacuoles. The pressure exerted by notochord vacuoles on the peri-notochordal basement membrane gives this structure its proper stiffness and mechanical strength (Adams et al., 2000). Moreover, it has been recently shown that notochord vacuoles are specialized post-Golgi structures whose biogenesis and maintenance require late endosomal trafficking (Ellis et al., 2013).
Despite its essential structural role, the notochord is also a source of developmental signals that patterns surrounding tissues. Among the signals secreted by the notochord are the Hedgehog (Hh) proteins. The Hedgehog signaling pathway is a central regulator of embryonic development, controlling the pattern and proliferation of a wide variety of organs, including neural tube

(Yamada et al., 1991), somites (Pourquié et al., 1993; Griffin and Kimelman, 2003), blood vessels (Fouquet et al., 1997), and pancreas (Roy et al., 2001). Sonic Hedgehog, in particular, induces a range of ventral spinal cord fates in a graded fashion, simultaneously suppressing the expression of characteristically dorsal genes (Placzek et al., 1993; Yamada et al., 1991). Notochord signals are also involved in establishing left-right asymmetry, and notochord ablation in *Xenopus* gastrulae results in randomisation of asymmetry (Danos and Yost, 1995; Lohr et al., 1997). In teleosts, notochord-derived Hh signals control the formation of the horizontal myoseptum, as well as specifying slow-twitch muscle fates (Barresi et al., 2000; Devoto et al., 1996). Moreover, notochord-derived signals are important for specifying the formation of the dorsal aorta (Cleaver et al., 2000; Fekany et al., 1999; Isogai et al., 2003; Lawson et al., 2002), as well as for normal specification of the cardiac field (Goldstein and Fishman, 1998). Finally, the notochord is important for the normal development of early endoderm and the pancreas (Cleaver and Krieg, 2001; Roy et al., 2001).
Several studies in zebrafish showed that the formation of a notochord sheath is closely linked to the differentiation of notochord cells, and their reciprocal interactions are fundamental for the proper development and function of the notochord itself (Parsons et al., 2002; Pagnon-Minot et al., 2008; Mangos et al., 2010; Yamamoto et al., 2010).

1.3 Structural and functional role of Emilin3 during notochord development.

The main focus of my PhD study was to elucidate the function of Emilin3 during embryonic development, using zebrafish as a model. The two zebrafish Emilin3 paralog genes, *emilin3a* and *emilin3b,* are specifically expressed in the most posterior part of the trunk during early development, in particular in the tail bud, chordoneural hinge and in the notochord. This pattern of expression is limited to the first developmental stages, until 24 hpf. In fact, by 48 hpf, expression in the notochord and floor plate disappears and the two transcripts

are found in the primordial cartilage elements of the developing craniofacial skeleton (Milanetto et al., 2008). Although these studies allowed determine the mRNA expression of the Emilin3 paralogs, the characterization of the protein distribution during zebrafish development was still missing. First of all, I found that Emilin3 is deposited in the notochord sheath, a specialized ECM structure that surrounds the notochord. Interestingly, the protein distribution strongly resembles the pattern observed for mRNA transcripts, since by 24 hpf no notochord labeling can be detected anymore. This indicates that, at difference from a number of other ECM proteins, Emilin3 has a relatively rapid turnover at least during early development.

To investigate the role of Emilin3 in notochord development, I injected one- to two-cell-stage zebrafish embryos with antisense morpholino oligonucleotides targeting the splice sites between the first exon and the first intron of *emilin3a* and *emilin3b* genes. Morpholino-mediated knockdown of both *emilin3* paralogs led to a marked distortion of the notochord due to structural defects of the notochord sheath as revealed by ultrastructural analysis. These data indicate that Emilin3 is a novel component of the notochord sheath, playing an essential role for the correct organization and the proper function of this structure. Next, I investigated whether the ablation of Emilin3 could affect the notochord patterning activity, a process that is mainly mediated by the secretion of Hedgehog (Hh) ligands. Notably, Emilin3 knockdown resulted in the upregulation of Hh signaling pathway. In particular, the generation of a transgenic zebrafish line that express the mCherry reporter gene under the transcriptional regulation of Gli1 allowed me to analyze the Hh signaling activity after Emilin3 depletion. Moreover, I generated a pCS-twhh-mEmilin3 construct carrying murine full- length Emilin3 cDNA under the control of a promoter that confers notochord-specific expression. Interestingly, and in agreement with the results obtained with the *loss-of-function* strategy, notochord-specific Emilin3 overexpression led to the downregulation of Hh target genes, as shown by *in situ* hybridization, real-time PCR and immunofluorescence experiments., *In vitro* experiments showed that Emilin3 modulates the release of Hh ligands, via a direct interaction with the permissive factor Scube2. Finally, *in vivo* knockdown

experiments confirmed that Emilin3 has a physiological role in limiting notochord-derived Hh signals, a function exerted through its interaction with the secreted protein Scube2 (Corallo et al., 2013).

Emilin3 is required for notochord sheath integrity and interacts with Scube2 to regulate notochord-derived Hedgehog signals.

Development ePress. Posted online 23 October 2013
 | Development (2013) 140, 4594-4601 doi:10.1242/dev.094078

RESEARCH ARTICLE

Emilin3 is required for notochord sheath integrity and interacts with Scube2 to regulate notochord-derived Hedgehog signals

Diana Corallo[1,*], Alvise Schiavinato[1,*], Valeria Trapani[1], Enrico Moro[1], Francesco Argenton[2] and Paolo Bonaldo[1,‡]

ABSTRACT

The notochord is a transient and essential structure that provides both mechanical and signaling cues to the developing vertebrate embryo. In teleosts, the notochord is composed of a core of large vacuolated cells and an outer layer of cells that secrete the notochord sheath. In this work, we have identified the extracellular matrix glycoprotein Emilin3 as a novel essential component of the zebrafish notochord sheath. The development of the notochord sheath is impaired in Emilin3 knockdown embryos. The patterning activity of the notochord is also affected by Emilin3, as revealed by the increase of Hedgehog (Hh) signaling in Emilin3-depleted embryos and the decreased Hh signaling in embryos overexpressing Emilin3 in the notochord. *In vitro* and *in vivo* experiments indicate that Emilin3 modulates the availability of Hh ligands by interacting with the permissive factor Scube2 in the notochord sheath. Overall, this study reveals a new role for an EMILIN protein and reinforces the concept that structure and function of the notochord are strictly linked.

KEY WORDS: Extracellular matrix, EMILIN, Notochord, Hedgehog, Scube2, Zebrafish

INTRODUCTION

EMILINs (elastin microfibril interface located proteins) are extracellular matrix (ECM) glycoproteins belonging to the EMILIN/multimerin family. Emilin1, the founding member of this family, was originally identified as an ECM component associated with microfibrils in blood vessels (Bressan et al., 1993). Emilin3 contains the characteristic cysteine-rich EMI domain at the N-terminal end, followed by a region forming three coiled-coil structures at the C-terminal end (Schiavinato et al., 2012). At variance with the other EMILIN/multimerin proteins, Emilin3 is not expressed in the cardiovascular system and it lacks the C-terminal gC1q domain, which is involved in cell attachment and integrin binding (Spessotto et al., 2003; Danussi et al., 2011). Emilin3 expression during mouse development is particularly abundant in the perichondrium of developing bones (Leimeister et al., 2002; Doi et al., 2004; Schiavinato et al., 2012). We have previously found that eight EMILIN/multimerin genes are present in the zebrafish genome in four pairs of duplicated paralogs (Milanetto et al., 2008). Thus, Emilin3 is present in zebrafish with two genetic paralogs that we termed *emilin3a* and *emilin3b*. Similarly to the murine Emilin3 ortholog, the two zebrafish paralogs are not expressed in the cardiovascular system, whereas they are abundantly expressed in the notochord and in the chordoneural hinge until 24 hpf, and in cartilage primordia of the developing craniofacial skeleton at 48 hpf (Milanetto et al., 2008).

In the present study, we focused on the role of the two zebrafish Emilin3 genes during notochord development. During the early phases of embryonic development, until the segmentation stage, the notochord is distinguishable from adjacent tissues by the expression of specific genes, such as *shh*, *ehh* and *col2a1* (Yan et al., 1995; Currie and Ingham, 1996). As the notochord develops, expression of these early-transcribed genes is turned off and notochord cells differentiate in two different cell populations, an outer sheath layer and an inner vacuolated cell layer. The choice between these two fates is determined by Notch signals (Yamamoto et al., 2010). The outer cell layer is responsible for the synthesis of the notochord sheath, a thick peri-notochordal basement membrane that is composed of several ECM proteins, whereas the inner cells contain large intracellular vacuoles. Recently, the nature of these vacuoles was elegantly identified as lysosome-related organelles (Ellis et al., 2013). Both the notochord sheath and the vacuolated cells are essential for conferring the proper stiffness and rigidity to the notochord (Stemple, 2005).

Several studies in zebrafish showed that the formation of a notochord sheath is closely linked to the differentiation of notochord cells, and their reciprocal interactions are fundamental for the proper development and function of the notochord itself (Parsons et al., 2009; Pagnon-Minot et al., 2008; Mangos et al., 2010; Yamamoto et al., 2010). Here, we provide evidence that Emilin3 is a novel component of the notochord sheath that plays an essential role for the correct organization and the proper function of this structure. Moreover, we found that Emilin3 has a physiological role for limiting notochord-derived Hh signals, a function entailing the interaction of Emilin3 with the secreted protein Scube2.

RESULTS

Emilin3 is a novel essential component of the notochord sheath

To study Emilin3 protein distribution in the zebrafish embryo, we carried out whole-mount immunofluorescence with a polyclonal Emilin3 antibody. At 20 hpf, a specific signal was present throughout the notochord with a distinct posteroanterior gradient, whereas no labeling was detected in embryos at eight somites (data not shown; see also supplementary material Fig. S5D). At 24 hpf, Emilin3 became restricted to the notochord sheath, as confirmed by colocalization with collagen II. In agreement with mRNA expression data (Milanetto et al., 2008), labeling of the notochord sheath was lost at 48 hpf, indicating that Emilin3 undergoes a rapid turnover in the ECM and may fulfill a temporally restricted function during notochord development (Fig. 1A).

To investigate the role of Emilin3 during notochord development, we injected one- to two-cell-stage zebrafish embryos

[1]Department of Biomedical Sciences, University of Padova, I-35121 Padova, Italy.
[2]Department of Biology, University of Padova, I-35121 Padova, Italy.
*These authors contributed equally to this work

‡Author for correspondence (bonaldo@bio.unipd.it)

Received 15 January 2013; Accepted 27 August 2013

Development (2013) doi:10.1242/dev.094078

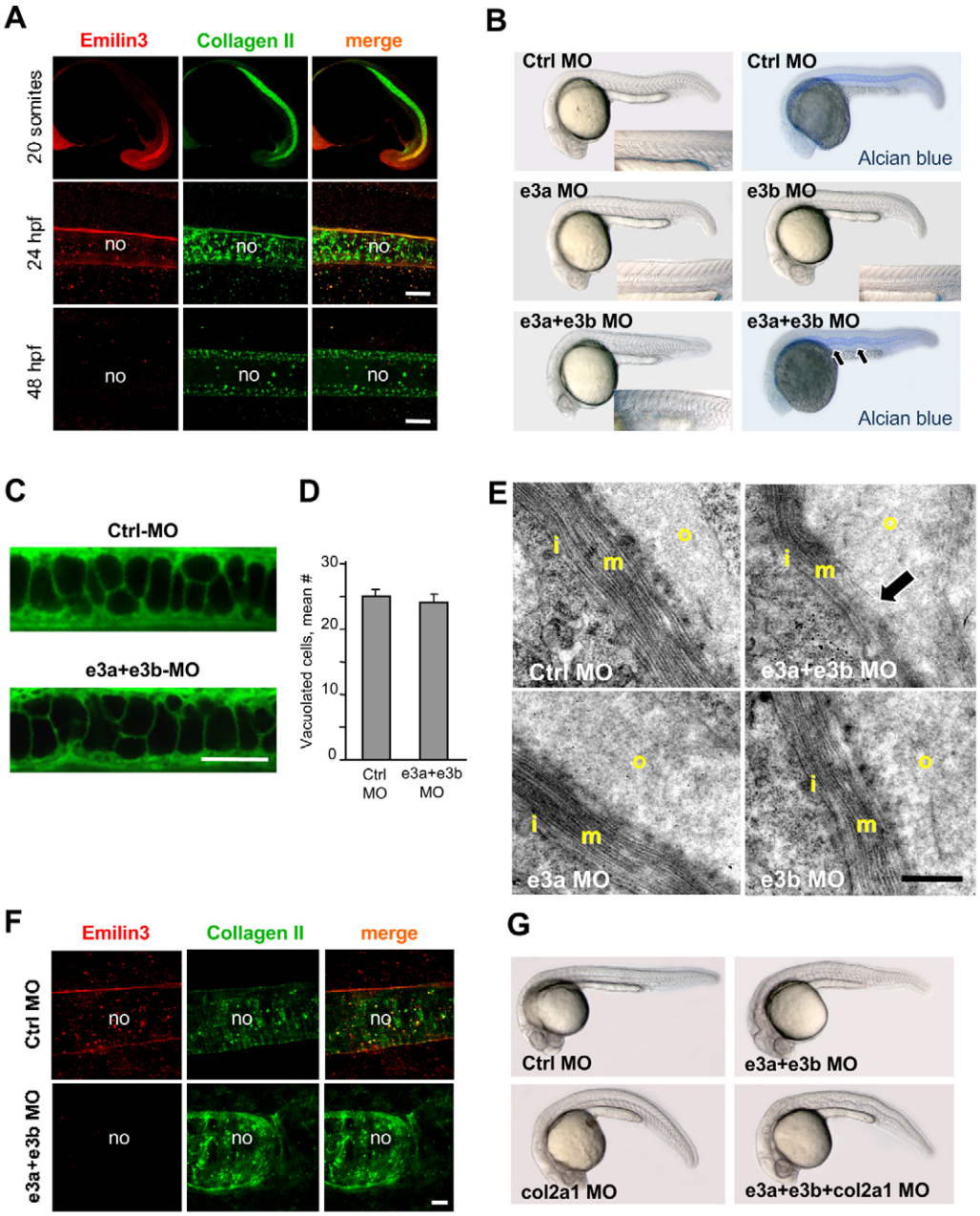

Fig. 1. Emilin3 is an essential component of the notochord sheath. (A) Lateral views of zebrafish embryos after immunofluorescence for Emilin3 and collagen II. Scale bars: 30 μm. (B) Lateral views of 24 hpf injected embryos. (C) BODIPY TR Ceramide staining of notochord cells in 24 hpf injected embryos. Scale bar: 50 μm. (D) Quantification of the mean number of vacuolated cells within the trunk region of control and treated notochord (not significantly different, n=10). Data are mean+s.e.m. (E) Transmission electron micrographs of the notochord sheath in transverse trunk sections of 30 hpf injected embryos. The arrow points at the medial layer of the notochord basement membrane, which is thinner and partially disorganized in Emilin3 double morphants. Scale bar: 500 nm. (F) Immunofluorescence for Emilin3 and collagen II in 24 hpf injected embryos. Scale bar: 10 μm. (G) Lateral views of 24 hpf injected embryos. col2a1 MO, *col2a1* morpholino; Ctrl MO, control morpholino; e3a MO, *emilin3a* morpholino; e3b MO, *emilin3b* morpholino; i, inner layer; m, medial layer; no, notochord; o, outer layer.

with antisense morpholino oligonucleotides targeting the splice sites between the first exon and the first intron of *emilin3a* and *emilin3b* genes. Co-injection of the two morpholinos resulted in the knockdown of the corresponding transcripts and proteins (supplementary material Fig. S1A,B), leading to a distinct distortion of the notochord with partial loss of the V-shaped conformation of somites and shortening of the main axis (Fig. 1B). Embryos injected with translation-blocking morpholinos for *emilin3a* and *emilin3b* showed a similar phenotype, and the same result was found in mixed experiments where a splice-blocking morpholino for one paralog was co-injected with a translation-blocking morpholino for the other paralog (supplementary material Fig. S1C; supplementary material Table S1). Injection of morpholinos targeting only one paralog did not cause a similar phenotype, even when injected at double concentration (Fig. 1B; supplementary material Table S1). As a further control, we performed p53 knockdown and found that co-injection of p53 morpholino was ineffective in rescuing the phenotypic defects induced by Emilin3 depletion (supplementary material Fig. S1D). Two different mechanisms could be inferred for the notochord phenotype of Emilin3 double morphants: (1) an increased pressure generated inside the notochord; or (2) a disruption of the sheath organization.

Quantification of total and vacuolated notochord cells in control and Emilin3 double morphant embryos did not reveal any significant difference, suggesting that Emilin3 deficiency is not grossly perturbing the morphology and commitment of notochord cells (Fig. 1C,D; supplementary material Fig. S2). Notch signaling is known to regulate the fate choice between vacuolated and non-vacuolated notochord cells (Yamamoto et al., 2010). Using the Tg_Hbb:EGFP Notch reporter zebrafish line (Parsons et al., 2009), we did not detect any major difference of Notch signaling activity in notochord cells of control and Emilin3 double morphant embryos (supplementary material Fig. S3).

Development (2013) doi:10.1242/dev.094078

We next investigated the structure of the notochord sheath by electron microscopy. At 30 hpf, in Emilin3 double morphants, but not in Emilin3 single morphants, the medial layer of the notochord basement membrane was not properly organized and many fibers appeared interrupted, whereas the outer and inner layers appeared normal (Fig. 1E). The medial and inner layers of the notochord sheath are thought to consist of collagen and laminin, respectively (Stemple, 2005). *In situ* hybridization and immunofluorescence showed that collagen II was more abundant in Emilin3-depleted embryos at both 24 and 48 hpf (Fig. 1F; supplementary material Fig. S4A,B), whereas laminin labeling was normal (supplementary material Fig. S4C). To exclude the possibility that the phenotype of Emilin3 morphants could be caused by an upregulation of collagen II, we performed concurrent knockdown of *emilin3a*, *emilin3b* and *col2a1*. Knockdown of *col2a1* caused ventral body curvature as expected (Mangos et al., 2010), whereas simultaneous knockdown of the three genes resulted in the overlap of the two phenotypes (Fig. 1G). Altogether, these data reveal that Emilin3 is essential for the normal structure of the notochord sheath.

Emilin3 knockdown results in the upregulation of Hh signaling

Next, we investigated whether knockdown of Emilin3 could affect notochord patterning activity, a process that is largely mediated by the secretion of Hh ligands (Stemple, 2005). Expression of *ptc1* (*ptch2* – Zebrafish Information Network), which is transcriptionally regulated by Hh signaling (Concordet et al., 1996), was strongly increased in the trunk of 24 hpf Emilin3 morphants and this effect was completely blocked by treatment with 100 µM cyclopamine, an inhibitor of Hh signaling, but was unaffected by p53 (Tp53 – Zebrafish Information Network) knockdown (Fig. 2A; supplementary material Fig. S5A,B). To assess whether *ptc1* upregulation was specifically due to Emilin3 ablation, we analyzed *ptc1* expression at eight somites, a stage where Emilin3 proteins are not yet present in the sheath. Consistently, at this stage, *ptc1* was not differently expressed in Emilin3 morphants (supplementary material Fig. S5C,D).

Next, we generated the Tg12x_Gli zebrafish line, which express the mCherry reporter under the transcriptional regulation of Gli1 (see Materials and methods). We co-injected *emilin3a* and *emilin3b* morpholinos in Tg12x_Gli embryos and investigated expression of the transgene at 24 hpf. Notably, Emilin3 morphants displayed a remarkable increase of transgene expression (Fig. 2A), as also confirmed by qPCR experiments (Fig. 2B). We investigated the expression of other genes that respond to notochord-derived Hh signals in different embryonic structures. Expression of *nkx2.2a*, *tbx20* and *myoD1* was consistently increased in Emilin3-depleted embryos (Fig. 2C). Similarly, *olig2*, *vegf* and *eng2a* were upregulated (supplementary material Fig. S6A). Overexpression of Hh ligands by notochord cells can lead to hyperactivation of the Hh pathway (Yamamoto et al., 2010). At 20 somites, *shh* and *ehh*, the only two Hh ligands produced in the notochord, were not

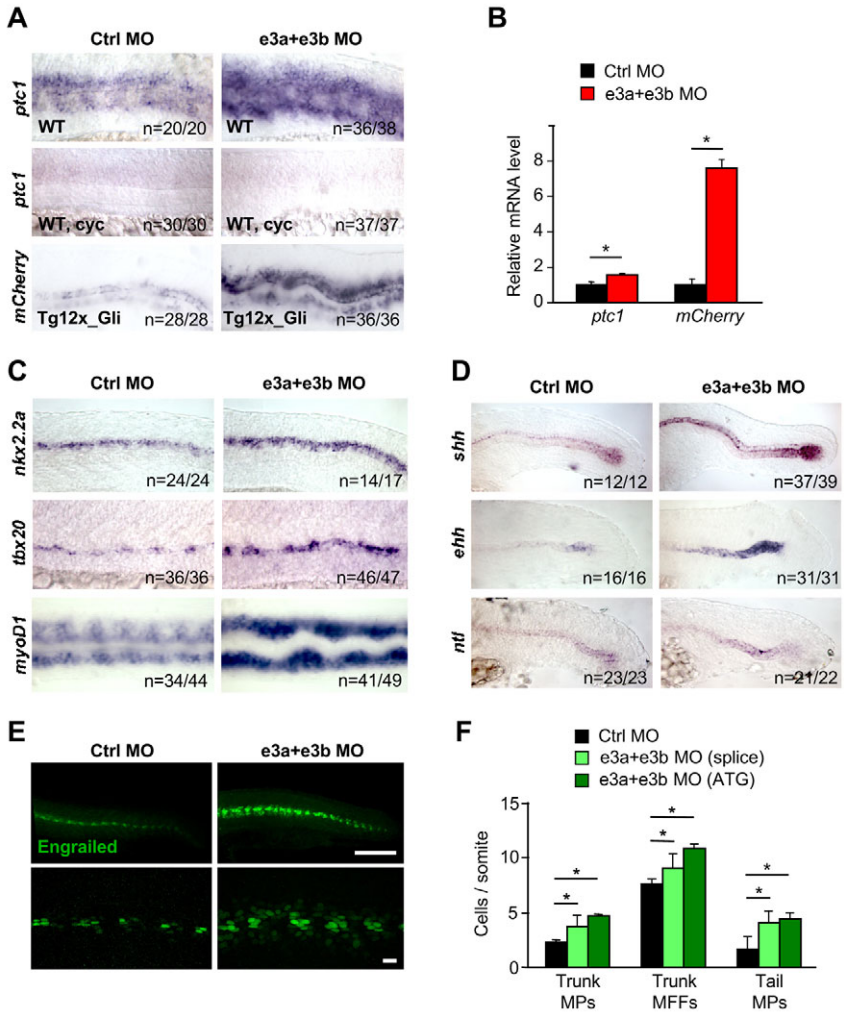

Fig. 2. Hh signaling is upregulated in Emilin3 morphant embryos. (A) Wild-type (WT) and Tg12x_Gli embryos were treated with 100 µM cyclopamine (cyc) and probed at 24 hpf by *in situ* hybridization for *ptc1* or *mCherry*. (B) qRT-PCR for *ptc1* and *mCherry* transcripts in Emilin3 morphant and control embryos (*P<0.05; n=30). (C) *In situ* hybridization for *nkx2.2a*, *tbx20* and *myoD1* in 24 hpf injected embryos. All images are lateral views, except for bottom panels (dorsal views). (D) *In situ* hybridization for *shh*, *ehh* and *ntl* in 24 hpf injected embryos. (E) Immunofluorescence for engrailed in 24 hpf injected embryos. Scale bars: 150 µm. (F) Quantification of engrailed-positive cells at 24 hpf (*P<0.05; n=10). Data are mean+s.e.m. Ctrl MO, control morpholino; e3a MO, *emilin3a* morpholino; e3b MO, *emilin3b* morpholino; e3a+e3b MO, *emilin3a* + *emilin3b* morpholinos; MPs, muscle pioneers; MFFs, medial fast fibers.

Development (2013) doi:10.1242/dev.094078

differently expressed in Emilin3 morphants when compared with control embryos (data not shown), whereas at 24 hpf they were upregulated in the distal part of the notochord (Fig. 2D). Therefore, the sole upregulation of *shh* and *ehh* did not explain the increased Hh activity in Emilin3 morphants. Moreover, expression of *ntl* and of the notochord-unrelated gene *fgf8* was not affected, thus excluding a developmental delay (Fig. 2D; supplementary material Fig. S6B).

We quantified engrailed-positive cells and found that both muscle pioneers (MPs) and medial fast fibers (MFFs) were significantly increased in Emilin3 morphants (Fig. 2E,F). It is known that engrailed expression in the zebrafish myotome is negatively regulated by BMP signaling (Du et al., 1997; Dolez et al., 2011), and high levels of Hh activity can prevent the accumulation of activated Smads in the medial part of the myotome (Maurya et al., 2011). Consistently, we found that expansion of the engrailed-positive domain in Emilin3 morphants was paralleled by a reduction of the pSmad1/5/8 domain in the medial part of the myotome. Treatment with low doses of cyclopamine was sufficient to rescue pSmad distribution in the somites of Emilin3 morphants, indicating that Hh pathway is primarily affected by Emilin3 knockdown (supplementary material Fig. S7A). To exclude the possibility that the observed effect on Hh signaling could be mediated by the pro-TGFβ inhibitory activity of Emilin3 (Schiavinato et al., 2012), we treated morphant embryos with two different selective inhibitors of TGFβ type I receptors, SB431542 and LY364947. Neither of these inhibitors was effective in decreasing *ptc1* expression, and pharmacological inhibition of TGFβ activity also exacerbated notochord distortion in Emilin3 morphants (supplementary material Fig. S7B).

Emilin3 overexpression leads to downregulation of Hh target genes

To investigate whether upregulation of the Hh pathway was directly caused by Emilin3 deficiency or was a broader effect caused by disruption of the notochord sheath, we analyzed *ptc1* expression in *emilin3a* and *emilin3b* single morphants. Interestingly, albeit to a lesser extent than in Emilin3 double morphants, *ptc1* expression was increased in the trunk of single morphants (Fig. 3A). To further assess the role of Emilin3 in notochord-derived Hh signaling, we generated a pCS-twhh-mEmilin3 construct carrying murine full-length *Emilin3* cDNA under the control of a promoter that confers notochord-specific expression (Du et al., 1997). Embryos injected with this construct developed normally but at 24 hpf they displayed mild notochord defects and a shorter axis, when compared with embryos injected with a control pCS-twhh-β-gal construct (Fig. 3B). Notably, embryos injected with pCS-twhh-mEmilin3 showed impaired *myoD1* expression, together with reduced number of engrailed-positive cells. Emilin3 overexpression in the notochord did not influence *ehh* transcription, indicating that expression of Hh ligands by notochord cells was not grossly affected (Fig. 3B,C). Moreover, injection of the pCS-twhh-mEmilin3 construct also rescued the effects of morpholino-mediated ablation of Emilin3 both on notochord development and Hh signaling (supplementary material Fig. S8).

Emilin3 functionally interacts with Scube2

As Emilin3 paralogs are expressed by notochord cells with a pattern closely similar to that of Hh ligands, we speculated that Emilin3 could influence the rate of synthesis and/or release of Hh proteins. Interestingly, when Emilin3 and Shh were transiently co-expressed in HEK293T cells, the amount of Shh released in media was

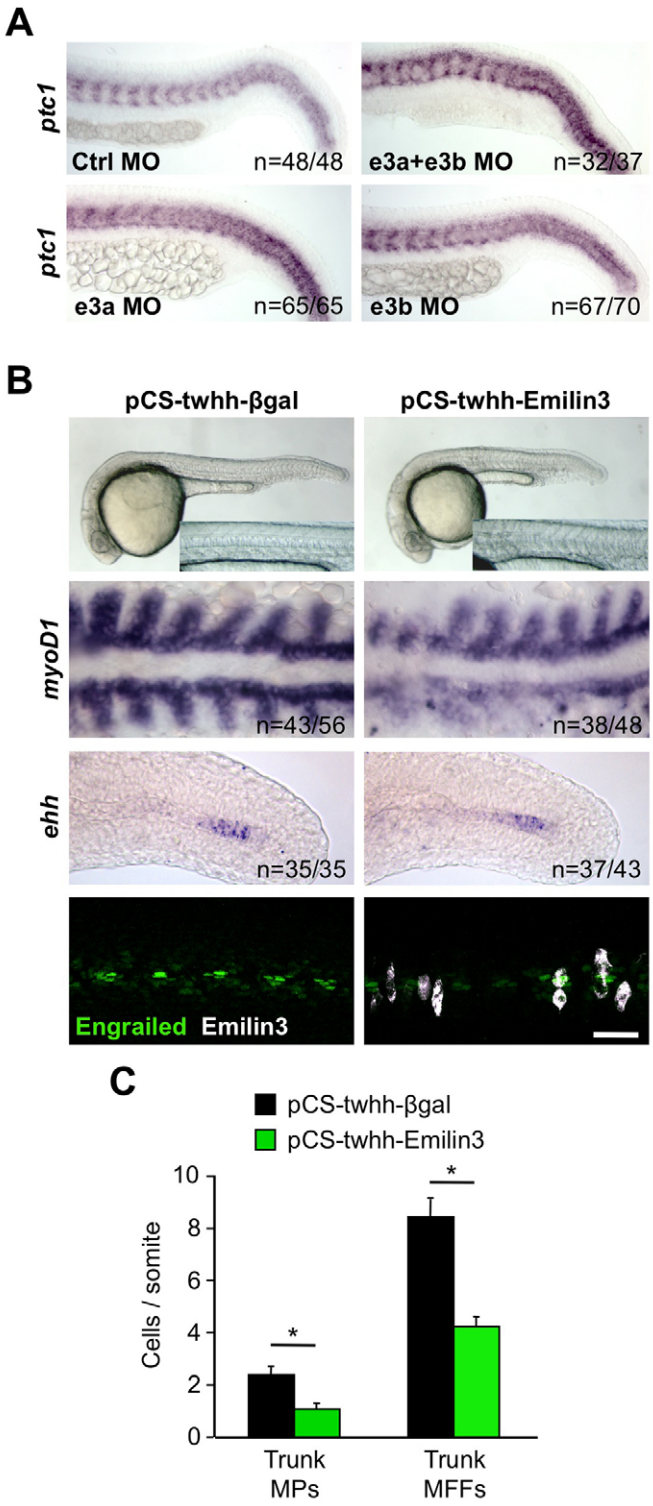

Fig. 3. Overexpression of Emilin3 affects notochord patterning activity. (A) Lateral views of 24 hpf embryos probed for *ptc1*. Embryos were injected with the indicated morpholinos. (B) Wild-type embryos were injected with the indicated constructs at 50 ng/µl and photographed at 24 hpf (upper panels), or probed by *in situ* hybridization for *myoD1* at eight somites and for *ehh* at 24 hpf (middle panels), or by immunofluorescence for engrailed and Emilin3 at 24 hpf (lower panels). Scale bar: 50 µm. (C) Quantification of engrailed-positive cells in 24 hpf embryos injected as in B (*P<0.05; n=15). Data are mean+s.e.m. Ctrl MO, control morpholino; e3a+e3b MO, *emilin3a* + *emilin3b* morpholinos; MPs, muscle pioneers; MFFs, medial fast fibers.

Development (2013) doi:10.1242/dev.094078

reduced (Fig. 4A). This effect was not dependent on the EMI domain and it was lost when Emilin3 was co-expressed with ShhN, a form of Shh lacking cholesterol modification (Fig. 4B,C). Co-immunoprecipitation experiments failed to reveal any interaction between Emilin3 and Shh (Fig. 4D). Therefore, we hypothesized that Emilin3 could interact with a factor secreted by HEK293T and involved in Shh release. To test this hypothesis, we used conditioned media derived from HEK293T transfected with empty vector or with Emilin3 construct to stimulate the release of Shh from stably transfected Shh-293 cells. Interestingly, the conditioned medium derived from mock-transfected cells strongly increased Shh release compared with fresh medium, whereas medium from Emilin3-transfected cells induced a much lower rate of Shh release (supplementary material Fig. S9).

Recent studies demonstrated a role for the secreted protein Scube2 in Shh release (Creanga et al., 2012; Tukachinsky et al., 2012). We therefore investigated whether Emilin3 could interact with Scube2. When HEK293T cells were co-transfected with Emilin3 and FLAG-tagged Scube2, Emilin3 was co-precipitated with Scube2 from media (Fig. 4E). Similarly, FLAG-tagged Scube2 was efficiently immunoprecipitated by HA-tagged Emilin3 (supplementary material Fig. S10A). This interaction was confirmed by *in vitro*-binding experiments and did not require the EMI domain or the coiled-coil region of Emilin3 (Fig. 4F,G). A similar *in vitro*-binding experiment showed that the EGF repeats of Scube2 are sufficient for Emilin3 binding (supplementary material Fig. S10B). To investigate whether the interaction of Emilin3 with Scube2 has any functional significance, we treated transfected HEK293T cells with conditioned media derived from Scube2-transfected cells. Notably, treatment with Scube2-conditioned media, as well as Scube2 co-transfection, were able to rescue the effect of Emilin3, whereas treatment with soluble heparin was ineffective (Fig. 4H; supplementary material Fig. S10C-E). We also prepared conditioned media derived from HEK293T transiently transfected with Scube2 alone or in combination with Emilin3, and found that the latter was less effective in releasing Shh from 293-Shh cells (Fig. 4I).

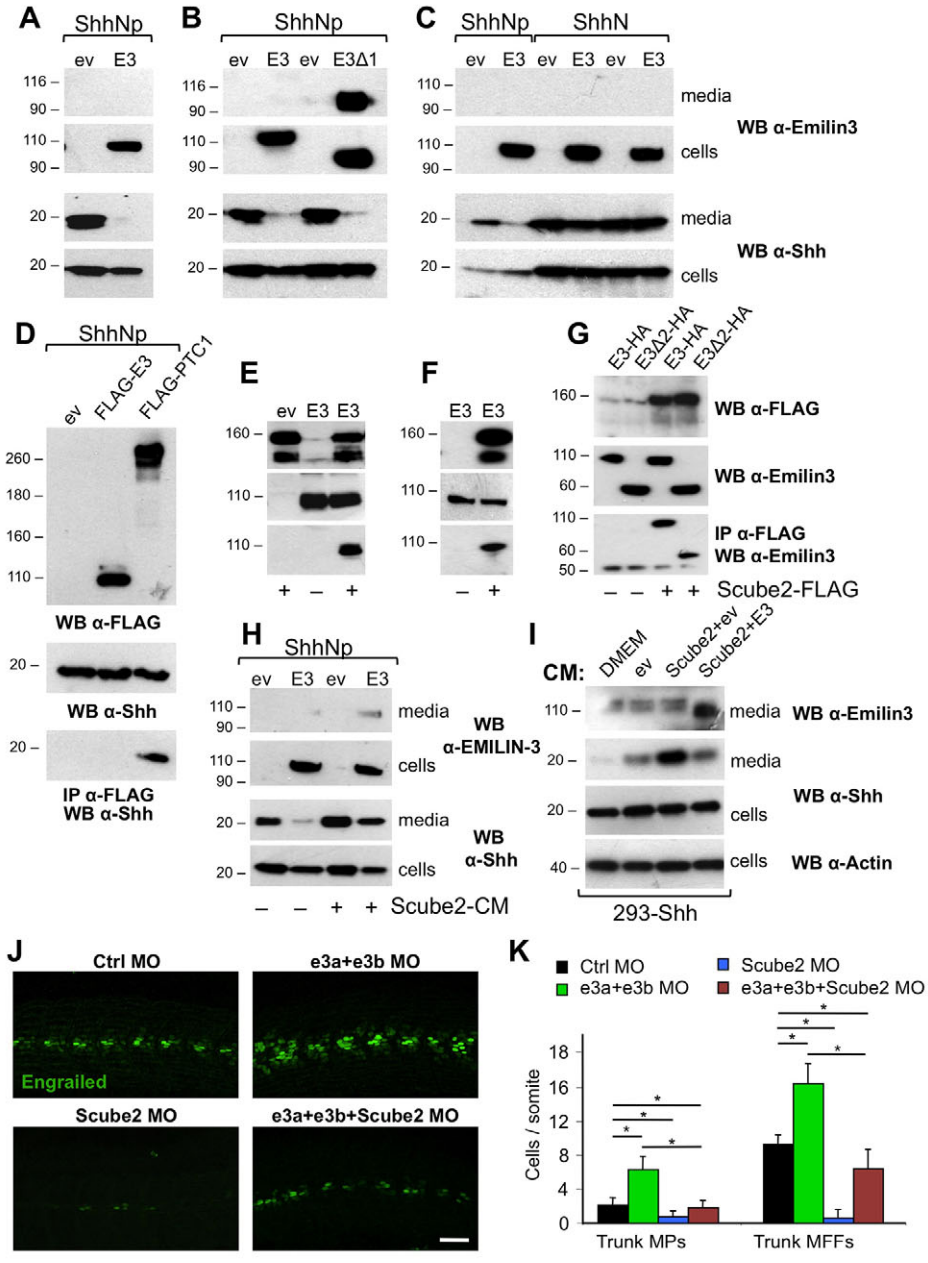

Fig. 4. Emilin3 functionally interacts with Scube2. (A-C) HEK293T were transiently co-transfected with the indicated constructs. Conditioned serum-free media and cell lysates were analyzed by western blot. (D) Cell lysates of HEK293T transfected with the indicated plasmids were analyzed by western blot or subjected to immunoprecipitation. (E-G) HEK293T were either co-transfected (E,G) or separately transfected (F) with the indicated plasmids. Media (E,F) and cell lysates (G) were analyzed by western blot or subjected to immunoprecipitation. (H) Transfected HEK293T were incubated for 24 hours with conditioned media derived from control or Scube2-transfected cells. (I) Stably transfected 293-Shh cells were incubated for 6 hours with fresh medium (DMEM) or with conditioned media derived from HEK293T co-transfected with the indicated plasmids. Media and cell lysates were analyzed by western blot. (J) Lateral views of 24 hpf embryos injected with the indicated morpholinos and immunostained for engrailed. Scale bar: 50 μm. (K) Quantification of engrailed-positive cells in injected embryos (*P<0.05; n=6). Data are mean+s.e.m. CM, conditioned media; E3, murine full-length Emilin3; E3Δ1, murine Emilin3 lacking the EMI domain; E3Δ2, murine Emilin3 lacking the EMI domain and the coiled-coil region; ev, empty vector; IP, immunoprecipitation; PTC1, human FLAG-patched-1; WB, western blot; Ctrl MO, control morpholino; e3a+e3b MO, *emilin3a* + *emilin3b* morpholinos; Scube2 MO, Scube2 morpholino; MPs, muscle pioneers; MFFs, medial fast fibers.

Development (2013) doi:10.1242/dev.094078

Finally, to investigate whether the interaction of Emilin3 with Scube2 was relevant *in vivo*, we injected embryos with morpholinos directed against *emilin3a*/*emilin3b* and *scube2*, as well as their combination. Emilin3 knockdown resulted in a robust increase of both MFFs and MPs, whereas Scube2 morphants lacked engrailed-positive cells as expected (Woods and Talbot, 2005). Interestingly, although co-injection of the three morpholinos resulted in the overlap of the two phenotypes (supplementary material Fig. S11A), the number of engrailed-positive cells was rescued almost to wild-type levels in triple morphants (Fig. 4J,K). qRT-PCR experiments showed that Scube2 expression was slightly, albeit not significantly, upregulated in Emilin3-depleted embryos (supplementary material Fig. S11B). Overall, these results support a physiological role for Emilin3 in limiting the activity of Scube2 on the release of Hh ligands by notochord cells.

DISCUSSION

In this work, we provided the first *in vivo* functional characterization of Emilin3, revealing both structural and functional roles for notochord development in zebrafish. Electron microscopy showed that Emilin3 is required for proper structural organization of the peri-notochordal basement membrane. In the absence of Emilin3, the sheath is not resistant enough to withstand the pressure generated by vacuolization of notochord cells, and this defect provides an explanation for the notochord distortion we observed in Emilin3 morphants.

Interestingly, the notochord phenotype of Emilin3 double morphant embryos is similar to that described for other ECM components. In particular, the ultrastructural alterations we found in the medial layer of the notochord sheath are reminiscent of those described for the zebrafish *gulliver* mutants, which carry a missense mutation in the globular C1q domain of the *col8a1* gene (Gansner and Gitlin, 2008). Intriguingly, unlike other EMILIN proteins, this domain is missing in Emilin3. It has been shown that the globular C1q domain is involved in the supramolecular organization of EMILINs by interacting with the EMI domain (Doliana et al., 2000), thus suggesting the possibility that Emilin3 and collagen VIII are interacting partners in the medial layer of the notochord sheath.

Our data also support previous findings, which indicated that defects in the notochord sheath can influence the gene expression pattern of notochord cells. However, at odds with what is observed in other models of notochord disruption (Parsons et al., 2002; Pagnon-Minot et al., 2008; Yamamoto et al., 2010), we found that *col2a1* and Hh ligands are not co-regulated. Indeed, in Emilin3 double morphants, *col2a1* expression is upregulated throughout the length of the notochord, whereas *shh* and *ehh* are overexpressed only in the expression field of *emilin3a* and *emilin3b*, at the level of the chordoneural hinge. Conversely, laminin mutants and collagen XV morphants display a similar upregulation of *col2a1* and *ehh* throughout the notochord (Parsons et al., 2002; Pagnon-Minot et al., 2008). This implies that notochord cells can respond to extracellular signals in a region-specific way.

The second function we report here for Emilin3 concerns the regulation of notochord-derived Hh signals. We show that Emilin3 interacts with Scube2 in the extracellular environment. Recently, Scube2 has been identified as a secreted, permissive factor, acting non-cell autonomously in the release of lipidated Shh from producing cells (Creanga et al., 2012; Tukachinsky et al., 2012). Scube2 is a multi-domain protein, with a signal peptide sequence at the N-terminal end followed by nine EGF repeats, one spacer region, three cysteine-rich motifs and one CUB domain at the C-terminal end. The CUB domain was found to interact with Shh and its presence is required for the activity of Scube2 on Shh release (Creanga et al., 2012; Tukachinsky et al., 2012). Our finding that Emilin3 is able to interact with the EGF repeats of Scube2 supports the hypothesis that this region of the protein may be important for targeting Scube2 to the ECM and fine-tuning its localization and activity in the extracellular milieu. We therefore propose that Emilin3 deficiency disturbs notochord sheath formation and causes abnormal localization and/or activity of Scube2 in the extracellular milieu, thus leading to increased Hh signals (Fig. 5). It is tempting to speculate that Emilin3, similar to Emilin1, associates with fibrillin microfibrils in the ECM, and thus the Scube2/Emilin3 interaction may represent a novel mechanism by which microfibrils control tissues homeostasis. Overall, our data indicate that the ECM endows a novel level of regulation for Hh signals through Scube2, and we propose that Emilin3 and Scube2 interaction in the notochord sheath is crucial for the proper notochord patterning activity.

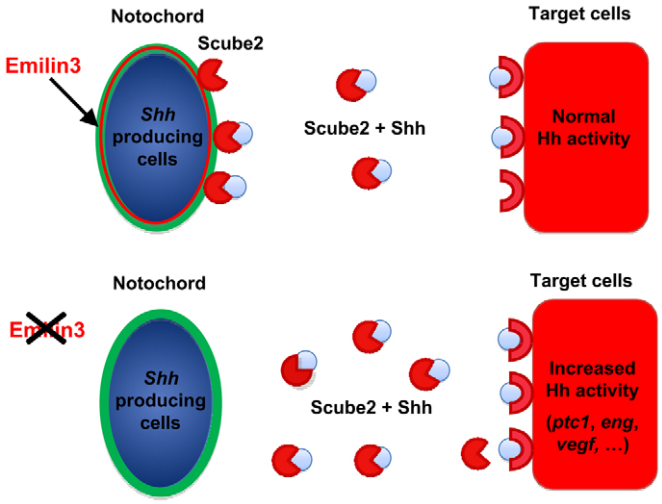

Fig. 5. Hypothetical model of Emilin3 and Scube2 interaction in the notochord sheath. Emilin3 is located in the extracellular matrix of the notochord sheath and interacts with Scube2, a secreted factor that mediates the release of lipid-modified Hh ligand. In wild-type embryos, Emilin3 ensures the integrity and function of the notochord sheath, which is necessary for proper notochord patterning activity. Emilin3 deficiency results in the disruption of the notochord sheath and affects Scube2 localization and activity in the extracellular milieu, thus leading to increased Hh signals.

MATERIALS AND METHODS

Zebrafish lines

Wild-type (AB/TU) zebrafish were maintained as described previously (Westerfield, 1995). For the generation of the *Tg(12xGli-HSVTK:nlsmCherry)ia10* zebrafish line (Tg12x_Gli), a cassette containing twelve multimerized Gli1-binding sites was isolated from the 12GLI-RE-TKO-luc construct (Kogerman et al., 1999) and ligated with the Herpes simplex virus thymidine kinase minimal promoter in the p5E-MCS Tol2 5′ entry vector. Positive clones were sequenced in both strands and recombined with a middle entry vector carrying the *mCherry* open reading frame and a 3′ entry vector carrying a SV40 poly-A tail. Entry plasmids were finally recombined into the pTol2 destination vector as previously described (Kwan et al., 2007). A total of 25 pg of Tol2 recombinant plasmids and 25-50 pg of *in vitro* synthesized transposase mRNA (Kawakami et al., 2004) were co-injected into zebrafish embryos at the one- to two-cell stage. Microinjected embryos were raised to adulthood and outcrossed to wild-type fish. Six out of 30 screened fish were identified as founders for the reporter line. The *Tg(EPV.TP1-Mmu.Hbb:EGFP)ia12* zebrafish line (Tg_Hbb:EGFP) has been previously described (Parsons et al., 2009).

Development (2013) doi:10.1242/dev.094078

Zebrafish embryo injection

Sequences of the morpholinos used in the study are reported in supplementary material Table S2. All morpholinos were splice blocked, except where indicated. Morpholinos were dissolved in 1×Danieu's buffer and injected at the doses reported in supplementary material Table S1. p53 morpholino (Robu et al., 2007) and Scube2 morpholino (Woods and Talbot, 2005) were injected at 6 ng/embryo and 2 ng/embryo, respectively. For DNA microinjection, linearized DNA was dissolved in deionised H_2O to a final concentration of at 50 ng/µl (Du et al., 1997), except where indicated. Murine *Emilin3* cDNA was cloned into the pCS-twhh-βgal vector (Du et al., 1997).

Pharmacological treatments

Cyclopamine hydrate (Sigma) was dissolved in DMSO and embryos were incubated at the indicated concentrations beginning at shield stage until fixation at 24 hpf. LY364947 (Zhou et al., 2011) and SB431542 (Ho et al., 2006) (Sigma) were dissolved in DMSO and diluted into embryo medium to a final concentration of 30 µM and 100 µM, respectively, and embryos were incubated with these compounds from 8 hpf until fixation at 24 hpf. Embryos incubated with DMSO were used as control.

Probes and plasmids

For *in situ* hybridization experiments, the used riboprobes were: *emilin3a* and *emilin3b* (Milanetto et al., 2008), *col2a1* (Yan et al., 1995), *ntl* (Schulte-Merker et al., 1994), *shh* (Krauss et al., 1993), *ehh* (Currie and Ingham, 1996), *ptc1* (Concordet et al., 1996), *nkx2.2a* (Barth and Wilson, 1995), *tbx20* (Ahn et al., 2000), *vegf* (Liang et al., 1998), *olig2* (Park et al., 2002), *eng2a* (Ekker et al., 1992), and *fgf8* (Reifers et al., 1998). The cDNA constructs for murine full-length Emilin3 and EMILIN-3Δ1, which lacks amino acid residues 54-189, have been described previously (Schiavinato et al., 2012). Murine EMILIN-3Δ2 cDNA construct, which lacks both the EMI domain (amino acid residues 54-189) and the coiled-coil region (amino acid residues 534-758), was prepared by PCR using the EMILIN-3Δ1 construct as a template and the following primers: SP6 (forward) and 5′-CTAAGCGTAATCTGGAACATCGTATGGGTACCAGGCCTTCACCTC-TGC-3′ (reverse). The EMILIN-3-HA cDNA construct was generated by adding the human influenza hemagglutinin (HA) tag sequence at the C-terminal end of murine full-length Emilin3. Murine full-length Shh, ShhN and Scube2 cDNAs were obtained by PCR and cloned into the pCS2+ vector. The Scube2-FLAG construct was generated by adding the FLAG tag sequence at the C-terminal end of murine Scube2. The EGF-FLAG construct, encompassing amino acids 1-479 of murine Scube2, was generated by PCR using the Scube2 full-length construct as a template with the following primers: 5′-GGTTGCATGCTGATGGGAGA-3′ (forward) and 5′-TTCTCGAGTCACTTGTCATCGTCGTCCTTGTAGTCTGACGAGA-GGTGAATGCC-3′ (reverse, coding for the FLAG tag sequence). The PCR product was then subcloned into the pCS2 vector. All constructs were sequenced prior to use.

Immunohistochemistry and BODIPY labeling

Immunohistochemical staining of whole zebrafish embryos was performed essentially as described previously (Dolez et al., 2011). Used antibodies were: monoclonal anti-engrailed (4D9, DSHB; 1:10 dilution); monoclonal anti-collagen II (II-II6B3, DSHB; 1:400); rabbit polyclonal anti-laminin (L9393, Sigma; 1:200); rabbit polyclonal anti-phospho-Smad1/Smad5/Smad8 (9511, Cell Signaling; 1:100); rabbit polyclonal anti-Emilin3 (Schiavinato et al., 2012; 1:500); mouse monoclonal anti-β-Catenin (C7207, Sigma; 1:500). Nuclei were stained with Hoechst (Invitrogen). Where indicated, embryos were stained with 100 µM BODIPY TR Ceramide (Invitrogen) in E3 medium for 2 hours. All embryos were imaged with a Leica SP5 confocal microscope.

Electron microscopy

Embryos were prepared essentially as described previously (Parsons, 2002) and ultrathin sections were viewed on a Zeiss 902 electron microscope.

RNA analysis

Total RNA was extracted from pools of 30 embryos using TRIzol Reagent (Invitrogen) as recommended by the manufacturer and 1 µg of RNA was used for cDNA synthesis, using the M-MLV Reverse Transcriptase kit (Invitrogen). The efficacy of splice-blocking morpholinos was tested by RT-PCR using the following primers: 5′-ACGTGCTGAAATTGGTGGA-3′ (*emilin3a*, forward); 5′-GGAACAGCTTGACCTTCGAG-3′ (*emilin3a*, reverse); 5′-ACTCAAGCAAGCTGGACCAT-3′ (*emilin3b*, forward); 5′-CCTTGTGTGTGGAGCGACA-3′ (*emilin3b*, reverse). Expression of *nlsmCherry*, *ptc1* and *scube2* transcripts was analyzed by real-time qualitative RT-PCR using the SYBR Green Realtime PCR Master Mix in an ABI PRISM 7900HT System (Applied Biosystems). Expression of *gapdh* was used as normalizer in each sample and triplicate PCR reactions were carried out. Primers used were: 5′-GTGGAGTCTACTGGTGTCTTC-3′ (*gapdh*, forward); 5′-GTGCAGGAGGCATTGCTTACA-3′ (*gapdh*, reverse); 5′-GAAGGTGACCAAGGGCGGCC-3′ (*nlsmCherry*, forward); 5′-CTGGGTCACGGTCACCACGC-3′ (*nlsmCherry*, reverse); 5′-CTTCAGTCGCCAAGGTCTTC-3′ (*ptc1*, forward); 5′-CCGATCAATCC-CATCATACC-3′ (*ptc1*, reverse); 5′-GCAAGGCTTTTTCCTGAGTG-3′ (*scube2*, forward); 5′-TTACCATGGTTGCAGGTCAA-3′ (*scube2*, reverse).

Cell culture and transfection

HEK293T were grown in DMEM supplemented with 10% FBS (Invitrogen) and transfected with LT-1 (Mirus). The next day cells were washed and incubated in serum-free medium. For the preparation of Scube2-conditioned medium, cells were transfected and kept in DMEM supplemented with 2% FBS for 72 hours. Stably transfected HEK-293 (293-Shh) cells were generated by transfection with the murine full-length Shh cDNA subcloned into the pcDNA3.1+ vector, followed by selection with G418 (Invitrogen) at a concentration of 400 µg/ml.

Western blot and immunoprecipitation

Cells and conditioned media were harvested 24 hours (western blot) or 72 hours (immunoprecipitation) after incubation in serum-free medium. Cells were lysed in ice-cold lysis buffer [25 mM Tris (pH 7.5), 150 mM NaCl, 2.5 mM EDTA, 10% glycerol, 1% Nonidet P-40] supplemented with proteases inhibitor (Roche) and media were TCA precipitated. Immunoprecipitation, SDS-PAGE and western blot were performed as previously described (Schiavinato et al., 2012). Used antibodies were: rabbit polyclonal anti-Emilin3 (Schiavinato et al., 2012), rabbit polyclonal anti-Shh (Santa Cruz), mouse monoclonal anti-FLAG (Sigma) and mouse monoclonal anti-HA (Sigma).

Statistical analysis

Data are expressed as mean±s.e.m. Statistical significance was determined by unequal variance Student's *t*-test. $P<0.05$ was considered significant.

Acknowledgements

We thank Walter Giuriati for help with electron microscopy. We are grateful to Professor Mats Paulsson and Dr Raimund Wagener for Emilin3 antibody and for critical reading of the manuscript.

Competing interests

The authors declare no competing financial interests.

Author contributions

D.C. and A.S. conceived and performed the majority of the experiments, and analyzed data. V.T. performed experiments and analyzed data. E.M. and F.A. provided zebrafish transgenic lines, contributed new reagents/analytic tools. P.B. and A.S. designed the study, analyzed data and wrote the paper. All authors discussed the results and commented on the manuscript.

Funding

This work was supported by grants from the University of Padova and the Italian Ministry of University and Research.

Supplementary material

Supplementary material available online at
http://dev.biologists.org/lookup/suppl/doi:10.1242/dev.094078/-/DC1

References

Ahn, D. G., Ruvinsky, I., Oates, A. C., Silver, L. M. and Ho, R. K. (2000). tbx20, a new vertebrate T-box gene expressed in the cranial motor neurons and developing cardiovascular structures in zebrafish. *Mech. Dev.* **95**, 253-258.

Barth, K. A. and Wilson, S. W. (1995). Expression of zebrafish nk2.2 is influenced by sonic hedgehog/vertebrate hedgehog-1 and demarcates a zone of neuronal differentiation in the embryonic forebrain. *Development* **121**, 1755-1768.

Bressan, G. M., Daga-Gordini, D., Colombatti, A., Castellani, I., Marigo, V. and Volpin, D. (1993). Emilin, a component of elastic fibers preferentially located at the elastin-microfibrils interface. *J. Cell Biol.* **121**, 201-212.

Concordet, J. P., Lewis, K. E., Moore, J. W., Goodrich, L. V., Johnson, R. L., Scott, M. P. and Ingham, P. W. (1996). Spatial regulation of a zebrafish patched homologue reflects the roles of sonic hedgehog and protein kinase A in neural tube and somite patterning. *Development* **122**, 2835-2846.

Creanga, A., Glenn, T. D., Mann, R. K., Saunders, A. M., Talbot, W. S. and Beachy, P. A. (2012). Scube/You activity mediates release of dually lipid-modified Hedgehog signal in soluble form. *Genes Dev.* **26**, 1312-1325.

Currie, P. D. and Ingham, P. W. (1996). Induction of a specific muscle cell type by a hedgehog-like protein in zebrafish. *Nature* **382**, 452-455.

Danussi, C., Petrucco, A., Wassermann, B., Pivetta, E., Modica, T. M., Del Bel Belluz, L., Colombatti, A. and Spessotto, P. (2011). EMILIN1-α4/α9 integrin interaction inhibits dermal fibroblast and keratinocyte proliferation. *J. Cell Biol.* **195**, 131-145.

Doi, M., Nagano, A. and Nakamura, Y. (2004). Molecular cloning and characterization of a novel gene, EMILIN-5, and its possible involvement in skeletal development. *Biochem. Biophys. Res. Commun.* **313**, 888-893.

Dolez, M., Nicolas, J. F. and Hirsinger, E. (2011). Laminins, via heparan sulfate proteoglycans, participate in zebrafish myotome morphogenesis by modulating the pattern of Bmp responsiveness. *Development* **138**, 97-106.

Doliana, R., Bot, S., Bonaldo, P. and Colombatti, A. (2000). EMI, a novel cysteine-rich domain of EMILINs and other extracellular proteins, interacts with the gC1q domains and participates in multimerization. *FEBS Lett.* **484**, 164-168.

Du, S. J., Devoto, S. H., Westerfield, M. and Moon, R. T. (1997). Positive and negative regulation of muscle cell identity by members of the hedgehog and TGF-beta gene families. *J. Cell Biol.* **139**, 145-156.

Ekker, M., Wegner, J., Akimenko, M. A. and Westerfield, M. (1992). Coordinate embryonic expression of three zebrafish engrailed genes. *Development* **116**, 1001-1010.

Ellis, K., Bagwell, J. and Bagnat, M. (2013). Notochord vacuoles are lysosome-related organelles that function in axis and spine morphogenesis. *J. Cell Biol.* **200**, 667-679.

Gansner, J. M. and Gitlin, J. D. (2008). Essential role for the alpha 1 chain of type VIII collagen in zebrafish notochord formation. *Dev. Dyn.* **237**, 3715-3726.

Ho, D. M., Chan, J., Bayliss, P. and Whitman, M. (2006). Inhibitor-resistant type I receptors reveal specific requirements for TGF-beta signaling in vivo. *Dev. Biol.* **295**, 730-742.

Kawakami, K. (2004). Transgenesis and gene trap methods in zebrafish by using the Tol2 transposable element. *Methods Cell Biol.* **77**, 201-222.

Kogerman, P., Grimm, T., Kogerman, L., Krause, D., Undén, A. B., Sandstedt, B., Toftgård, R. and Zaphiropoulos, P. G. (1999). Mammalian suppressor-of-fused modulates nuclear-cytoplasmic shuttling of Gli-1. *Nat. Cell Biol.* **1**, 312-319.

Krauss, S., Concordet, J. P. and Ingham, P. W. (1993). A functionally conserved homolog of the Drosophila segment polarity gene hh is expressed in tissues with polarizing activity in zebrafish embryos. *Cell* **75**, 1431-1444.

Kwan, K. M., Fujimoto, E., Grabher, C., Mangum, B. D., Hardy, M. E., Campbell, D. S., Parant, J. M., Yost, H. J., Kanki, J. P. and Chien, C. B. (2007). The Tol2kit: a multisite gateway-based construction kit for Tol2 transposon transgenesis constructs. *Dev. Dyn.* **236**, 3088-3099.

Leimeister, C., Steidl, C., Schumacher, N., Erhard, S. and Gessler, M. (2002). Developmental expression and biochemical characterization of Emu family members. *Dev. Biol.* **249**, 204-218.

Liang, D., Xu, X., Chin, A. J., Balasubramaniyan, N. V., Teo, M. A. L., Lam, T. J., Weinberg, E. S. and Ge, R. (1998). Cloning and characterization of vascular endothelial growth factor (VEGF) from zebrafish, *Danio rerio*. *Biochim. Biophys. Acta* **1397**, 14-20.

Mangos, S., Lam, P. Y., Zhao, A., Liu, Y., Mudumana, S., Vasilyev, A., Liu, A. and Drummond, I. A. (2010). The ADPKD genes pkd1a/b and pkd2 regulate extracellular matrix formation. *Dis. Model. Mech.* **3**, 354-365.

Maurya, A. K., Tan, H., Souren, M., Wang, X., Wittbrodt, J. and Ingham, P. W. (2011). Integration of Hedgehog and BMP signalling by the engrailed2a gene in the zebrafish myotome. *Development* **138**, 755-765.

Milanetto, M., Tiso, N., Braghetta, P., Volpin, D., Argenton, F. and Bonaldo, P. (2008). Emilin genes are duplicated and dynamically expressed during zebrafish embryonic development. *Dev. Dyn.* **237**, 222-232.

Pagnon-Minot, A., Malbouyres, M., Haftek-Terreau, Z., Kim, H. R., Sasaki, T., Thisse, C., Thisse, B., Ingham, P. W., Ruggiero, F. and Le Guellec, D. (2008). Collagen XV, a novel factor in zebrafish notochord differentiation and muscle development. *Dev. Biol.* **316**, 21-35.

Park, H. C., Mehta, A., Richardson, J. S. and Appel, B. (2002). olig2 is required for zebrafish primary motor neuron and oligodendrocyte development. *Dev. Biol.* **248**, 356-368.

Parsons, M. J., Pollard, S. M., Saude, L., Feldman, B., Coutinho, P., Hirst, E. M. and Stemple, D. L. (2002). Zebrafish mutants identify an essential role for laminins in notochord formation. *Development* **129**, 3137-3146.

Parsons, M. J., Pisharath, H., Yusuff, S., Moore, J. C., Siekmann, A. F., Lawson, N. and Leach, S. D. (2009). Notch-responsive cells initiate the secondary transition in larval zebrafish pancreas. *Mech. Dev.* **126**, 898-912.

Reifers, F., Böhli, H., Walsh, E. C., Crossley, P. H., Stainier, D. Y. R. and Brand, M. (1998). *Fgf8* is mutated in zebrafish acerebellar (ace) mutants and is required for maintenance of midbrain-hindbrain boundary development and somitogenesis. *Development* **125**, 2381-2395.

Robu, M. E., Larson, J. D., Nasevicius, A., Beiraghi, S., Brenner, C., Farber, S. A. and Ekker, S. C. (2007). p53 activation by knockdown technologies. *PLoS Genet.* **3**, e78.

Schiavinato, A., Becker, A. K., Zanetti, M., Corallo, D., Milanetto, M., Bizzotto, D., Bressan, G., Guljelmovic, M., Paulsson, M., Wagener, R. et al. (2012). EMILIN-3, peculiar member of elastin microfibril interface-located protein (EMILIN) family, has distinct expression pattern, forms oligomeric assemblies, and serves as transforming growth factor β (TGF-β) antagonist. *J. Biol. Chem.* **287**, 11498-11515.

Schulte-Merker, S., Hammerschmidt, M., Beuchle, D., Cho, K. W., De Robertis, E. M. and Nüsslein-Volhard, C. (1994). Expression of zebrafish goosecoid and no tail gene products in wild-type and mutant no tail embryos. *Development* **120**, 843-852.

Spessotto, P., Cervi, M., Mucignat, M. T., Mungiguerra, G., Sartoretto, I., Doliana, R. and Colombatti, A. (2003). beta 1 Integrin-dependent cell adhesion to EMILIN-1 is mediated by the gC1q domain. *J. Biol. Chem.* **278**, 6160-6167.

Stemple, D. L. (2005). Structure and function of the notochord: an essential organ for chordate development. *Development* **132**, 2503-2512.

Tukachinsky, H., Kuzmickas, R. P., Jao, C. Y., Liu, J. and Salic, A. (2012). Dispatched and scube mediate the efficient secretion of the cholesterol-modified hedgehog ligand. *Cell Reports* **2**, 308-320.

Westerfield, M. (1995). *The Zebrafish Book*. Eugene, OR: University of Oregon Press.

Woods, I. G. and Talbot, W. S. (2005). The you gene encodes an EGF-CUB protein essential for Hedgehog signaling in zebrafish. *PLoS Biol.* **3**, e66.

Yamamoto, M., Morita, R., Mizoguchi, T., Matsuo, H., Isoda, M., Ishitani, T., Chitnis, A. B., Matsumoto, K., Crump, J. G., Hozumi, K. et al. (2010). Mib-Jag1-Notch signalling regulates patterning and structural roles of the notochord by controlling cell-fate decisions. *Development* **137**, 2527-2537.

Yan, Y. L., Hatta, K., Riggleman, B. and Postlethwait, J. H. (1995). Expression of a type II collagen gene in the zebrafish embryonic axis. *Dev. Dyn.* **203**, 363-376.

Zhou, Y., Cashman, T. J., Nevis, K. R., Obregon, P., Carney, S. A., Liu, Y., Gu, A., Mosimann, C., Sondalle, S., Peterson, R. E. et al. (2011). Latent TGF-β binding protein 3 identifies a second heart field in zebrafish. *Nature* **474**, 645-648.

Supplementary Figure S1. Morpholino-mediated knockdown of zebrafish Emilin3 transcripts. (**A**) RT-PCR analysis of RNA extracted from 24 hpf non-injected embryos (WT) and embryos injected with the indicated morpholinos. β-actin was used as a loading control. (**B**) Whole mount immunofluorescence labeling for Emilin3 in 24 hpf embryos injected with 4 ng control morpholino (Ctrl MO), 2 ng/each of *emilin3a* and *emilin3b* splice-blocking morpholinos (e3a+e3b MO splice), or 2 ng/each of *emilin3a* and *emilin3b* translation-blocking morpholinos (e3a+e3b MO ATG). Scale bar, 50 μm. (**C**) Lateral views of 24 hpf embryos injected with 4 ng control morpholino (Ctrl MO) or 2 ng/each of *emilin3a* and *emilin3b* translation-blocking morpholinos (e3a+e3b MO ATG). Arrows point at notochord distortions in Emilin3 double morphants. (**D**) Lateral views of 24 hpf embryos injected with 10 ng control morpholino (Ctrl MO), 2 ng/each of *emilin3a* and *emilin3b* splice-blocking morpholinos (e3a+e3b MO), 6 ng p53 translation-blocking morpholino (p53 MO) and the combination of p53, *emilin3a* and *emilin3b* morpholinos (e3a+e3b+p53 MO). no, notochord.

Supplementary Figure S2. Quantification of the mean number of notochord cells. (**A**) Notochord cell nuclei of the same trunk region from 24 hpf control and Emilin3 double morphant embryos were stained with Hoechst. Scale bar, 50 μm. (**B**) Nuclei, stained as in (A), were counted and reported as mean number of nuclei/somite (not significant; *n*=15). Ctrl MO, control morpholino; e3a+e3b MO, *emilin3a* + *emilin3b* morpholinos.

Supplementary Figure S3. Notch activity is not grossly affected in the notochord of Emilin3 depleted embryos. (**A**) Notch-responsive reporter zebrafish (Tg_Hbb:EGFP) were injected with the indicated morpholinos and the fluorescence analyzed at 24 hpf. Scale bar, 50 μm. (**B**) Quantification of the mean number of GFP-positive notochord cells in the trunk region (250 μm in length) (not significant; *n*=10). Ctrl MO, control morpholino; e3a+e3b MO, *emilin3a* + *emilin3b* morpholinos.

Supplementary Figure S4. Analysis of collagen II and laminin expression in Emilin3 morphant embryos. (**A**, **B**) Zebrafish embryos were injected with the indicated morpholinos and probed for *col2a1* expression at 24 and 48 hpf, respectively. The fraction of embryos displaying the corresponding phenotype is provided in each panel. Note that at 24 hpf, even embryos injected with *emilin3a* or *emilin3b* morpholino alone displayed a slight increase in *col2a1* expression. (**C**) Lateral views of controls and Emilin3 morphant embryos labeled by immunohistochemistry for laminin at 24 hpf. The panels display projection of confocal sections around somite 10, showing the notochord. Scale bar, 25 μm. Ctrl MO, control morpholino; e3a MO, *emilin3a* morpholino; e3b MO, *emilin3b* morpholino; e3a+e3b MO, *emilin3a* + *emilin3b* morpholinos.

Supplementary Figure S5. Hedgehog upregulation in Emilin3 morphant embryos is dependent on Emilin3 protein depletion. (**A, B**) Embryos were injected with the indicated splice- or translation-blocking morpholinos (ATG) and probed for *ptc1* expression at 24 hpf. Lateral view of the trunk, head is on the left. (**C**) Control and Emilin3 double morphant embryos were probed for *ptc1* expression at 8-somite stage. (**D**) Dorsal view of wild-type embryos immunostained for Emilin3 and β-catenin at at 8-somite stage. Note the absence of Emilin3 in the notochord (marked by the asterisks) at this stage of development. Scale bar, 100 μm. The fraction of embryos displaying the corresponding phenotype is provided in each panel. Ctrl MO, control morpholino; e3a+e3b MO, *emilin3a* + *emilin3b* morpholinos; p53 MO, p53 morpholino.

Supplementary Figure S6. Upregulation of Hedgehog target genes in Emilin3 morphant embryos. (**A**) Lateral views of 24 hpf embryos injected with the indicated morpholinos and probed for *olig2*, *vegfa* and *eng2a* expression. (**B)** Expression of *fgf8* is similar between control and Emilin3 double morphant embryos, thus excluding a generalized developmental delay. Head is on the left. The fraction of embryos displaying the corresponding phenotype is provided in each panel. Ctrl MO, control morpholino; e3a+e3b MO, *emilin3a* + *emilin3b* morpholinos.

Supplementary Figure S7. Hedgehog upregulation in Emilin3 morphant embryos is not dependent on BMP or TGF-β signaling. **(A**) Lateral views of 24 hpf embryos injected with the indicated morpholinos and treated at 8 hpf with 5 μM cyclopamine (lower panels) or with the corresponding volume of ethanol as a control (upper panels). Embryos were then stained with the monoclonal 4D9 antibody (green) and the polyclonal pSMAD1/5/8 antibody (purple). The panels show magnifications around somite 10. Scale bar, 50 μm. (**B**) Wild-type embryos were injected with the indicated morpholinos. Embryos were then left untreated or treated at 8 hpf with 30 μM of the selective TGF-β receptor inhibitor LY364947 from 8 hpf and probed for *ptc1* expression at 24 hpf. The fraction of embryos displaying the corresponding phenotype is provided in each panel. Ctrl MO, control morpholino; e3a+e3b MO, *emilin3a* + *emilin3b* morpholinos.

Supplementary Figure S8. Injection of Emilin3 cDNA rescues the phenotype of Emilin3 morphants. (A) Lateral views of 24 hpf embryos co-injected with the indicated morpholinos (4 ng/embryo) and with the indicated cDNA constructs (25 ng/μl). Arrows point at notochord distortions in Emilin3 double morphants, which are largely rescued by co-injection with the pCS-twhh-mEmilin3 construct. The fraction of embryos displaying the corresponding phenotype is provided in each panel. (**B)** Whole mount immunofluorescence labeling for engrailed and Emilin3 in 24 hpf embryos injected as in (A). Scale bar, 25 μm. (**C**) Quantification of engrailed-positive cells in 24 hpf co-injected embryos (*, $P < 0.05$; n.s., not significant; $n = 10$). Ctrl MO, control morpholino; e3a+e3b MO, *emilin3a* + *emilin3b* morpholinos; Trunk MPs, trunk muscle pioneers; Trunk MFFs, trunk medial fast fibers.

Supplementary Figure S9. **Conditioned medium from HEK293T cells can stimulate Shh release**. 293-Shh cells were incubated for 6 hr with fresh medium (DMEM) or with conditioned media derived from HEK293T transfected with the indicated plasmids. The release rate of Shh was assessed by immunoblot of media and cell lysates. CM, conditioned media; E3, murine full-length Emilin3; ev, empty vector; WB, western blot.

Supplementary Figure S10. Emilin3 and Scube2 functionally interact. (**A**) Cell lysates of HEK293T transfected with the indicated plasmids were either analyzed directly by western blot or subjected to immunoprecipitation with an anti-HA affinity gel followed by western blot for Scube2 (anti-FLAG). (**B**) *In vitro* binding between Emilin3 and the EGF fragment of Scube2. HEK293T were transiently co-transfected with Emilin3 or Scube2-EGF constructs. Media were then harvested, and subjected to western blot and immunoprecipitation with the indicated antibodies. (**C**) HEK293T were co-transfected with the Shh plasmid and the indicated constructs and left untreated or treated overnight with 50 μg/ml of soluble heparin in serum free medium. Cell lysates and conditioned media were then analyzed by immunoblotting. (**D**,**E**) HEK293T were co-transfected with the Shh plasmid and the indicated constructs (D) or transfected and then treated with increasing concentration of Scube2-conditioned medium (E). Shh release was then studied by western blot. E3, murine full-length Emilin3 cDNA; E3-HA, murine full-length HA-tagged Emilin3 cDNA; ev, empty vector; IP, immunoprecipitation; Scube2-FLAG, murine full-length FLAG-tagged Scube2 cDNA; WB, western blot.

Supplementary Figure S11. Morpholino-mediated knockdown of zebrafish Emilin3 and Scube2. (**A**) Lateral views of 24 hpf embryos injected with 6 ng of control morpholino (Ctrl MO) or 2 ng/each of the indicated morpholinos. (**B**) qRT-PCR for *scube2* transcript in control and Emilin3 double morphant embryos (not significant; $n = 30$). Ctrl MO, control morpholino; e3a+e3b MO, *emilin3a* + *emilin3b* morpholinos; Scube2 MO, Scube2 morpholino.

Supplementary Table S1. Summary of the phenotypic defects detected after injection of morpholino oligonucleotides. Wild-type zebrafish embryos were injected with the indicated morpholinos and examined at 24 hpf. The dose for each morpholino, the total number of injected embryos, and the number and percentage of embryos displaying the indicated phenotypic defects is provided. Embryos were assigned to one of the following three classes based on their phenotype: *a)* normal (no evidence of morphological defect); *b)* notochord defects; *c)* radialized embryos. Ctrl, control morpholino; e3a splice, *emilin3a* splicing-blocking morpholino; e3b splice, *emilin3b* splicing-blocking morpholino; e3a ATG, *emilin3a* translation-blocking morpholino; e3b ATG, *emilin3b* translation-blocking morpholino.

Supplementary Table S2. Sequences of morpholino oligonucleotides used in the study. The table describes the sequences of morpholinos targeting the donor splice site between the first exon and the first intron of *emilin3a* or *emilin3b* (e3a MO splice and e3b MO splice), the splice site between the first exon and the first intron of *col2a1* (col2a1 MO splice; Mangos et al., 2010), the translation initiation codon of *emilin3a* or *emilin3b* (e3a MO ATG and e3b MO ATG), the translational initiation codon of *scube2* (scube2 MO ATG; Woods et al., 2005), the translation initiation codon of p53 (p53 MO ATG; Robu et al., 2007) and a standard control morpholino (Ctrl MO). All sequences were provided by Gene tools, LLC.

Figure S1

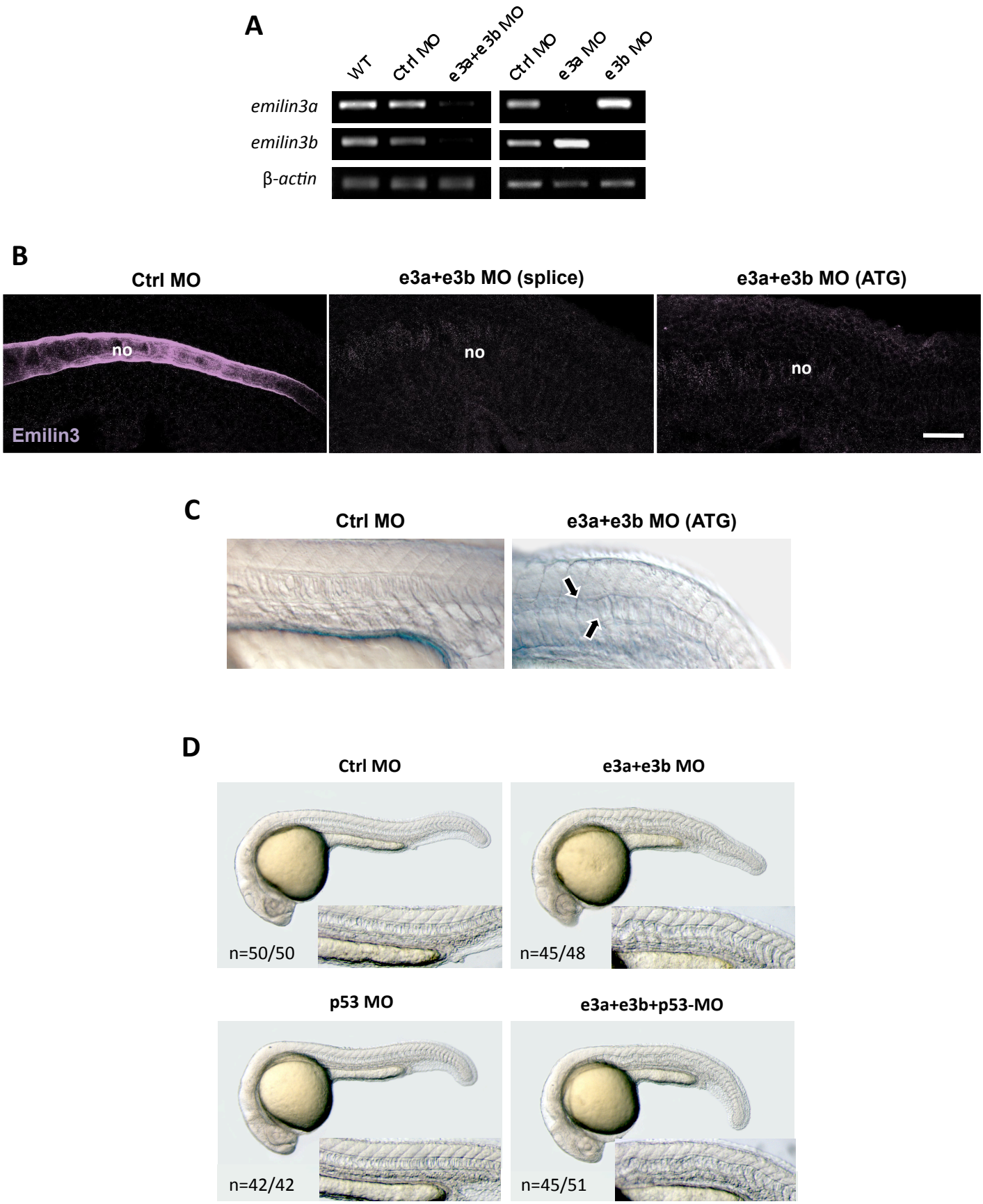
A
WT
Ctrl MO
e3a+e3b MO
Ctrl MO
e3a MO
e3b MO
emilin3a
emilin3b
β-actin
B
Ctrl MO
e3a+e3b MO (splice)
e3a+e3b MO (ATG)
no
no
no
Emilin3
C
Ctrl MO
e3a+e3b MO (ATG)
D
Ctrl MO
e3a+e3b MO
n=50/50
n=45/48
p53 MO
e3a+e3b+p53-MO
n=42/42
n=45/51

Figure S2

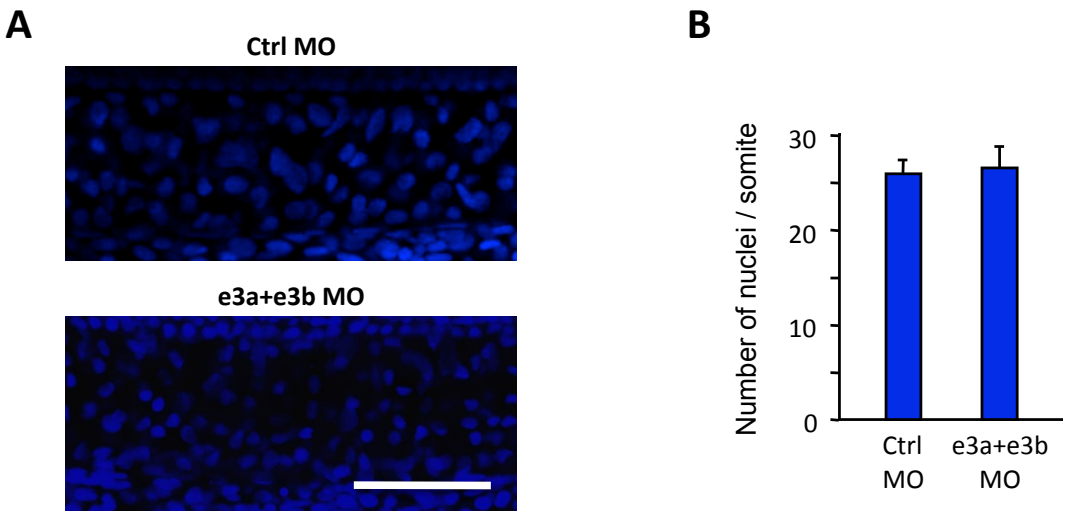
A
Ctrl MO
e3a+e3b MO
B
Number of nuclei / somite
30
20
10
0
Ctrl MO
e3a+e3b MO

Figure S3

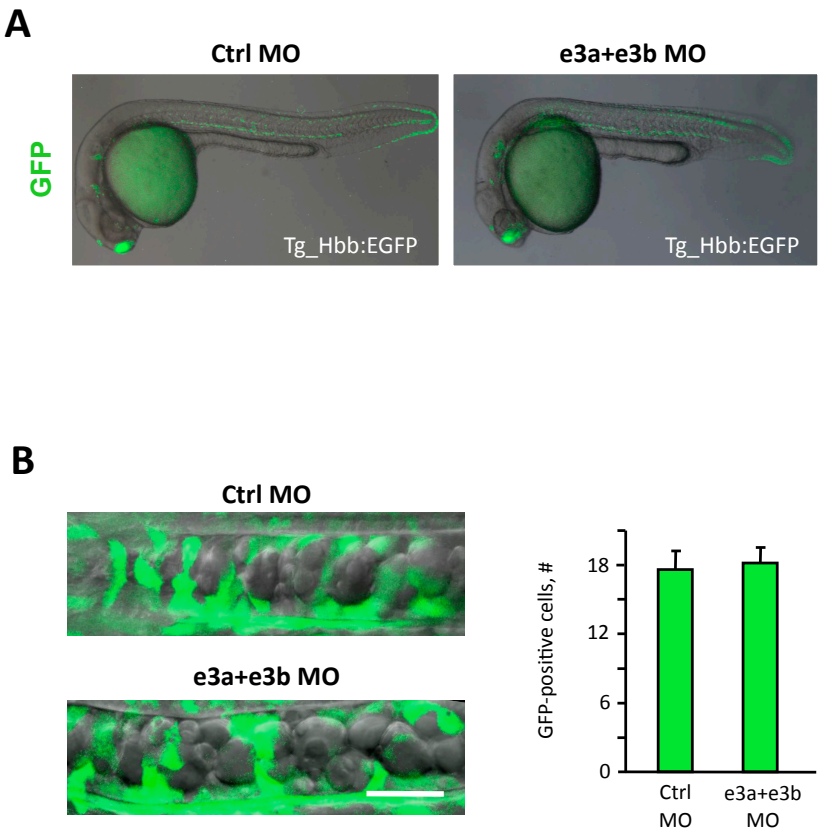
A
Ctrl MO
e3a+e3b MO
GFP
Tg_Hbb:EGFP
Tg_Hbb:EGFP
B
Ctrl MO
e3a+e3b MO
GFP-positive cells, #
18
12
6
0
Ctrl MO
e3a+e3b MO

Figure S4

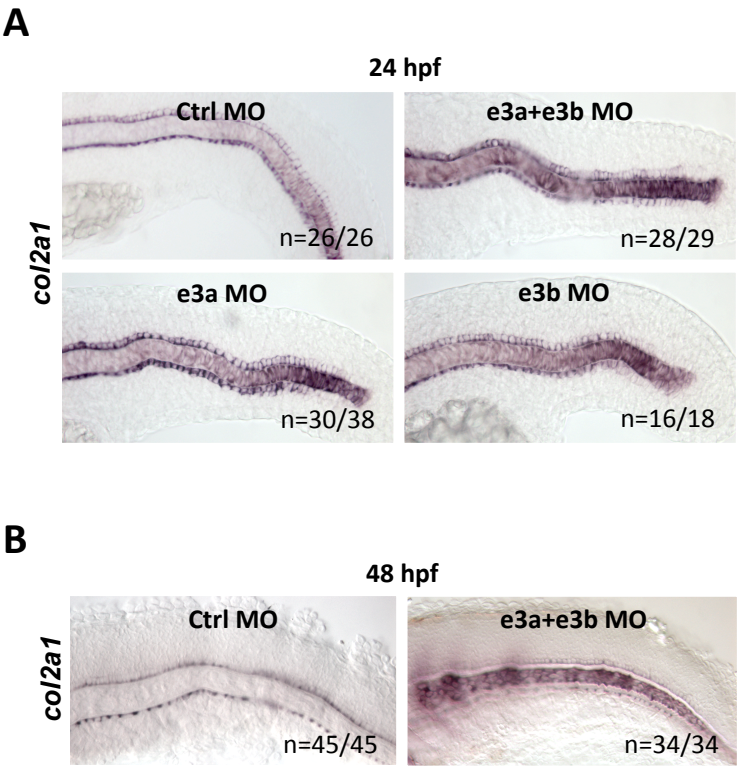
A
24 hpf
col2a1
Ctrl MO
n=26/26
e3a+e3b MO
n=28/29
e3a MO
n=30/38
e3b MO
n=16/18
B
48 hpf
col2a1
Ctrl MO
n=45/45
e3a+e3b MO
n=34/34

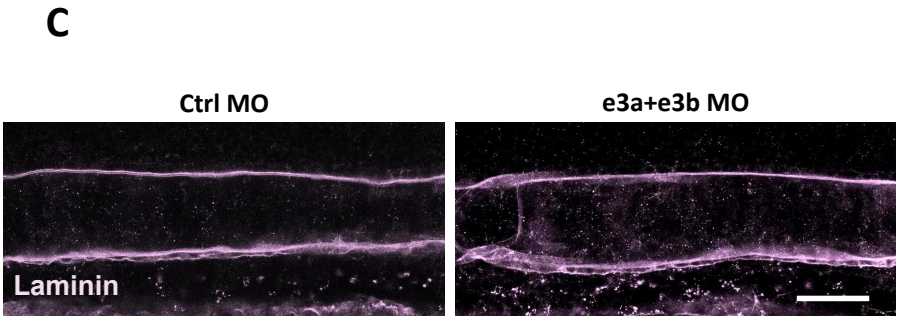
C
Ctrl MO
e3a+e3b MO
Laminin

Figure S5

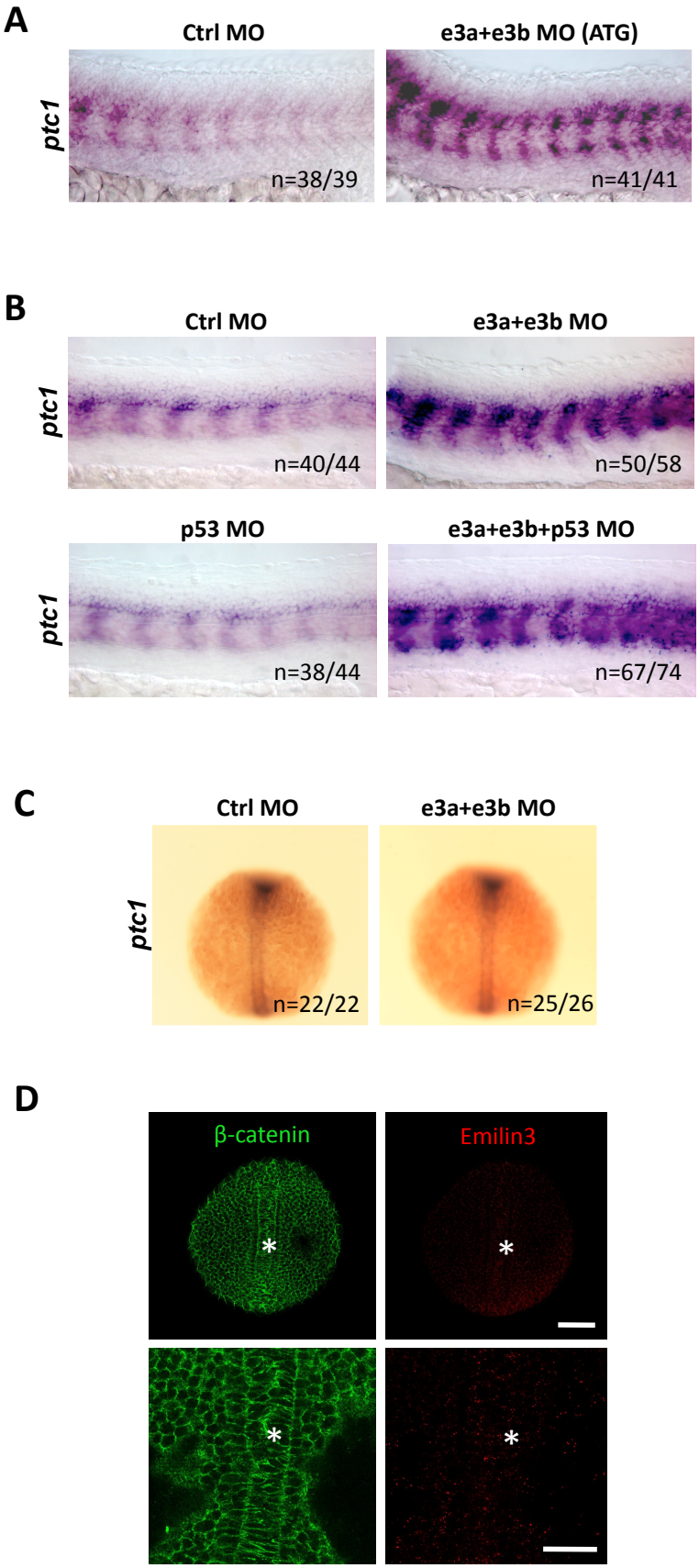
A
Ctrl MO
e3a+e3b MO (ATG)
ptc1
n=38/39
n=41/41
B
Ctrl MO
e3a+e3b MO
ptc1
n=40/44
n=50/58
p53 MO
e3a+e3b+p53 MO
ptc1
n=38/44
n=67/74
C
Ctrl MO
e3a+e3b MO
ptc1
n=22/22
n=25/26
D
β-catenin
Emilin3

Figure S6

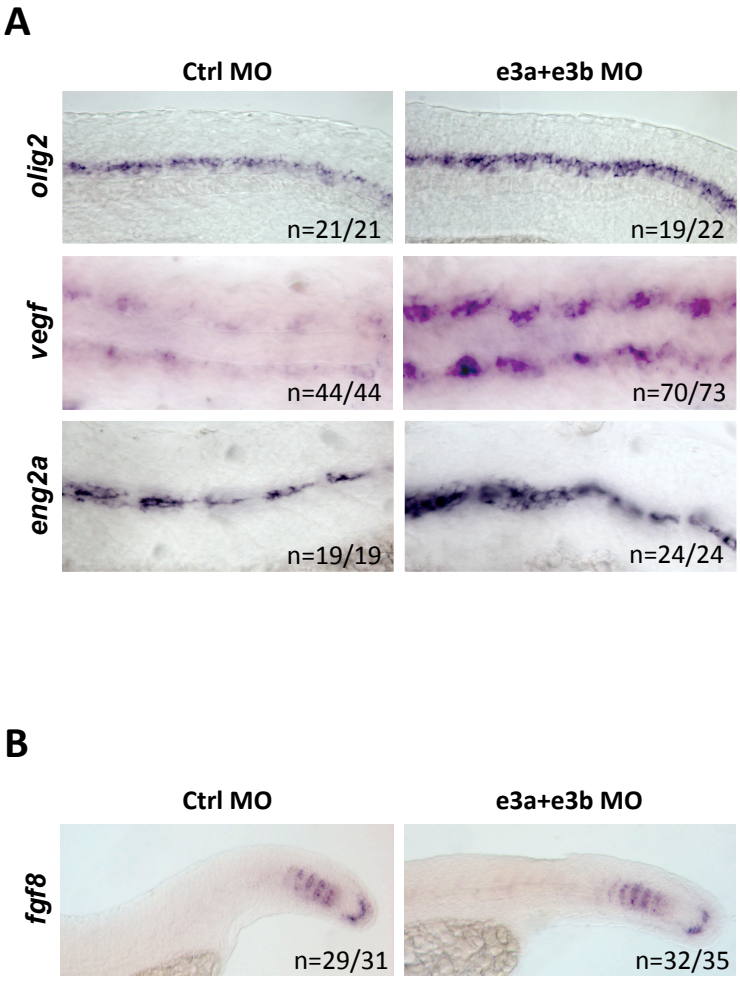
A
Ctrl MO
e3a+e3b MO
olig2
n=21/21
n=19/22
vegf
n=44/44
n=70/73
eng2a
n=19/19
n=24/24
B
Ctrl MO
e3a+e3b MO
fgf8
n=29/31
n=32/35

Figure S7

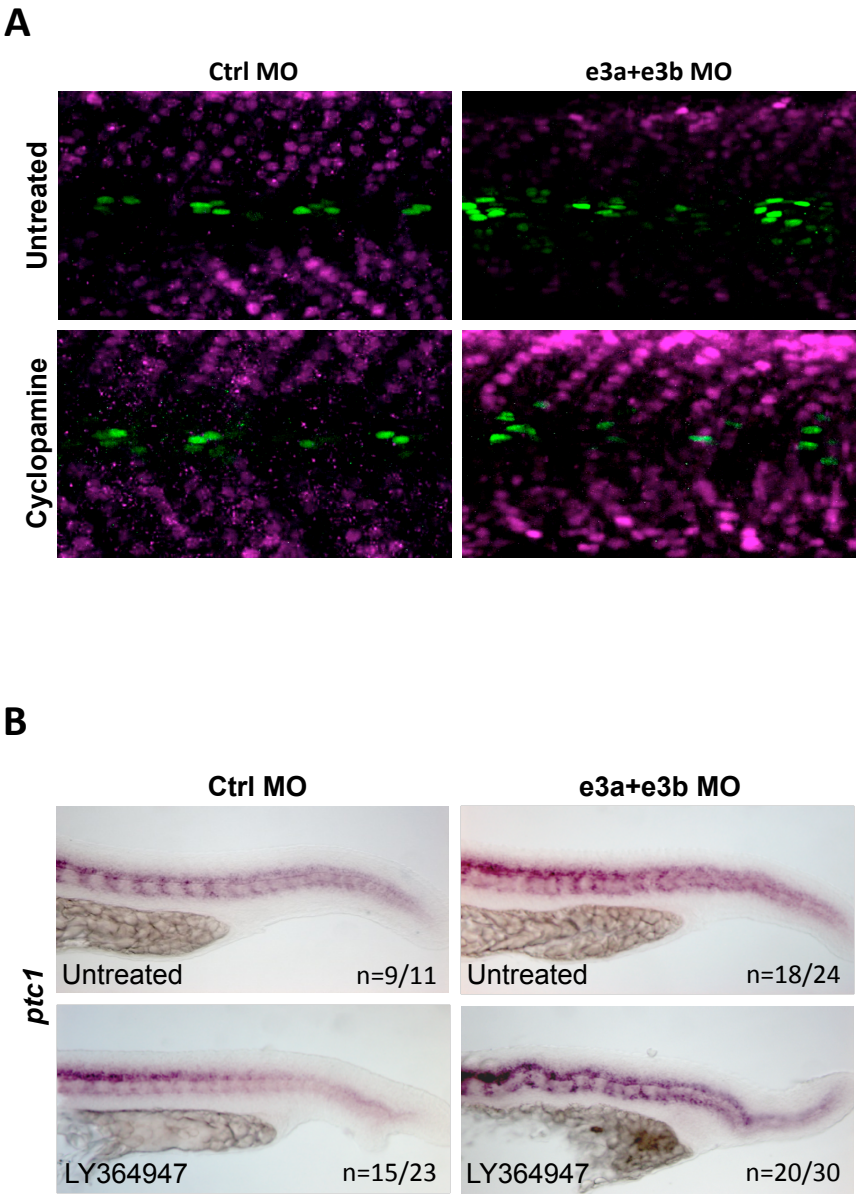
A
Ctrl MO
e3a+e3b MO
Untreated
Cyclopamine
B
Ctrl MO
e3a+e3b MO
ptc1
Untreated
n=9/11
Untreated
n=18/24
LY364947
n=15/23
LY364947
n=20/30

Figure S8

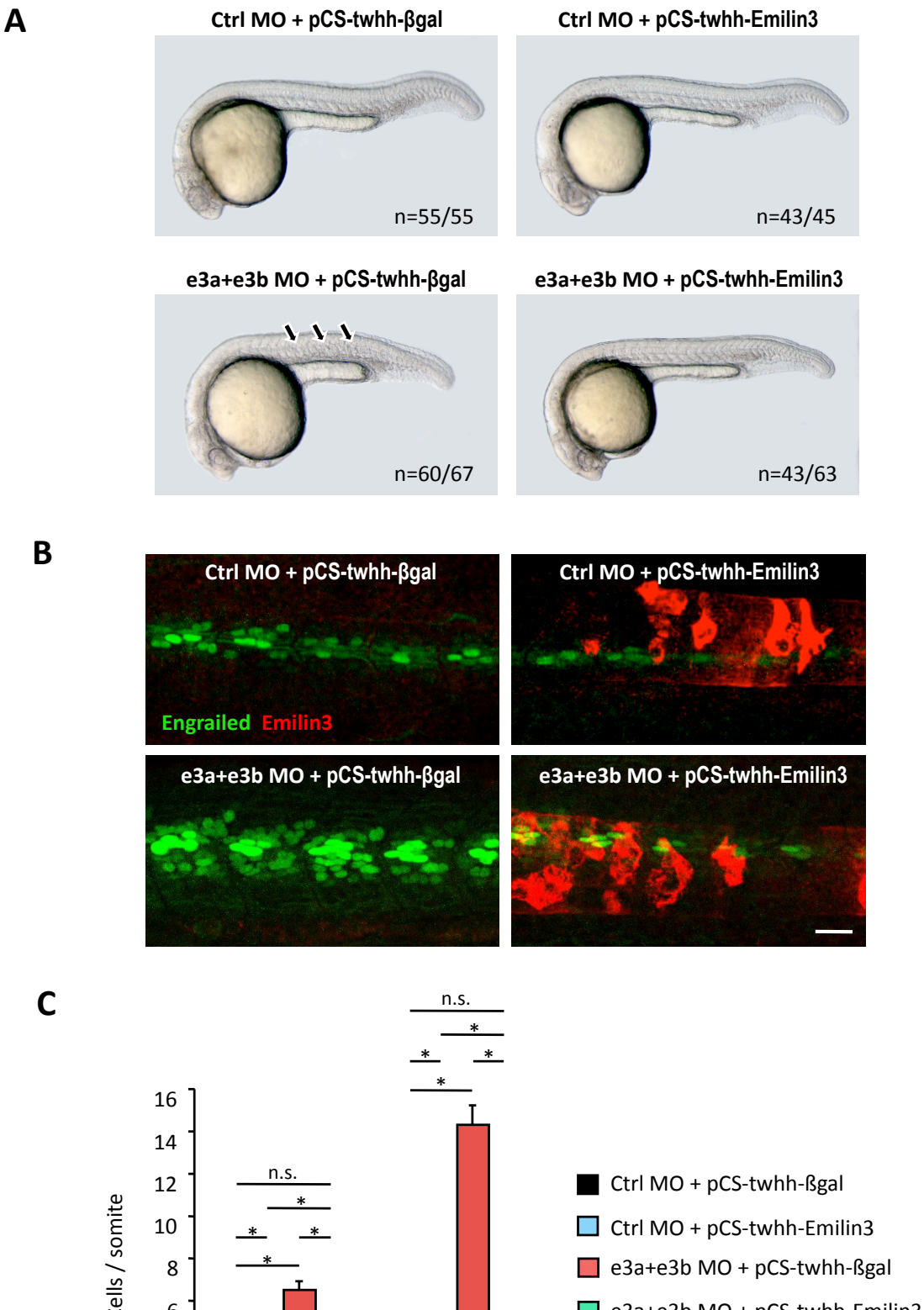
A
Ctrl MO + pCS-twhh-βgal
n=55/55
Ctrl MO + pCS-twhh-Emilin3
n=43/45
e3a+e3b MO + pCS-twhh-βgal
n=60/67
e3a+e3b MO + pCS-twhh-Emilin3
n=43/63
B
Ctrl MO + pCS-twhh-βgal
Engrailed Emilin3
Ctrl MO + pCS-twhh-Emilin3
e3a+e3b MO + pCS-twhh-βgal
e3a+e3b MO + pCS-twhh-Emilin3
C
Cells / somite
16
14
12
10
8
6
4
2
0
n.s.
*
*
*
*
n.s.
*
*
*
*
Trunk MPs
Trunk MFFs
Ctrl MO + pCS-twhh-ßgal
Ctrl MO + pCS-twhh-Emilin3
e3a+e3b MO + pCS-twhh-ßgal
e3a+e3b MO + pCS-twhh-Emilin3

Figure S9

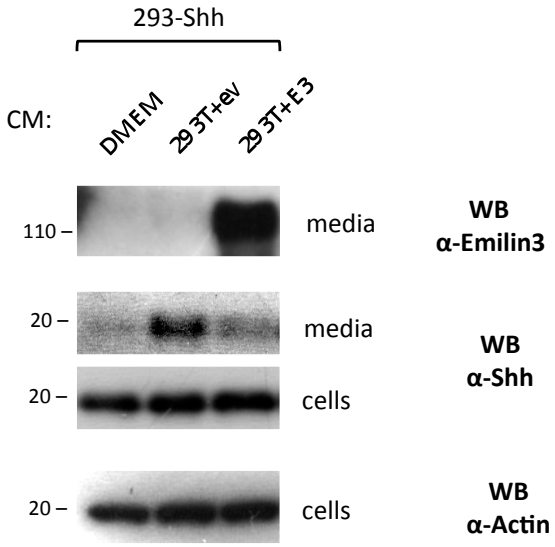
293-Shh
CM:
DMEM
293T+ev
293T+E3
110 –
media
WB
α-Emilin3
20 –
media
20 –
cells
WB
α-Shh
20 –
cells
WB
α-Actin

Figure S10

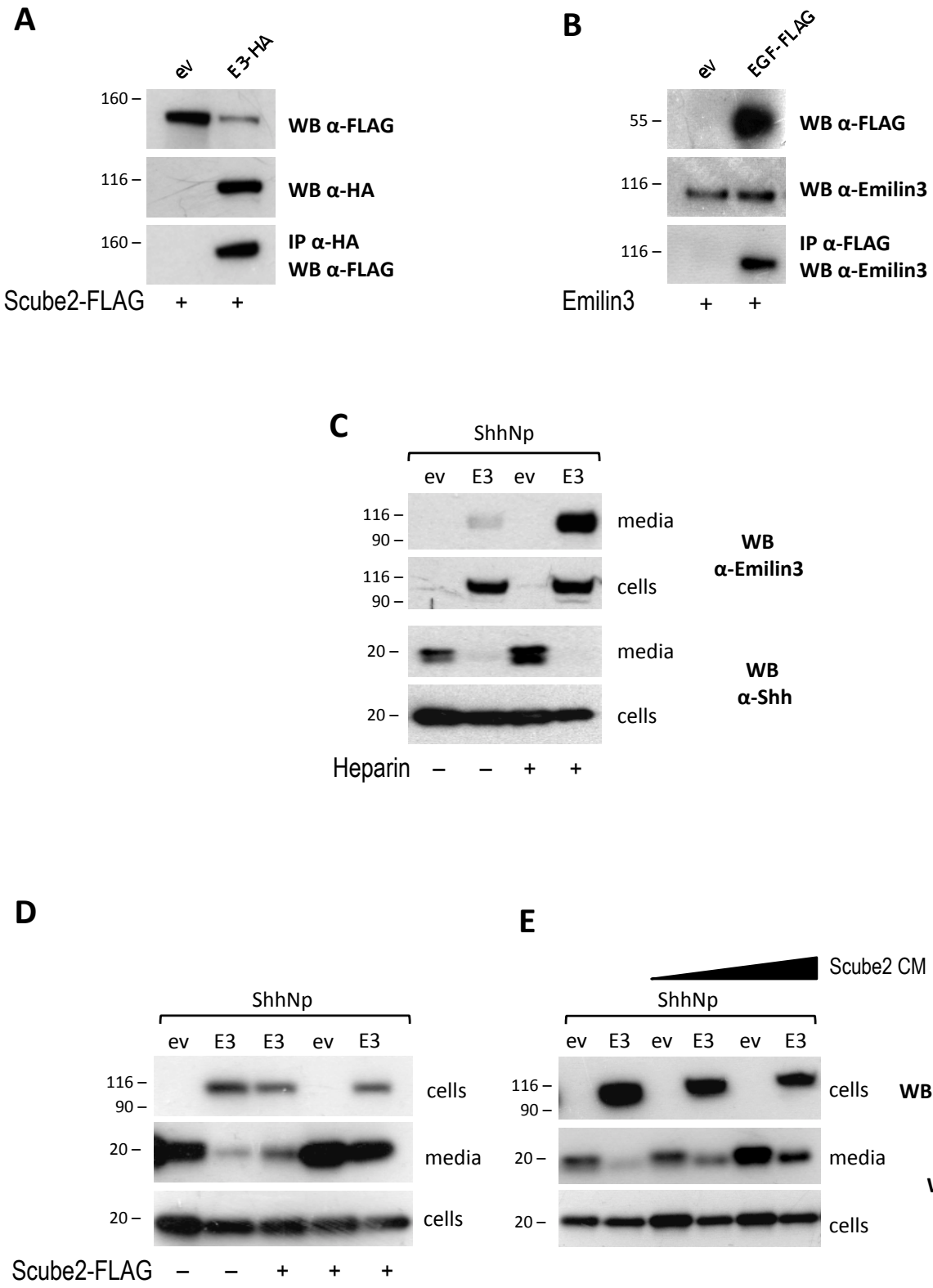
A
ev
E3-HA
160 –
WB α-FLAG
116 –
WB α-HA
160 –
IP α-HA
WB α-FLAG
Scube2-FLAG + +
B
ev
EGF-FLAG
55 –
WB α-FLAG
116 –
WB α-Emilin3
116 –
IP α-FLAG
WB α-Emilin3
Emilin3 + +
C
ShhNp
ev E3 ev E3
116 –
90 –
media
116 –
90 –
cells
WB
α-Emilin3
20 –
media
20 –
cells
WB
α-Shh
Heparin – – + +
D
ShhNp
ev E3 E3 ev E3
116 –
90 –
cells
20 –
media
20 –
cells
Scube2-FLAG – – + + +
E
Scube2 CM
ShhNp
ev E3 ev E3 ev E3
116 –
90 –
cells
WB α-Emilin3
20 –
media
WB α-Shh
20 –
cells

Figure S11

A

B

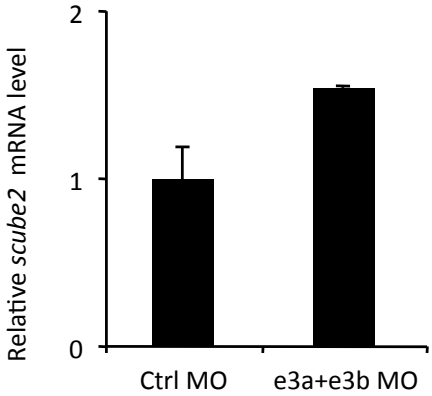

Table S1

Type of morpholino	Dose (ng)	Embryos examined	Phenotype		
			Normal	Notochord defects	Radialized embryos
Ctrl	4	153	151 (99%)	0 (0%)	2 (1%)
e3a (splice)	2	63	61 (97%)	1 (1.5%)	1 (1.5%)
e3a (splice)	4	68	50 (74%)	17 (25%)	1 (1%)
e3b (splice)	2	63	58 (92%)	3 (5%)	2 (3%)
e3b (splice)	4	63	54 (86%)	7 (11%)	2 (3%)
e3a (splice) + e3b (splice)	4 + 4	80	3 (5%)	58 (92%)	2 (3%)
	2 + 2	231	33 (14%)	195 (84%)	3 (2%)
	0.5 + 0.5	55	61 (97%)	1 (1.5%)	1 (1.5%)
e3a (ATG)	2	69	51 (74%)	17 (24%)	1 (2%)
e3b (ATG)	2	51	38 (75%)	13 (25%)	0 (0%)
e3a (ATG) + e3b (ATG)	2 + 2	106	12 (11%)	94 (89%)	0 (0%)
Ctrl	3.5	40	37 (92%)	0 (0%)	3 (8%)
e3a (splice)	2	63	61 (97%)	1 (1.5%)	1 (1.5%)
e3b (ATG)	1.5	42	42 (100%)	0 (0%)	0 (0%)
e3a (splice) + e3b (ATG)	2 + 1.5	62	27 (44%)	33 (53%)	2 (3%)

Table S2

Type of morpholino	Sequence
e3a MO (splice)	5’ –TTACTCATGGATACTTACTTGTGCC– 3’
e3b MO (splice)	5’ –TAGCGTTTACTTACTTATGATGCCC– 3’
col2a1 MO (splice)	5’ –TGAAAAACTCCAACTTACGGTCATC– 3’
e3a MO (ATG)	5’ –TGCAAAATCTTCTCC AGTAGCATGA– 3’
e3b MO (ATG)	5’ –ACGGAAATGCAAGAATCCACCTCAT– 3’
scube2 MO (ATG)	5’ –GCCGTACAGTCCAAACAGCTCCCAT– 3’
p53 MO (ATG)	5’ –GCGCCATTGCTTTGCAAGAATTG– 3’
Ctrl MO	5’ –CCTCTTACCCTAGTTACAATTTATA– 3’

1. Introduction

1.1 The structure of the skin

The skin has a vital role in maintaining body homeostasis by forming an effective barrier between the organism and the environment, preventing invasion of pathogens, and fending off chemical and physical assaults, as well as the unregulated loss of water and solutes (Proksch et al., 2008).
Mammalian skin is a complex organ consisting of several layers. The epidermis is the outermost layer creating a barrier against dehydration and external aggressions. It comprises interfollicular epidermis, hair follicles, sebaceous glands and sweat glands. The underlying dermis provides nutrients to the epidermis and stimulates proliferation. The subcutis contains adipocytes and serves as a nutrient storage for epidermis and dermis (Montagna, 1974b).

1.2 The interfollicular epidermis

The interfollicular epidermis is a multilayered epithelium of the epidermis that lies between hair follicles; it forms the barrier that protects the skin from the external environment. The interfollicular epidermis, as well as many other tissues, is maintained by stem cells that are responsible for the maintenance of tissue homeostasis and repair following injuries.
Undifferentiated, proliferatively active keratinocytes are attached to the basement membrane constituting the stratum basale and remain in contact with the dermis through hemidesmosomes and integrin-based adhesions that provide connections to the underlying ECM (Simpson et al., 2011). Basal keratinocytes express different intermediate filament keratins (K), such as K5, K14 and K15 (Whitbread et al., 1998; Liu et al., 2003). Upon terminal differentiation, basal keratinocytes detach from the basement membrane and move into the stratum spinosum, switching off the expression of K5 and K14.

Concomitantly, spinous cells switch on the expression of genes encoding for K1 and K10, forming an even more robust interfilament network. Cells of the stratum granulosum express further structural cross-linked proteins, like filaggrin and loricrin, that function as scaffolds for lipid bilayers and are important for waterproofing the skin barrier (Blanpain and Fuchs, 2009; Candi et al., 2005). Cells of the stratum granulosum originate the outermost cornified layer of the interfollicular epidermis, the stratum corneum, made of dead cells that serve as the barrier keeping harmful microbes out and essential body fluids in.

1.3 The hair follicle

Hair follicles (HFs) represent the most prominent miniorgan of the skin and one of the defining features of mammals. Primarily, HFs are scattered in the interfollicular epidermis and give rise to the hair shafts. Moreover, due to their nature as a stem cell reservoire, HFs also display high regenerative potential. In fact, the HF is the only organ in the mammalian body which, for its entire lifetime, undergoes cyclic transformations, from periods of organ regeneration and rapid growth (anagen) to apoptosis-driven regression (catagen) (Schmidt-Ullrich and Paus, 2005).

The mature HF can be divided into a 'permanent' upper part and a lower part that is continuously remodelled in each hair cycle (Figure 1). The upper part consists of the infundibulum, the junctional zone, the isthmus and the bulge. The sebaceous gland duct is inserted at the lower end of the infundibulum, thus allowing the secretion of sebum produced from the sebaceous gland to the epidermis. The lower part of the HF consists of the hair shaft factory, the hair bulb, containing the matrix keratinocytes and the HF pigmentary unit. Differentiating keratinocytes that colonize the matrix give rise to the various cell lineages of the hair shaft and the inner root sheath, while the outer root sheath is derived from separated progenitor cells (Legué et al., 2005; Cotsarelis et al., 2006). While infundibulum, isthmus, bulge and hair bulb are all part of the

HF epithelium (i.e. of ectodermal origin), the dermal papilla is mesoderm-derived. Dermal papilla consists of a small cluster of packed mesenchymal fibroblasts that determine hair bulb size, hair shaft diameter and length, and anagen duration.

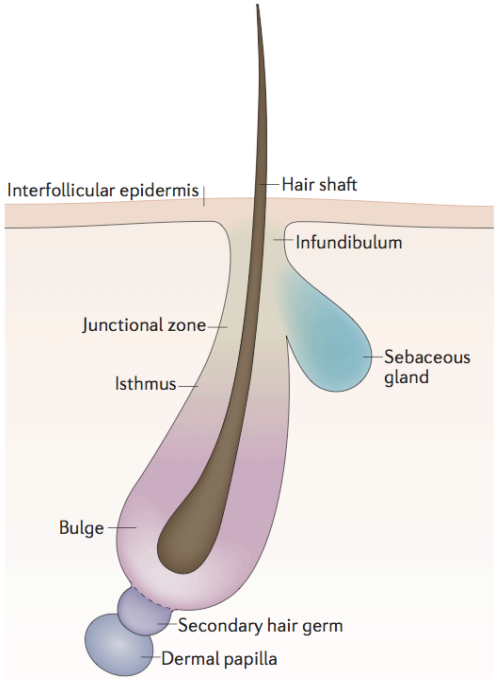

Figure 1. Structure of HFs. The diagram shows a HF in the resting phase (telogen). The interfollicular epidermis forms a barrier against external aggressions. HFs are associated to the interfollicular epidermis and give rise to the hair shafts. The permanent portion of the HF is composed by the infundibulum, the junctional zone, the isthmus and the bulge. Attached to the side of the HF is the sebaceous gland, which contributes to the isolating barrier of the epidermis with its secretions.

1.3.1 Morphogenesis of the hair follicle

Murine HF development can be divided into three phases: induction, organogenesis and cytodifferentiation. These three phases can be subdivided into eight morphologically defined developmental stages (Fig. 2). The key prerequisite for HF development is the molecular communication between the

epidermis and the underlying mesenchyme. In mice, both Wnt and BMP are essential for the development of skin epithelium, which originates from the ectoderm, whereas Wnt/β-catenin signaling alone decides on dermal fate around stage E10.5 of embryonic development (Fuchs, 2007; Atit et al., 2006). Once mesenchymal cells populate the dermis, they start interacting with the overlying epidermis to induce the growth of regularly interspaced epithelial ingrowth into the dermis, called hair placodes (Schmidt-Ullrich et al., 2005; Atit et al., 2006). Epithelial placode cells signal to the underlying mesenchyme to form the dermal condensate, which will give rise to the dermal papilla. In subsequent stages, the hair placode (now called hair germ) becomes visible to the eye and downward growth is initiated. When the HF enters stage 3 of morphogenesis, keratinocytes of the lower part enclose the dermal condensate forming the dermal papilla. During this stage, Shh is an essential growth signal for HF maturation (St-Jacques et al., 1998; Chiang et al., 1999). At stage 5, HFs display an elongated inner root sheath, melanin granules are visible at the precortex, and the dermal papilla is almost completely enclosed by keratinocytes of the HF. At this time, the outer root sheath maintains contact with the basement membrane while the inner layers begin to differentiate to form the inner root sheath, which will serve as the channel for the protruding hair. At stage 6 of HF morphogenesis, a cluster of sebocytes can be seen in the upper part of the HF, the hair canal (infundibulum) becomes visible and a hair shaft is formed within the inner root sheath. At stage 7 of HF morphogenesis, the tip of the hair shaft reaches the hair canal and, at the last stage of HF morphogenesis (stage 8) the hair shaft emerges through the infundibulum and the HF, reaching its maximal length. Besides Wnt/β-catenin and BMP, the signals controlling epidermal-dermal communication include members of the TGF-β, FGF and TNF families (Schmidt-Ullrich et al., 2005; Fuchs et al, 2007). Once HF morphogenesis is completed, the lower part of the HF enters the cyclic renewal and undergoes phases of regression (catagen), rest (telogen) and growth (anagen). Also these phases are tightly controlled by different signaling events.

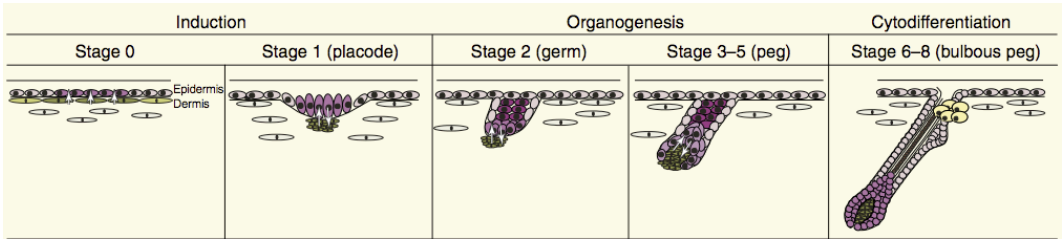

Figure 2. Embryonic stages of HF development. During stage 0, interaction between the epidermis and the underlying dermis is required for the formation of the placode. Different growth signals (such as Wnt/β-catenin and BMP) are needed to form an inductive area. At stage 1, a visible hair germ is formed and during organogenesis the HF growth is initiated. At these stages (3-8) the dermal papilla is formed, the orientation of the HF is defined and the different hair lineages are developed (modified from Schneider et al, 2009).

1.3.2 The hair cycle

Following morphogenesis, existing follicles undergo cycles of regression (catagen), quiescence (telogen) and growth (anagen) throughout life, providing a constant supply of new hairs. After around postnatal day 6 in mice, the HF becomes fully mature as its bulb nears the bottom of the dermis. At this stage, matrix cells located in the bulb continue to proliferate, promoting the formation of the growing hair. After the first 2 weeks of postnatal mouse life, the initial supply of matrix cells declines, hair shaft and inner root sheath differentiation slow, and the HF enters a destructive phase known as catagen. During this phase, the lower "cycling" portion of the HF regresses in a process that includes apoptosis of epithelial cells of the bulb, outer and inner root sheath keratinocytes, while bulge HF stem cells escape apoptosis. This moves the dermal papilla upward to reach the permanent, non-cycling upper follicle (Fig. 3), in close proximity to the bulge. Notably, cells of the secondary hair germ (the epithelial aggregate that appears after the first catagen between the bulge and the dermal papilla) are the first cells that respond to activating signals at the onset of anagen (Lyle et al., 1999; Muller-Rover et al., 2001; Panteleyev et al., 2001). Following catagen, follicles enter in a resting phase (telogen), where HF

stem cells are thought to be quiescent. The proximity between dermal papilla and bulge is maintained throughout telogen and only when a critical concentration of growth activating signals is reached, anagen phase occurs. During this third phase, the bulge progressively moves away from the dermal papilla and epithelial HF stem cells re-adopt quiescence. More distally in the precortical hair matrix, keratinocytes stop proliferating and differentiate into cells of the inner root sheath and hair shaft. As hair shaft cells terminally differentiate, they become tightly packed with cross-linked keratin filaments, which give flexibility and tensile strength to the hair (Fig. 3).

Although multiple molecular regulators have been identified, the molecular players in HF cycling need to be still defined. For example, Wnt/β-catenin, BMP antagonists and Shh act as anagen-inducing signals (Blanpain et al., 2004; Horsley et al., 2008; Kobielak et al., 2007; Rendl et al., 2008). More recently, it has been proposed that cells of the dermal papilla emit TGF-β2, thus repressing active BMP signaling and leading to activation of secondary hair germ cells (Oshimori and Fuchs, 2012). Moreover, FGF5 plays a key role in inducing catagen (Hebert et al., 1994; Paus and Foitzik, 2004; Stenn and Paus, 2001).

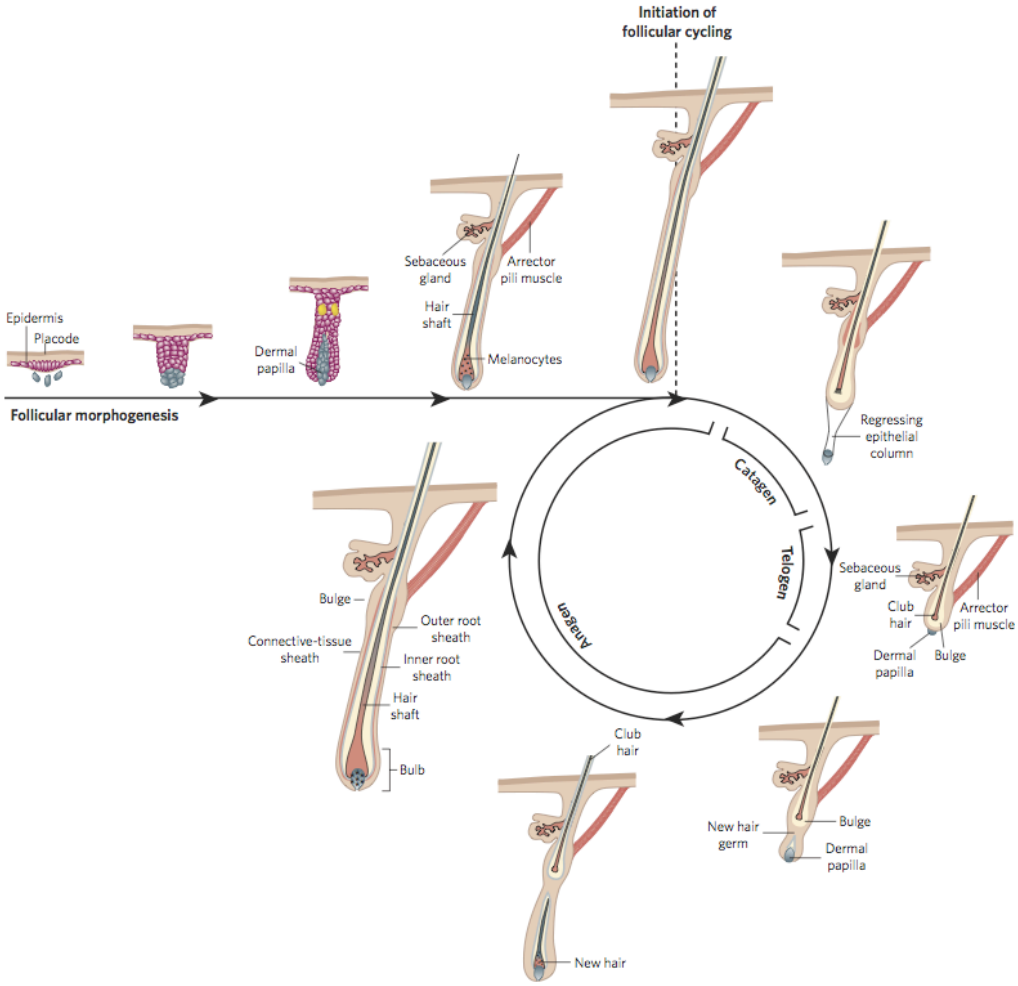

Figure 3. Key stages of the hair cycle. Stages of embryonic hair development (upper left) and HF cycle are shown. The hair cycle can be divided into three phases: anagen (growth phase), catagen (regression phase) and telogen (quiescent phase). Once HF has matured, it enters the regression phase during which the lower-cycling portion of the HF is degraded. This process brings the dermal papilla in close proximity to the bulge and this interaction is maintained throughout the telogen phase. Only when a critical concentration of activating factors is reached, the stem cells become activated to re-growth the hair through a new anagen (From Fuchs, 2007).

1.3.3 The hair follicle stem cell compartment

In order to produce a new hair, pre-existing HFs need to regenerate. For this purpose, and for the maintenance of the epidermis and sebaceous gland, several populations of stem cells are present in HFs (Figure 4). The role of these resident stem cells is fundamental for maintaining the correct skin homeostasis,

as well for repairing damaged areas. Previous studies revealed the presence of reservoirs of multipotent epithelial stem cells found in the lowest, permanent portion of the HF – the bulge (Taylor et al., 2000; Morris et al., 2006). It was shown that bulge stem cells are able to regenerate the cycling portion of the HF, whereas they do not contribute to the interfollicular epidermis unless it has been damaged (Ito et al., 2005; Levy et al., 2007). More recently, it has been shown that different epidermal stem cell pools are distributed along the longitudinal and vertical axes of the HF. These pools are characterized by the expression of different genetic markers and they contribute to different temporal phases of the hair cycle and to different regions of the HF above the bulge.

The more proliferative cells in the lower portion of the bulge are in close contact with the secondary hair germ and are enriched in the expression of LGR5 (leucine-rich repeat-containing G protein-coupled receptor 5; Barker et al., 2007). These LGR5-positive cells also express the Hh-activated transcription factor GLI1, which is absent in mid bulge cells but, interestingly, present again in the upper bulge region (Brownell et al., 2011). While during telogen the high expression of LGR5 and GLI1 extends also to the secondary hair germ, in anagen HF the localization of these markers shifts to the lower part of the outer root sheath. This changed expression is indicative of a cellular trafficking from the bulge to the growing portion of HF (Hsu et al., 2011). Interestingly, secondary hair germ cells are molecularly similar to bulge stem cells, showing a multipotent capacity and the ability to de-differentiate into bulge stem cells when this compartment is depleted (Ito et al., 2004). A separate cell population at the lower part of the bulge express high levels of SOX9, K15 and CD34, whereas another pool of upper bulge stem cells express high levels of GLI1, but not CD34 and K15. Strikingly, although lower bulge and hair germ stem cells are the first to contribute to the HF cycling, upper bulge stem cells are efficient as the lower counterpart in giving rise to all the HF lineages during anagen.

Besides the bulge, other progenitor compartments have been described during the past years. In the juctional zone, cells are defined by the expression of LGR6 (leucine-rich repeat-containing G protein-coupled receptor 6) and high levels of

the epithelial stem cell marker MTS24 (Nijhof et al., 2006). Lineage tracing experiments showed that these cells contribute to the maintenance of the junctional zone and sebaceous gland (Snippert et al., 2010). A further stem cell population residing in the upper part of the junctional zone and expressing LRIG1 (leucine-rich repeats and Ig-like domains protein 1) has been recently described. It was suggested that LRIG1-positive cells contribute to the interfollicular epidermis and sebaceous glands during normal homeostasis (Jensen et al., 2009), whereas in a wounded area they act as multipotent stem population that contribute to all the follicular, sebaceous and interfollicular lineages (Jensen et al., 2009). Finally, at least three different types of cells, LRIG1-positive, LGR6-positive and bulge cells, contribute to the maintenance of the sebaceous gland. Apart from these, a fourth population of cells arising from the bulge and expressing BLIMP1 (B lymphocyte-induced maturation protein 1) acts as a unipotent sebaceous gland progenitor lineage (Horsley et al., 2006).

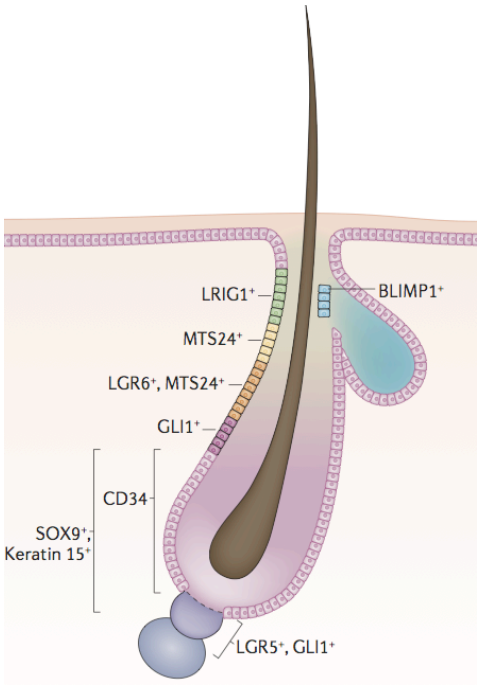

Figure 4. The HF stem cell pool. The diagram represents the different stem cell populations distributed among the vertical axis of the HF.

30

2. METHODS

2.1 Mice

Emilin1$^{-/-}$ mice were generated as previously described (Zanetti et al., 2004) and maintained on a C57BL/6J background. Animal procedures were approved by the Ethics Committee of the University of Padova and authorized by the Italian Ministry of Health.

2.2 Genotyping

Genotyping of Emilin3 null mice was performed by polymerase chain reaction on genomic DNA extracted from tail biopsies of 1 month-old animals, using the following primers:
Emilin3: 5'– ACA GCC CAG TGC CTC CCG TTA CA –3' (forward), 5'– CAG GGT GCC ATA TGC TTG CGA CA –3' (reverse), reaction product: 487 bp; neo cassette: 5'-ATC TCC GGG CCT TTC GAC -3' (forward), 5'- GAC TTA CAG CGG ATC CCT CA -3' (reverse), reaction products: 696 bp.
Polymerase chain reaction consisted in an initial step of denaturation at 94°C for 3 min, followed by 35 cycles of denaturation (94°C for 30 sec), primer annealing (58°C for 30 sec) and elongation (72°C for 1 min and 30 sec). After a final elongation step at 72°C for 7 min, the reaction products were separated in 1% agarose gels. All PCR reactions were done in a *MJ Mini 48-well* gradient thermal cycler (BioRad).

2.3 Southern blotting

Genomic DNA was isolated from ES cells or tail biopsies as previously described (Laird et al., 1991), digested with *Sph*I or *Nco*I, separated on 0.8% agarose gels, transferred to a Gene Screen membrane (PerkinElmer Life Sciences), and

hybridized with two different 1.0-kb genomic fragments as external probes (Fig. 3A). Insertion of the *neo* cassette in the *Emilin3* gene introduced new *Sph*I and *Nco*I restriction sites that were used to distinguish between the wild-type and the targeted *Emilin3* alleles, which produced 8.4- and 7.2-kb or 5.5- and 4.1-kb fragments, respectively.

2.4 Histology

For the histological analysis, newborn, 10-days, 15-days, 17-days, 20-days, 30-days old mice were sacrificed by cervical dislocation and the skin was isoated as described before (Paus et al., 1999).
For cryo-sectioning, the unfixed skin was embedded in OCT (Histo-Line Laboratories), allowed to freeze slowly in liquid nitrogen and stored at -80°C. Cryostat sections (8 μm) were collected on SuperfrostPlus slides (BHD), air dried at room temperature and kept at -20°C.

2.5 Haematoxilin-eosin staining

To visualize skin morphology, sections were stained with haematoxilyn (Sigma Aldrich) for 3 min, followed by tab water to develop the staining. After brief washing in distilled water, sections were counterstained with eosin (Sigma Aldrich) for 1 min and dehydrated in 100% ethanol and 100% xylene. Finally, samples were mounted with Pertex (Leica) and observed in a Zeiss Axioplan microscope equipped with epifluorescence optics.

2.6 Immunofluorescence

After a short wash in PBS buffer, frozen sections were fixed for 5 min in cold 100% methanol. Then, sections were saturated with 1% BSA in PBS (Sigma) for 30 min. The antibodies used were the following: polyclonal guinea pig anti-Emilin3 (1:1000; Schiavinato et al., 2012), polyclonal rat anti-Emilin1 (1:250, Zanetti et al., 2003), monoclonal mouse anti-cytokeratin 15 (1:200; Thermo

Scientific, MA5-11344), monoclonal rabbit anti-nidogen 1 (1:3000; kind gift of Dr. Christian Frie, University of Cologne).

Reactions were developed by incubation with Cy-2 conjugated donkey anti-guinea pig IgG antibody (1:500; Jackson ImmunoResearch), Cy-3 conjugated goat anti-mouse IgG antibody (1:1000; Jackson ImmunoResearch), Cy-3 conjugated goat anti-rabbit IgG antibody (1:800; Jackson ImmunoResearch), Cy-3 goat anti-rat IgG antibody (1:300; Jackson ImmunoResearch).

Nuclei were visualized with Hoechst and slides were mounted using fluorescent mounting medium (DAKO). Images were taken with a Leica SP5 confocal microscope.

3. Results

3.1 Emilin3 has a restricted distribution in adult mouse tissues and colocalizes with Emilin1.

We recently demonstrated that Emilin3 has a restricted protein distribution, and it is not present in the cardiovascular system and parenchymatous organs, such as heart, blood vessels, kidneys, spleen and liver (Schiavinato et al., 2012). To compare Emilin3 and Emilin1 distribution in adult tissues, double immunofluorescence were carried out using an affinity-purified antiserum guinea pig raised against mouse Emilin3 and a rat antiserum against mouse Emilin1.

In agreement with our previous findings, strong Emilin3 labeling was detected in the pericondrium surrounding the elastic cartilage of the trachea, and Emilin3 labeling almost entirely overlapped with Emilin1 (Fig. 1A). A colocalization of Emilin3 and Emilin1 was also detected in the myenteric plexus of the gastrointestinal tract, but not in epithelium lining the villus, where only Emilin1 is deposited (Fig. 1B, C). In testis, Emilin3 and Emilin1 labeling colocalization was found in the collagenous structure of the tunica albuginea, in which Emilin1 appeared more abundant whereas Emilin3 seemed to be restricted only in the most external layer. Colocalization of the two proteins was also observed in the basement membrane surrounding each seminiferous tubule (Fig. 1D). Finally, the epimysium and the endomysium of many (but not all) quadriceps myofibers were labeled for Emilin3, and a partial colocalization with Emilin1 could be observed in these structures.

To test whether the deposition of Emilin3 might be affected by the absence of Emilin1, we carried out immunofluorescence analysis of testis from adult wild-type and Emilin1 null mice. As expected, in wild-type testis Emilin1 and Emilin3 were particularly abundant in the collagenous structure of the tunica albuginea and in the basement membrane surrounding each seminiferous tubule. Despite the absence of Emilin1, Emilin3 was still present and normally distributed in

Emilin1 null testis, suggesting that Emilin1 is not required for the normal deposition of Emilin3 in the ECM (Fig. 2 and data not shown).

Altogether, this analysis showed that Emilin3 largely colocalizes with Emilin1 but has a much more restricted distribution in adult mouse tissues. Furthermore, Emilin1 is dispensable for the ECM deposition of Emilin3 in adult tissues.

3.2 Emilin3 is expressed in hair bulge and contacts the bulge basement membrane.

We examined the distribution of Emilin3 in the skin at different postnatal stages. After birth, Emilin3 was highly expressed as a thick network in the dermis around each growing HF. Interestingly, no Emilin3 labeling could be detected in the epidermis (Fig. 3A). When HF growth had begun (P10), Emilin3 expression decreased and it became detectable only in the basement membrane of K15-positive early bulge stem cells as well as at the base of the follicle (Fig. 3B). At this time, Emilin3 deposition in the bulge was asymmetrically distributed at the posterior side. During the first telogen and the first anagen phases (P20, P30) Emilin3 labeling was maintained in the bulge and more strongly at the anchoring site of the arrector pili muscle (Fig. 3C and data not shown). To evaluate whether Emilin3 could be localized in the basement membrane surrounding HF, double immunofluorescence with nidogen1 were carried out. Although no strong colocalization was observed, many Emilin3-positive fibrils appeared to contact the basal membrane, reaching up K15-positive early bulge stem cells (Fig. 3D).

Altogether, these results indicate that Emilin3 has a very peculiar and dynamic deposition pattern in postnatal mouse skin, where it is asymmetrically confined in the hair bulge and contacts the basement membrane of each HF.

3.3 Generation of Emilin3-deficient mice.

In order to study the function of Emilin3, targeted inactivation of the *Emilin3*

gene was carried out by partial deletion of exon 1 and insertion of a *neo* cassette (Fig. 4A). This deletion removed the sequence coding for the first 50 amino acid residues, including the signal peptide. Consequently, following insertion of the targeting construct into the ES cell genome and homologous recombination with the endogenous *Emilin3* allele, no functional domains of Emilin3 should be contained in the translation product of the mutated gene. Targeted ES clones were characterized by *Sph*I digestion and Southern blotting, revealing expected fragments for the wild-type allele (8.4 kb) and for the targeted allele (7.2 kb) in the four targeted ES clones, while the non-targeted ES clones contain only the fragment corresponding to the wild-type allele (Fig. 4B). These correctly targeted ES clones were injected into host blastocysts, and different chimerice mice successfully transmitting the ES-derived *Emilin3* null allele in their germline were obtained, giving rise to heterozygous (*Emilin3*$^{+/-}$) mice. Litters generated by *Emilin3*$^{+/-}$ animals allowed to obtain homozygous mutant (*Emilin3*$^{-/-}$) mice, as revealed by Southern blotting using *Nco*I-digested genomic DNA (Fig. 4C). To confirm that *Emilin3*$^{-/-}$ mice had a complete ablation of Emilin3 protein, tissue sections from adult animals were analyzed by immunofluorescence. A network of short and fine fibrils was present in the tissues of wild-type mice, whereas Emilin3 was completely absent in sections prepared from *Emilin3*$^{-/-}$ mice (Fig. 4D and data not shown). Interestingly, immunofluorescence analysis with Emilin1 antibodies showed similar labeling in tissue sections from wild-type and *Emilin3*$^{-/-}$ mice, suggesting that ablation of Emilin3 does not affect the deposition of Emilin1 fibrils (Fig. 4D and data not shown).

3.4 Emilin3 null mice display pronounced hair phenotype, body weight loss and reduced lifespan.

To investigate the role of Emilin3 in postnatal life, I carried out a first characterization of *Emilin3* null mice. Lack of Emilin3 did not result in any gross macroscopic change or anatomical alterations within the first 15 days after birth. However, starting from postnatal day 17 (P17), *Emilin3*$^{-/-}$ mice developed

an increasingly pronounced hair phenotype, characterized by different extents of hair loss (Fig. 5A). At the same time, body size was also affected in *Emilin3*$^{-/-}$ mice. Whereas at birth and until two weeks of age the mean body weight of wild-type and *Emilin3*$^{-/-}$ animals was not different, starting from P17 Emilin3 null mice displayed a significantly lower body weight than wild-type littermates (Fig. 5B). This reduction became more evident between the third and the fourth week of age, and the phenotype was frequently correlated with an increased mortality of *Emilin3*$^{-/-}$ mice that reached about the 65% of the animals (Fig. 5C). Interestingly, the shortened lifespan of *Emilin3*$^{-/-}$ mice had a partial penetrance: surviving animals were fertile, had growth rates indistinguishable from that of controls, and did not display any gross abnormality. To confirm that the absence of Emilin3 was directly affecting the lifespan of mice, we determined the survival curves of another independent *Emilin3*$^{-/-}$ mouse line, obtained from chimeras generated from a different ES cell clone. Interestingly, these mice displayed the same trend of survival rate we observed in the first *Emilin3*$^{-/-}$ mouse line (Fig. 5C). Altogether, these data indicate that lack of Emilin3 leads to a progressive loss of body weight and reduced lifespan, suggesting a protective role of this ECM protein during the first weeks of mouse postnatal life.

3.5 Emilin3 ablation is dispensable for hair follicle formation but affects normal hair growth.

As discussed in detail above (section 3.2), immunofuorescence analysis of postnatal skin samples showed that Emilin3 has a very peculiar and dynamic expression pattern that is asymmetrically confined in the hair bulge and only in part in the basement membrane of each HF. To assess whether Emilin3 is involved in the proper development and cycling of HFs, haematoxilin-eosin stainings were performed on cryostat sections from wild-type and Emi3$^{-/-}$ mice. Inactivation of Emilin3 did not result in any obvious histological change in newborn and in 10-day old mice, where HFs appeared normally formed. Also during the first catagen at 15 days of postnatal age, histological analysis did not reveal any gross abnormality (Fig. 6A). However, starting from postnatal day 17,

Emilin3$^{-/-}$ mice developed an expansion of the upper areas of the HF, the so-called junctional zone and infundibulum, and a progressively increased number of irregularly shaped HFs. Notably, during the first resting phase (telogen), more than 80% of *Emilin3*$^{-/-}$ HFs were bent and coiled when entering the hair canal, subsequently dilating the infundibulum. By postnatal day 30, when the first anagen had begun, most hair canals were dilated and contained cornified debris as well as a small and curly keratinized hair shaft that did not penetrate the epidermis (Fig. 6B). Moreover, many HFs containing cystic infundibulum domains that possessed larger luminal areas were found in *Emilin3*$^{-/-}$ mice (Fig. 6B).

Notably, no significant difference in the mean number of HFs was found at all the analyzed stages (Fig. 7A), whereas only at the first anagen a significantly increased thickness of dermis was observed in *Emilin3*$^{-/-}$ mouse skin (Fig. 7B).

Although further studies will be needed to fully address the role of Emilin3 in hair growth, these results suggest that Emilin3 might be important during the first HF cycle progression.

3.6 Lack of Emilin3 results in the reduction of K15-positive bulge stem cells.

Since Emilin3 was detected in the basement membrane of K15-positive early bulge stem cells and its distribution was confined in this compartment during the first hair cycle, we investigated whether the morphological defects of *Emilin3*$^{-/-}$ HFs was accompanied by alterations in bulge stem cell identity. Strikingly, staining for the bulge stem cell marker K15 revealed a strongly reduced signal at P17 (data not shown) and P20 in *Emilin3*$^{-/-}$ HFs compared with controls (Fig. 8A). This reduction was also quantified by counting the mean number of K15-positive cells in the bulge of wild-type and *Emilin3*$^{-/-}$ mice (Fig. 8B). Notably, the loss of K15-positive cells was not extended to the interfollicular epidermis of *Emilin3*$^{-/-}$ animals, where this keratin appeared normally expressed. These data suggest that the HF stem cells located in the bulge may have lost quiescence. Future mechanistic studies will allow

characterize in better detail this HF stem cell phenotype, thus unraveling a possible role of Emilin3 in the regulation of HF stem cells quiescence and in the maintenance of skin homeostasis.

4. Discussion

The ECM is a macromolecular scaffold present in all the tissues of metazoan organisms, providing mechanical support and cell anchorage, as well as essential biochemical and biomechanical signals, through which ECM can instruct and influence many cellular functions in both physiological and pathological conditions. The ECM is a complex meshwork of crosslinked insoluble proteins and displays a high degree of compositional heterogeneity in different tissues (Hay, 1991; Adams and Watt, 1993). In mammals, around 300 ECM proteins (divided in collagens, proteoglycans and glycoproteins) constitute the "matrisome" (Hynes and Naba, 2011). An important functional subgroup of the "matrisome" is composed of proteins forming the elastic fibers, which include elastin, fibrillins, fibulins, LTBPs, MAGPs and versican. Emilins are glycoproteins of the ECM that are characterized by the presence of a highly conserved cysteine-rich EMI domain at their N-terminus. Emilin1 has been originally isolated as a component of elastic fibers in the chicken aorta (Bressan et al., 1983) and Emilin2 and Emilin3 were subsequently identified (Braghetta et al., 2004). We recently found that Emilin2 and Emilin3 are novel components of the elastic fibers, where they are deposited in association with fibrillin microfibrils (Bonaldo and coll., unpublished data). Emilin1 knockout mice display multiple phenotypes that highlight the function of this protein in the homeostasis of structures enriched in elastic fibers (Zanetti et al., 2004, Zacchigna et al. 2006, Danussi et al., 2013).

We have recently demonstrated that Emilin3 has a restricted protein distribution. The most remarkable difference between Emilin3 and other members of the Emilin/Multimerin family is its absence from the cardiovascular system (Milanetto et al., 2008; Schiavinato et al., 2012). In adult mouse tissues, Emilin3 is particularly abundant in the basement membrane of seminiferous tubules and throughout the gastro-intestinal tract, in close association with the myoenteric plexus. Emilin3 is also present in skin and in adult skeletal muscle, with a peculiar distribution around some muscle fibers (Schiavinato et al.,

2012).

The data obtained in this part of my PhD thesis work demonstrate that Emilin3 distribution, although restricted, largely overlaps with that of Emilin1 in normal adult tissues, suggesting that these two ECM proteins could indeed interact *in vivo*. The data obtained in *Emilin1*$^{-/-}$ mice indicate that the deposition of Emilin3 is not modified by Emilin1 deficiency, thus providing an *in vivo* evidence that Emilin1 is not essential for the incorporation of Emilin3 fibers in the ECM. Further *in vitro* and *in vivo* studies will be required to explore the nature of the interaction between Emilin1 and Emilin3, as well as the interactions of both proteins with other components of elastic fibers and the ECM.

Among the tissues mentioned above, one the most interesting distribution patterns of Emilin3 is related to skin. The data obtained in wild-type animals show an abundant deposition of Emilin3 in newborn dermis, where Emilin3-positive fibrils form a reinforced network around each growing HF that reaches the interfollicular epidermis. As the development proceeds, Emilin3 becomes confined to the bulge basement membrane, irrespective to the hair cycle, and particularly reinforced to the permanent attachment site of the arrector pili muscle, which is responsible for raising the hair follicles (piloerection) to trap body heat and express emotions. Moreover, the data indicate that Emilin3 does not fully colocalize with nidogen 1, one of the major components of basement membranes (Breitkreutz et al. 2013; Mokkapati et al., 2008). Notably, Emilin3 fibrils appear to contact nidogen1 only in the hair bulge. The Emilin3 association with the hair bulge basement membrane suggests that this protein could be linked to an elastic microfibril network deposited in the dermis and anchored to the basement membrane components.

The basement membrane is an essential structure that allows epidermal-dermal communication that is essential for skin homeostasis (Grose et al., 2007). It provides links to both the intracellular cytoskeletal keratins in keratinocytes and connective tissue proteins of the dermis (i.e., collagen fibers and elastic microfibrils; Masunaga et al., 1997). For example, the basement membrane protein Laminin-511 mediates epidermal-dermal papilla signaling during hair development (Gao et al., 2008). The basement membrane of the skin exhibits

local variation in structure and composition (Timpl, 1996) and these characteristics may assign and influence distinct stem cell niches and could also result in local differences in signaling with adjacent mesenchymal cells (Akiyama et al., 1995; Fuchs, 2008). Gene expression profiling of the bulge compartment revealed that bulge stem cells express different ECM proteins that differs from those of other epidermal cells (Morris et al., 2004; Ohyama et al., 2006; Tumbar et al., 2004). For example, nephronectin is an ECM protein deposited from bulge stem cells into the underlying basement membrane and in arrector pili muscle, which creates a smooth muscle stem niche and induces arrector pili muscle differentiation and anchorage to the bulge (Fujiwara et al., 2011). Our immunofluorescence data show that Emilin3 has a peculiar distribution in mouse skin in comparison with other mouse tissues and with the zebrafish ortologs (see Results 3.1; Corallo et al., 2013), since it is not a basement membrane component. Moreover, the restricted deposition of Emilin3 confined to the hair bulge and particularly reinforced in the attachment site of the arrector pili muscle suggests that this ECM protein might have a specific role in the development/homeostasis of the HF bulge.

In order to elucidate the function of Emilin3 *in vivo*, I carried out an initial phenotypic characterization of two different *Emilin3* knockout mouse lines that were previously engineered in our laboratory. The phenotypes of these two *Emilin3* knockout mouse lines were remarkably similar, thus confirming that the observed defects are directly related to the absence of Emilin3. Emilin3 depletion results in a progressively severe hair phenotype that becomes evident during the first catagen phase. At this time, histological analysis showed the expansion of the upper areas of the junctional zone and infundibulum, together with an increasing number of irregularly shaped HFs containing cornified debris. When the first anagen occurrs, small and curly keratinized hair shafts that do not penetrate the epidermis can be visualized, together with the onset of epidermoid cysts. In addition, Emilin3 depletion results in a gradual loss of quiescent epidermal bulge stem cells expressing the K15 marker.

These data point at a role for Emilin3 in maintaining the correct HF homeostasis and different mechanisms may be proposed. Previous *in vitro* studies indicated

that Emilin3, as Emilin1, participate in the extracellular regulation of the bioavailability of TGF-β ligands (Schiavinato et al, 2012; Zacchigna et al., 2006). In addition, other data obtained during my PhD work indicate a physiological role of zebrafish Emilin3 orthologs in limiting notochord-derived Hh signals (see Section 3.2; Corallo et al., 2013). These two signaling pathways are known to be important molecular regulators that drive HF development and cycling. In particular, TGF-β1 has been described as a catagen inducer (Paus and Foitzik, 2004), and more recently it has been proposed that TGF-β2 secreted from the dermal papilla leads to the activation of secondary hair germ cells (Oshimori and Fuchs, 2012), resulting in an anagen-inducing stimulus. Despite its role in controlling ingrowth and morphogenesis of the HF (St-Jacques et al., 1998), the Hh pathway is also required for hair growth phases of the hair cycle in juvenile and adult mice (Chiang et al., 1999). Moreover, previous studies pointed out a role of the Hh signaling in sebocyte cell fate decisions and sebaceous gland formation and activity (Allen et al., 2003). Therefore, the most likely hypothesis is that loss of Emilin3 perturbs the deposition or the activation of secreted growth factors associated to the basement membrane. The possibility that Emilin3 could be a regulatory component of these signaling pathways, required to maintain the normal structure and homeostasis of HFs, will be the aim of future studies.

As discussed above, Emilin3 is associated with the basement membrane component nidogen1. In Emilin3 null animals, as a result of the loss of this interaction, the production of stable microfibril macroaggregates might be impaired, thus leading to structural defects. Moreover, Emilin3 may regulate cell attachment to the bulge basement membrane, promoting cell growth, differentiation and migration. In Emilin1, the gC1q domain confers the ability for the attachment of smooth muscle cells to elastic fibers (Doliana et al., 1999; Colombatti et al., 2000). Despite the lack of the gC1q domain in Emilin3, the cell adhesion properties of Emilin3 were never investigated before. Further studies will be required to understand the fate of lower bulge stem cells in Emilin3 null mice and whether this phenotype may lead to a loss of proliferative potential, stem cell exhaustion, and premature aging.

Previous works showed that mice where Shh responsiveness was abrogated in skin keratinocytes survived at least 12 days after birth, up to a maximum of about 3 months (Gritli-Linde et al., 2007). In addition, transgenic mice with an expanded pool of keratinocytes in which the Shh pathway is active, generated by a gain-of-function Smoothened mutant driven by K5 promoter, displayed a perinatal lethality (Xie et al., 1998; Allen et al., 2003). Interestingly, starting from postnatal day 17, Emilin3 null mice display an increased lethality between the third and the fourth week of age, reaching about the 65% of the animals. Although the ablation of Emilin3 was not specifically restricted to the skin epithelium and the increased lethality did not show a full penetrance in our knockout mouse model, a relationship between the observed skin phenotype and the lower survival rate could not be excluded. Further studies will help elucidating whether and how the absence of Emilin3 may alter the protective role carried out by the skin barrier.

In summary, the skin morphological abnormalities detected within this part of my PhD work in Emilin3 null mice reveal a new role of this ECM protein in the regulation of skin homeostasis.

Figure 1

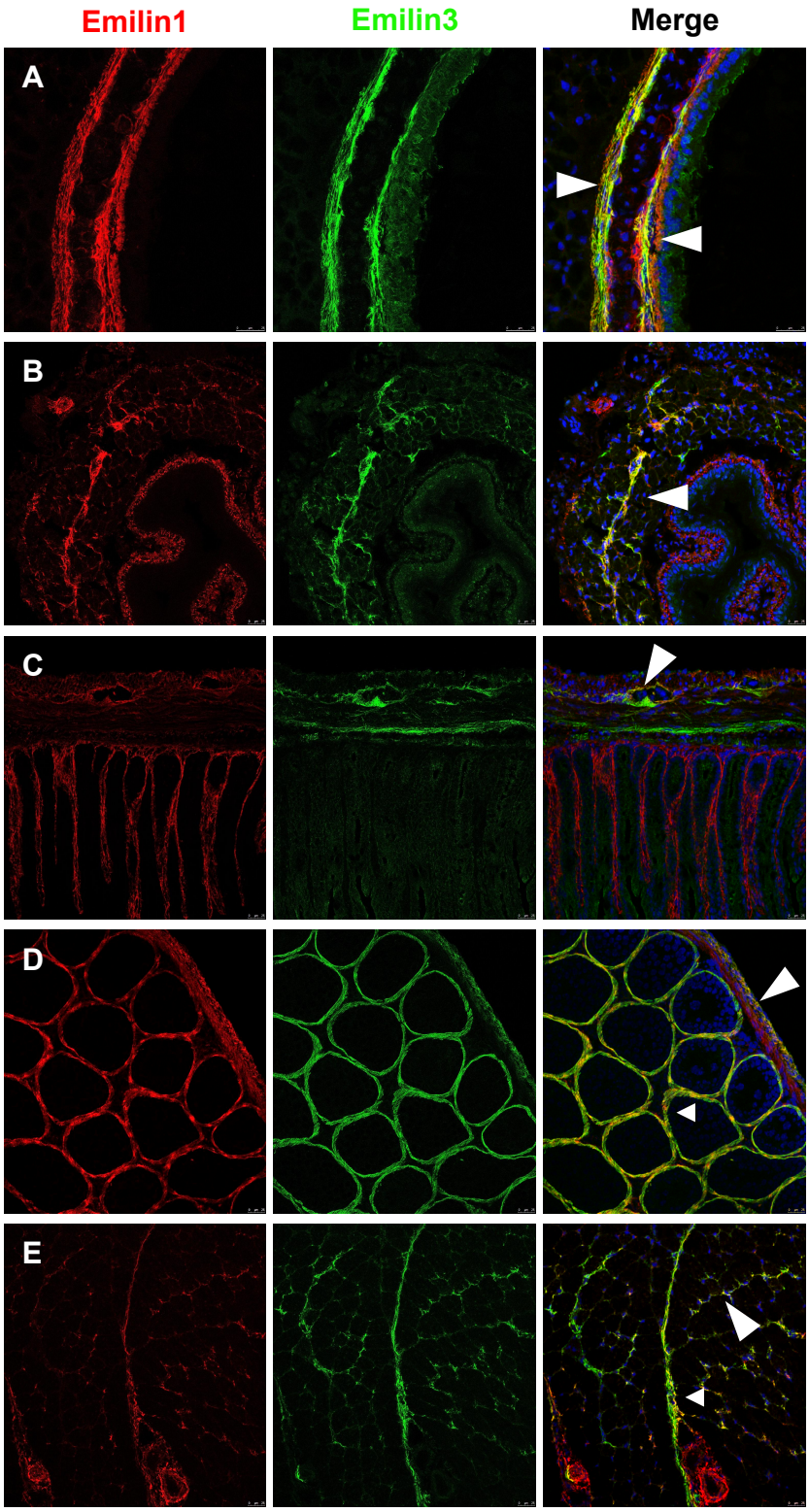

Figure 1. Emilin3 colocalizes with Emilin1 in wild-type adult mouse tissues. Cryostat sections of 1-month-old mouse tissues were analyzed by immunofluorescence with Emilin1 (Emi1; red) and Emilin3 (Emi3; green) antibodies, showing colocalization in (**A**) the pericondrium surrounding trachea cartilage (arrowheads), the myenteric plexus of (**B**) esophagus and (**C**) colon (arrowheads), (**D**) the tunica albuginea (arrow) and the basement membranes of seminiferous tubules (arrowhead), (**E**) the perimysium (arrow) and endomysium (arrowheads) of several quadriceps myofibers. Nuclei were stained with Hoechst (blue). Scale bar, 25 μm.

Figure 2

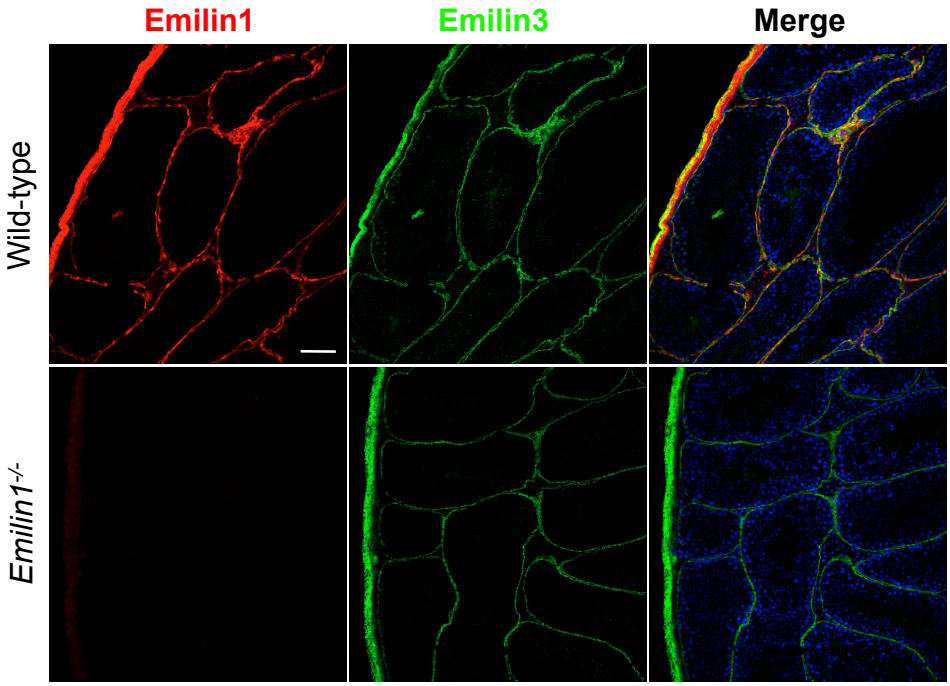

Figure 2. Emilin1 is dispensable for Emilin3 deposition. Cryostat sections from 3-month-old wild-type and Emilin1 null mouse testis, immunostained for Emilin1 (red) and Emilin3 (green) together with DAPI counterstain (blue). Emilin3 is still present in *Emilin1*$^{-/-}$ testis, indicating that Emilin1 is not required for the normal deposition of Emilin3 in the ECM. Scale bar, 75 μm.

Figure 3

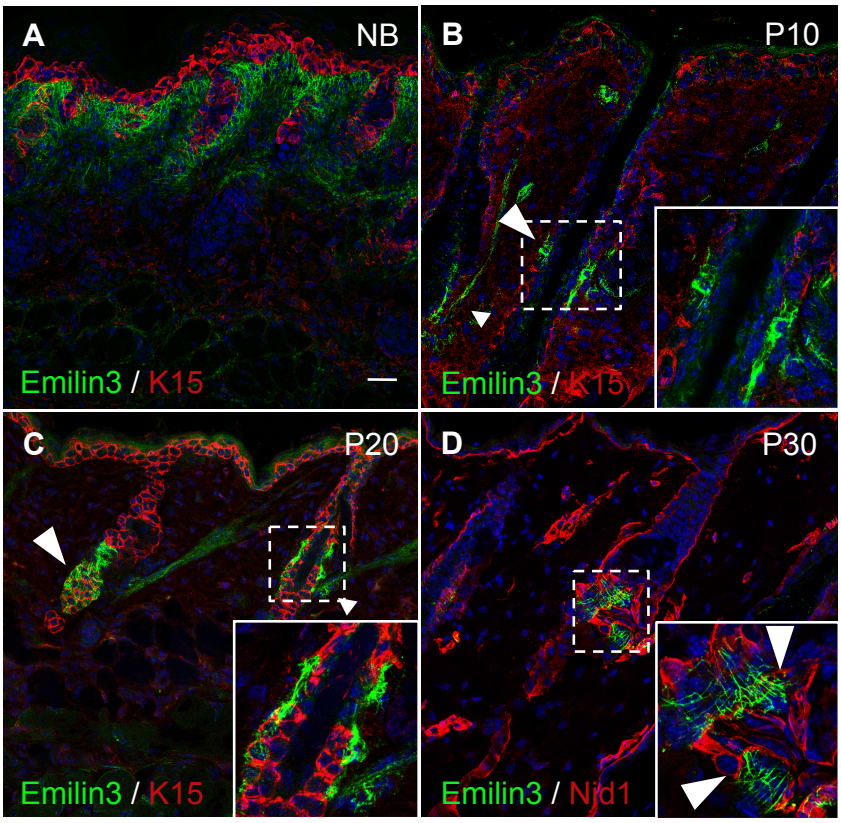

Figure 3. Emilin3 localization in skin. Cryostat sections of (**A**) newborn, (**B**) P10 and (**C**) P20 back skin were immunostained for Emilin3 (green) and for the bulge stem cell marker K15 (red), together with DAPI counterstain (blue). Emilin3 localizes in the upper dermis of newborn skin, whereas its expression decreases and becomes restricted in bulge (arrowhead) and arrector pili muscle (arrows). Cryostat sections of (**D**) P30 skin were immunostained for Emilin3 (green) and nidogen1 (Nid1; red). Emilin3 only partially colocalizes with nidogen1 in the basement membrane of HF (arrows). Nuclei were stained with Hoechst (blue). The insets show higher magnification details of the corresponding panel. Scale bar, 25 μm.

Figure 4

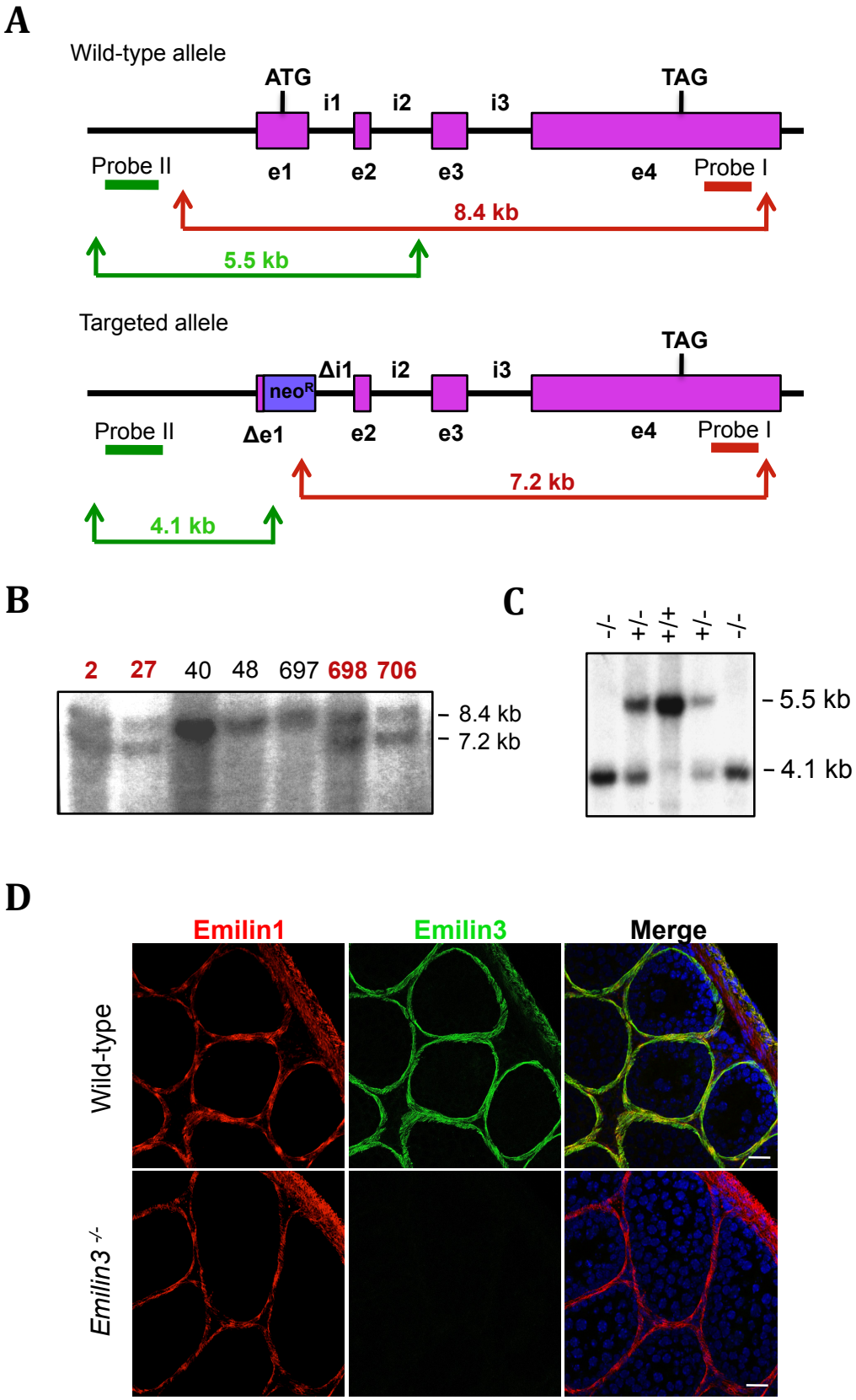
A
Wild-type allele
ATG
TAG
i1
i2
i3
Probe II
e1
e2
e3
e4
Probe I
8.4 kb
5.5 kb
Targeted allele
TAG
Δi1
i2
i3
neoR
Probe II
Δe1
e2
e3
e4
Probe I
7.2 kb
4.1 kb
B
2
27
40
48
697
698
706
8.4 kb
7.2 kb
C
-/-
+/-
+/+
+/-
-/-
5.5 kb
4.1 kb
D
Emilin1
Emilin3
Merge
Wild-type
Emilin3 -/-

Figure 4. Generation of Emilin3 knockout mice. (**A**). Schematic representation of *Emilin3* wild-type allele and the expected targeted allele after homologous recombination in ES cells. The diagram represents the wild-type and targeted alleles, with the position of external probes (probe I and probe II) and the fragments generated by digestion with restriction enzymes *Sph*I and *Nco*I, respectively. (**B**) Characterization of four targeted ES cell clones (2, 27, 698, 706) and three non-targeted ES clone (40, 48, 697) by Southern blotting of genomic DNA digested with *Sph*I and hybrided with external probe I. (**C**) Southern blot analysis of DNA extracted from adult wild-type (+/+), heterozygous (+/-) and Emilin3-deficient mice (-/-), digested with *Nco*I and hybrided with external probe II. (**D**) Immunofluorescence analysis of cryostat sections from 1-month-old wild-type and *Emilin3*$^{-/-}$ mouse testis with Emilin3 (green) and Emilin1 (red) antibodies, showing the absence of Emilin3 protein deposition in *Emilin3*$^{-/-}$ tissue. Nuclei were stained with Hoechst (blue). Scale bar, 25 μm.

Figure 5

A

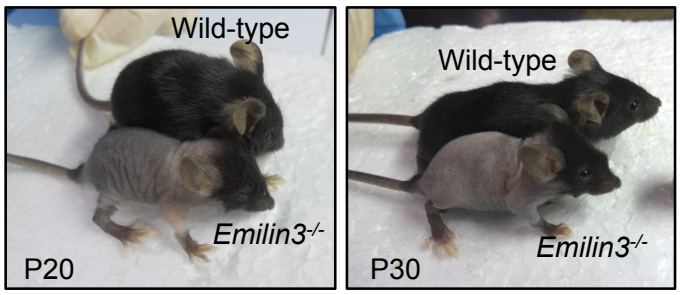
Wild-type
Emilin3-/-
P20
Wild-type
Emilin3-/-
P30

B

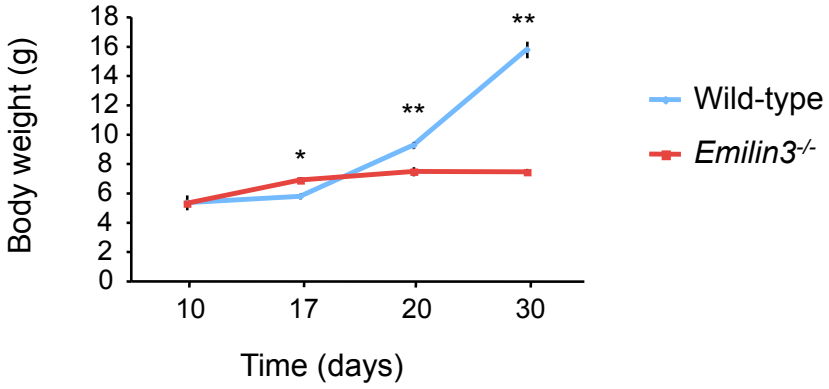
Body weight (g)
18
16
14
12
10
8
6
4
2
0
10
17
20
30
Time (days)
*
**
**
Wild-type
Emilin3-/-

C

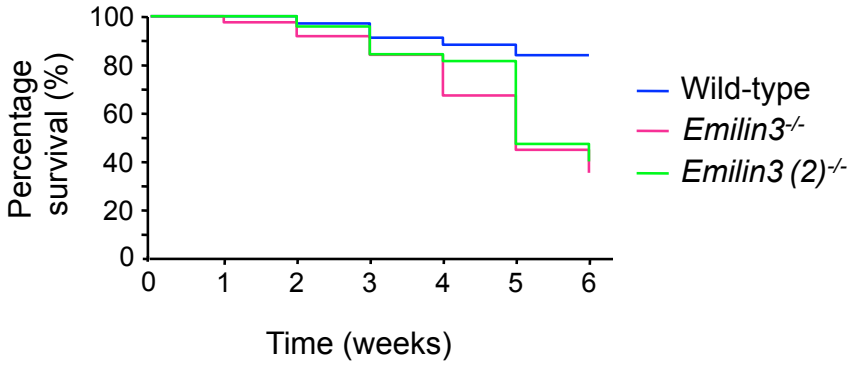
Percentage survival (%)
100
80
60
40
20
0
0
1
2
3
4
5
6
Time (weeks)
Wild-type
Emilin3-/-
Emilin3 (2)-/-

Figure 5. Loss of Emilin3 results in pronounced hair phenotype, body weight loss and reduced lifespan. (**A**) Macroscopic appearance of wild-type and *Emilin3*$^{-/-}$ mice at the indicated postnatal (P) days of age. (**B**) Body weight measurements of wild-type and *Emilin3*$^{-/-}$ mice, taken at 10, 17, 20 and 30 days after birth, showing a significant body weight loss in Emilin3 null animals starting from P17. Data are presented as mean ± SD (n = 30 mice/genotype; *, $P < 0.05$; **, $P < 0.01$. (**C**) Kaplan-Meier survival curves of wild-type and two different Emilin3-deficient mouse lines obtained from two independent targeted ES clones (706 and 2). Measurements were taken every week, from 1 to 6 (n = 70 mice/ genotype). *Emilin3*$^{-/-}$ mice display a reduced lifespan, particularly after the 4th-5th week of age.

Figure 6

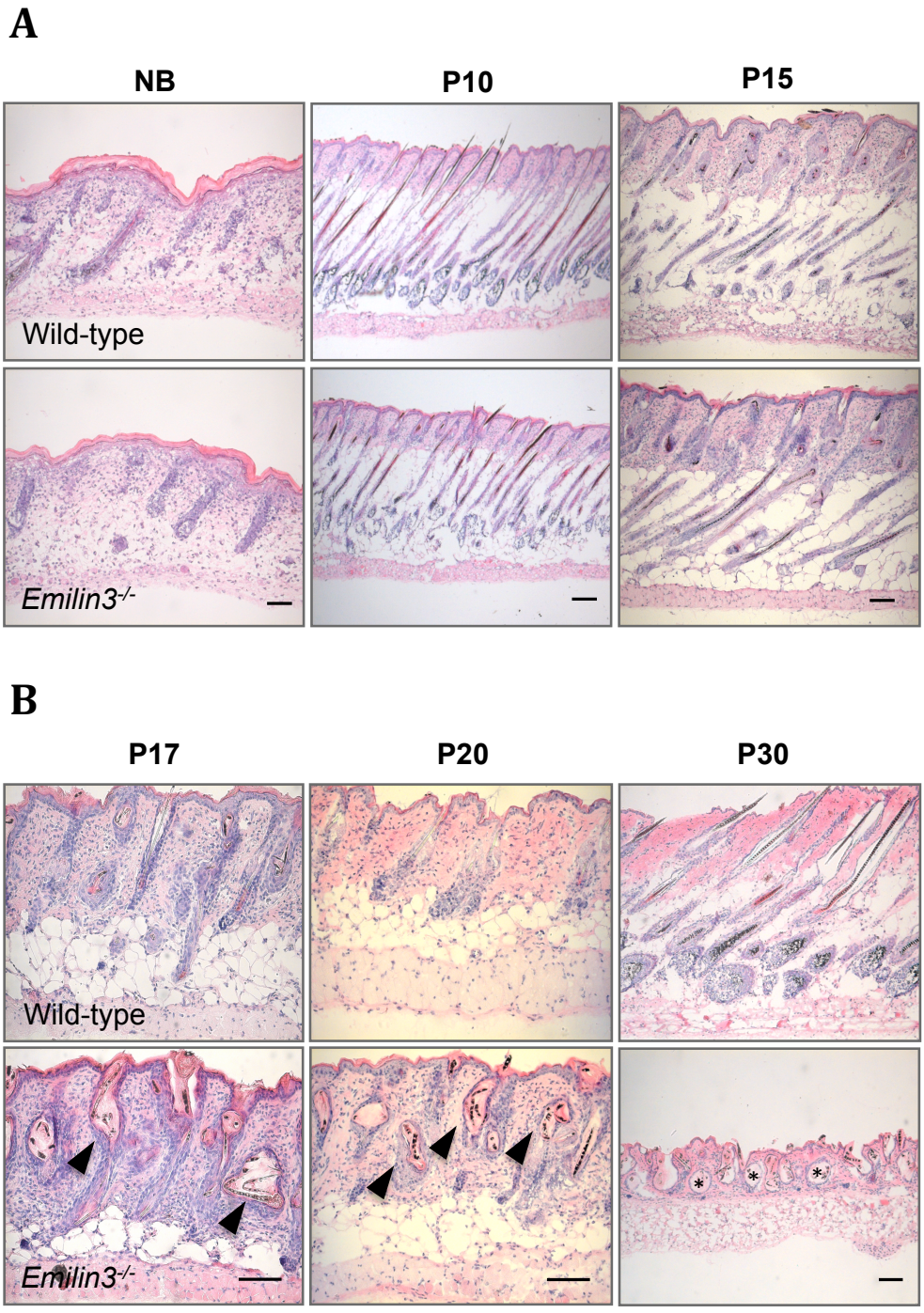

Figure 6. Emilin3 ablation is dispensable for HF formation but affects normal hair growth. (**A, B**) Haematoxylin-eosin staining of cryostat sections of back skin from wild-type and *Emilin3*$^{-/-}$ mice at the indicated postnatal (P) days of age. Arrows indicate the presence of a weakly stained, twisted hair shaft resulting in progressive dilation of the infundibulum, encompassed by increasing amounts of cornified debris. Asterisks indicate the formation of cysts-like structures. Scale bar, 100 μm.

Figure 7

A

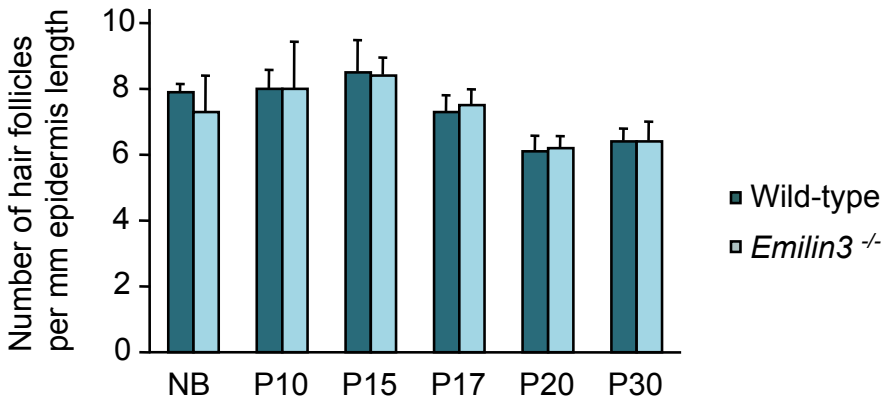
Number of hair follicles per mm epidermis length
10
8
6
4
2
0
NB
P10
P15
P17
P20
P30
Wild-type
Emilin3 -/-

B

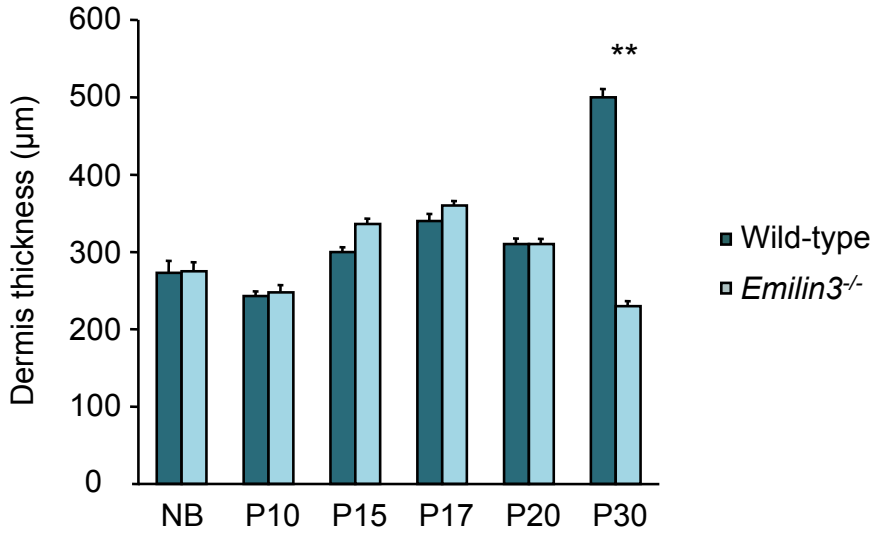
Dermis thickness (µm)
600
500
400
300
200
100
0
**
NB
P10
P15
P17
P20
P30
Wild-type
Emilin3-/-

Figure 7. Analysis of dermal thickness and mean number of HFs in the dorsal skin of wild-type and *Emilin3*$^{-/-}$ mice. (**A**) Quantification of the mean number of HFs per mm of epidermis length in wild-type and *Emilin3*$^{-/-}$ mice at the indicated postnatal (P) days of age, showing no significant differences between the two genotypes. (**B**) Quantification of dermis thickness in wild-type and *Emilin3*$^{-/-}$ mice at the indicated postnatal (P) days of age. A significant reduction in the dermis thickness is detected in *Emilin3*$^{-/-}$ sections at P30. For this analysis, three H&E-stained sections for each mouse were examined. Data are presented as mean values ± SD (n= 3 mice/genotype; **, $P < 0.01$).

Figure 8

A

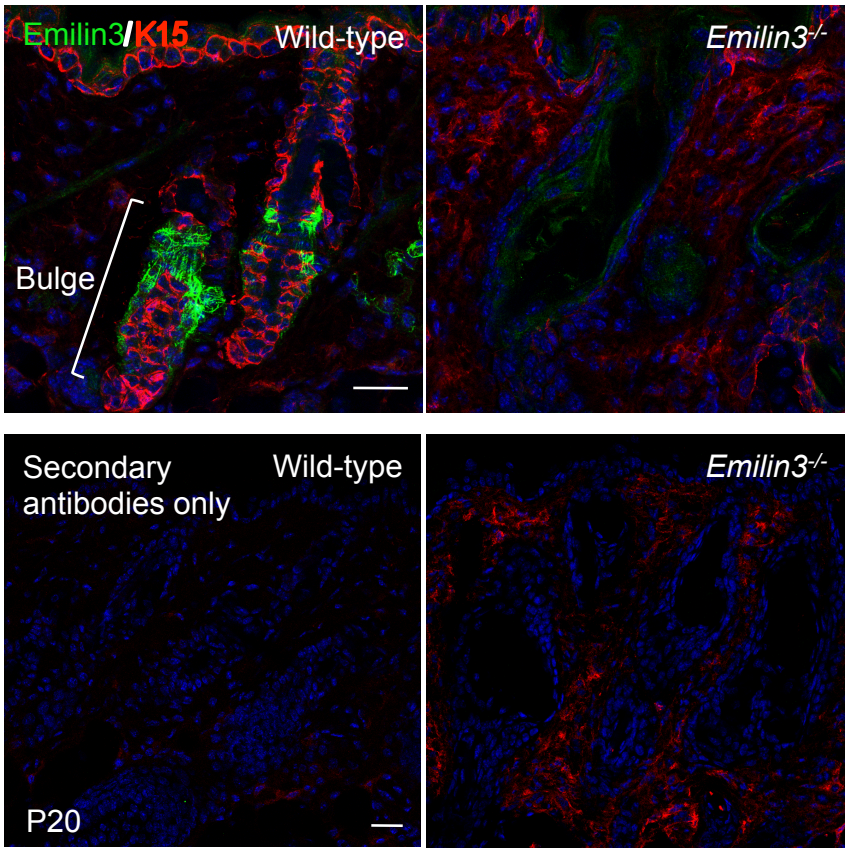
Emilin3/K15
Wild-type
Emilin3-/-
Bulge
Secondary antibodies only
Wild-type
Emilin3-/-
P20

B

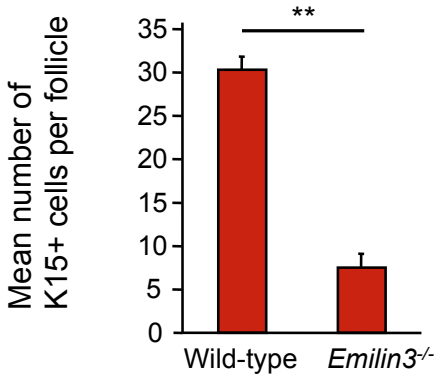
Mean number of K15+ cells per follicle
**
35
30
25
20
15
10
5
0
Wild-type
Emilin3-/-

Figure 8. Lack of Emilin3 results in the reduction of K15-positive bulge stem cells. (**A**) Cryostat sections of P20 wild-type and *Emilin3*$^{-/-}$ back skin were immunostained for Emilin3 (green) and for the bulge stem cell marker K15 (red), together with DAPI counterstain (blue). In the lower panel, sections were stained only with secondary antibodies as a control. Images show the complete loss of K15-positive cells in the bulge of *Emilin3*$^{-/-}$ skin. Scale bar, 25 μm. (**B**) Quantification of the mean number of K15-positive cells per follicle in wild-type and *Emilin3*$^{-/-}$ back skin at 20 days of age. Data are presented as mean ± SD (n=3 mice/genotype; **, $P < 0.01$).

References

Abrams, W. R., Ma, R. I., Kucich, U., Basher, M. M., Decker, S., Tsipouras, P., McPherson, J. D., Wasmuth, J. J., Rosenbloom, J. (1995). Molecular cloning of the microfibrillar protein MFAP3 and assignment of the gene to human-chromosome 5q32-q33.2. *Genomics* 26, 47-54.

Adams, D. M., Keller, R., Koehl, M. A. (1990). The mechanics of notochord elongation, straightening and stiffening in the embryo of Xenopus laevis. *Development* 110(1), 115-30.

Adams, J. C., Watt, F. M. (1993). Regulation of development and differentiation by the extracellular matrix. *Development* 117, 1183-98.

Akiyama, M., Dale, B. A., Sun, T. T., Holbrook, K. A. (1995). Characterization of hair follicle bulge in human fetal skin: the human fetal bulge is a pool of undifferentiated keratinocytes. J Invest Dermatol. 105, 844–850.

Allen M, Grachtchouk M, Sheng H, Grachtchouk V, Wang A, Wei L, Liu J, Ramirez A, Metzger D, Chambon P, Jorcano J, Dlugosz AA. (2003). Hedgehog signaling regulates sebaceous gland development. *Am J Pathol.* 163(6), 2173-8.

Atit, R., Sgaier, S. K., Mohamed, O. A., Taketo, M. M., Dufort, D., Joyner, A. L., Niswander, L., Conlon, R. A. (2006). Beta-catenin activation is necessary and sufficient to specify the dorsal dermal fate in the mouse. *Dev Biol*. 296(1), 164-76.

Barker, N., van Es, J. H., Kuipers, J., Kujala, P., van den Born, M., Cozijnsen, M., Haegebarth, A., Korving, J., Begthel, H., Peters, P. J., Clevers, H. (2007). Identification of stem cells in small intestine and colon by marker gene Lgr5. *Nature* 449, 1003-7.

Barresi, M. J., Stickney, H. L., Devoto, S. H. (2000). The zebrafish slow-muscle-omitted gene product is required for Hedgehog signal transduction and the development of slow muscle identity. *Development* 127(10), 2189-99.

Berrier, A. and Yamada, K. (2007). Cell-matrix adhesion. *J Cell Physiol.* 213(3), 565-73.

Blanpain, C., Lowry, W. E., Geoghegan, A., Polak, L., Fuchs, E. (2004). Self-renewal, multipotency, and the existence of two cell populations within an epithelial stem cell niche. *Cell* 118, 635-48.

Blanpain, C., Fuchs, E. (2009), Epidermal homeostasis: a balancing act of stem cells in the skin. *Nat Rev Mol Cell Biol* 10, 207-17.

Borel, A., Eichenberg, D., Farjanel, J., Kessles, E., Gleyzal, C., Hulmes, D., Sommer, P., Font, B. (2001). Lysil oxidase-like protein from bovine aorta. J. Biol. Chem. 276, 48944-48949.

Braghetta, P., Ferrari, A., De Gemmis, P., Zanetti, M., Volpin, D., Bonaldo, P., Bressan, G. M. (2004). Overlapping, complementary and site-specific expression pattern of genes of the EMILIN/Multimerin family. *Matrix Biol*. 22(7), 549-556.

Breitkreutz, D., Koxholt, I., Thiemann, K., Nischt, R. (2013). Skin basement membrane: the foundation of epidermal integrity-BM functions and diverse roles of bridging molecules nidogen and perlecan. *Biomed Res Int.* 2013, 2013:179784

Bressan, G. M., Daga-Gordini, D., Colombatti, A., Castellani, I., Marigo, V., Volpin, D. (1993). Emilin, a component of elastic fibers preferentially located at the elastin-microfibrils interface. *J. Cell Biol.* 121, 201-212.

Brownell, I., Guevara, E., Bai, C. B., Loomis, C. A., Joyner, A. L. (2011). Nerve-derived sonic hedgehog defines a niche for hair follicle stem cells capable of

becoming epidermal stem cells. *Cell Stem Cell* 8(5), 552-65.

Candi, E., Schmidt, R., Melino, G. (2005). The cornified envelope: a model of cell death in the skin. *Nat Rev Mol Cell Biol* 6, 328-40.

Chiang, C., Swan, R. Z., Grachtchouk, M., Bolinger, M., Litingtung, Y., Robertson, E. K., Cooper, M. K., Gaffield, W., Westphal, H., Beachy, P. A., Dlugosz, A. A. (1999). Essential role for Sonic hedgehog during hair follicle morphogenesis. *Dev Biol.* 205(1), 1-9.

Christoffels, A., Koh, E. G., Chia, J. M., Brenner, S., Aparicio, S., Venkatesh, B. (2004). Fugu genome analysis provides evidence for a whole-genome duplication early during the evolution of ray-finned fishes. *Mol Biol Evol* 21, 1146–1151.

Cleaver, O., Seufert, D. W., Krieg, P. A. (2000). Endoderm patterning by the notochord: development of the hypochord in Xenopus. *Development* 127(4), 869-79.

Cleaver, O., Krieg, P. A. (2001). Notochord patterning of the endoderm. *Dev Biol.* 234(1), 1-12.

Corallo, D., Schiavinato, A., Trapani, V., Moro, E., Argenton, F., Bonaldo, P. (2013). Emilin is required for notochord sheath integrity and interacts with Scube2 to regulate notochord-derived Hedgehog signals. *Development* 140(22), 4594-601.

Cotsarelis, G., Sun, T. T., Lavker, R. M. (1990). Label-retaining cells reside in the bulge area of pilosebaceous unit: implications for follicular stem cells, hair cycle, and skin carcinogenesis. *Cell* 61, 1329-37.

Danos, M. C., Yost, H. J. (1995). Linkage of cardiac left-right asymmetry and dorsal-anterior development in Xenopus. *Development* 121(5), 1467-74.

Danussi, C., Spessotto, P., Petrucco, A., Wassermann, B., Sabatelli, P., Montesi, M., Doliana, R., Bressan, G. M., Colombatti, A. (2008). Emilin1 deficiency causes structural and functional defects of lymphatic vasculature. *Mol Cell Biol.* 28(12), 4026-39.

Danussi, C., Petrucco, A., Wassermann, B., Pivetta, E., Modica, T. M., Del Bel Belluz, L., Colombatti, A., Spessotto, P. (2011). EMILIN1-α4/α9 integrin interaction inhibits dermal fibroblast and keratinocyte proliferation. *J Cell Biol*. 195(1), 131-45.

Devoto, S. H., Melançon, E., Eisen, J. S., Westerfield, M. (1996). Identification of separate slow and fast muscle precursor cells in vivo, prior to somite formation. *Development* 122(11), 3371-80.

Discher, D., Mooney, D. and Zandstra, P. (2009). Growth factors, matrices, and forces combine and control stem cells. *Science* 324(5935), 1673-7.

Doliana, R., Mongiat, M., Bucciotti, F., Giacomello, E., Deutzman, R., Volpin, D., Bressan, G. M., Colombatti, A. (1999). EMILIN, a component of elastic fiber and a new member of the C1q/tumor necrosis factor superfamily of proteins. *J Biol Chem.* 274, 16773-16781.

Dupont, S., Morsut, L., Aragona, M., Enzo, E., Giulitti, S., Cordenonsi, M., Zanconato, F., Le Digabel, J., Forcato, M., Bicciato, S., Elvassore, N., and Piccolo, S. (2011). Role of YAP/TAZ in mechanotransduction. *Nature* 474(7350), 179-83.

Ellis, K., Bagwell, J., Bagnat, M. (2013). Notochord vacuoles are lysosome-related organelles that function in axis and spine morphogenesis. *J Cell Biol.* 200(5), 667-79.

Fekany, K., Yamanaka, Y., Leung., T., Sirotkin, H. I., Topczewski, J., Gates, M. A.,

Hibi, M., Renucci, A., Stemple, D., Radbill, A., Schier, A. F., Driever, W., Hirano, T., Talbot, W. S., Solnica-Krezel, L. (1999). The zebrafish bozozok locus encodes Dharma, a homeodomain protein essential for induction of gastrula organizer and dorsoanterior embryonic structures. *Development* 126(7), 1427-38.

Fouquet, B., Weinstein, B. M., Serluca, F. C., Fishman, M. C. (1997). Vessel patterning in the embryo of the zebrafish: guidance by notochord. *Dev Biol.* 183(1), 37-48.

Fuchs, E. (2007). Scratching the surface of skin development. *Nature* 445, 834-42.

Fuchs, E. (2008). Skin stem cells: rising to the surface. *J Cell Biol.* 180, 273–284.

Fujiwara, H., Ferreira, M., Donati, G., Marciano, D. K., Linton, J. M., Sato, Y., Hartner, A., Sekiguchi, K.,Reichardt, L. F., Watt, F. (2011). The basement membrane of hair follicle stem cells is a muscle cell niche. *Cell* 144, 577–589.

Gao, J., DeRouen, M. C., Chen, C. H., Nguyen, M., Nguyen, N. T., Ido, H., Harada, K., Sekiguchi, K., Morgan, B. A., Miner, J. H., et al. (2008). Laminin-511 is an epithelial message promoting dermal papilla development and function during early hair morphogenesis. *Genes Dev.* 22, 2111–2124.

Gibson, M. A., Hatzinikolas, G., Davis, E. C., Baker, E., Sutherland, G. R., Mecham, R. P. (1995). Bovine latent transforming factor β1-binding protein-2: molecular cloning, identification of tissue isoforms and immunolocalization to elastin-associated microfibrils. *Mol Cell Biol.* 15, 6932-6942.

Gibson, M. A., Kumaratilake, J. S., Cleary, E. G. (1997). Immunohistochemical and ultrastructural localization of MP78/70 (betaig-h3) in extracellular matrix of developing and mature bovune tissues. *J Histochem Cytochem.* 45(12), 1683-1696.

Giltay, R., Kostka, G., Timpi, R. (1997). Sequence and expression of a novel member (LTBP-4) of the family of latent transforming growth factor-β binding proteins. *FEBS Lett*. 411, 164-168.

Griffin, K. J., Kimelman, D. (2003). Interplay between FGF, one-eyed pinhead, and T-box transcription factors during zebrafish posterior development. *Dev Biol.* 264(2), 456-66.

Gritli-Linde, A., Hallberg, K., Harfe, B. D., Reyahi, A., Kannius-Janson, M., Nilsson, J., Cobourne, M. T., Sharpe, P. T., McMahon, A. P., Linde, A. (2007). Abnormal hair development and apparent follicular transformation to mammary gland in the absence of hedgehog signaling. *Dev Cell.* 12(1), 99-112.

Grose, R., Fantl, V., Werner, S., Chioni, A. M., Jarosz, M., Rudling, R., Cross, B., Hart, I. R., Dickson, C. (2007). The role of fibroblast growth factor receptor 2b in skin homeostasis and cancer development. *EMBO J.* 26(5), 1268-78.

Hardingham, T. E., Fosang, A. J. (1992). Proteoglycans: many forms and many functions. *FASEB J.* 6(3):861-70.

Hatzinikolas, G., Gibson, M. A. (1998). The exon structure of the human MAGP-2 gene. Similarizy with the MAGP-1 gene is confined to the exons encoding a cysteine-rich region. *J Biol Chem.* 273, 29309-29314.

Hay, E. D. (1981). Extracellular matrix. *J Cell Biol.* 91(3 Pt 2), 205s-223s.

Hebert, J. M., Rosenquist, T., Gotz, J., Martin, G. R. (1994). FGF5 as a regulator of the hair growth cycle: evidence from targeted and spontaneous mutations. *Cell* 78, 1017-25.

Horsley, V., O'Carroll, D., Tooze, R., Ohinata, Y., Saitou, M., Obukhanych, T.,

Nussenzweig, M., Tarakhovsky, A., Fuchs, E. (2006). Blimp1 defines a progenitor population that governs cellular input to the sebaceous gland. *Cell* 126, 597-609.

Horsley, V., Aliprantis, A. O., Polak, L., Glimcher, L. H., Fuchs, E. (2008). NFATc1 balances quiescence and proliferation of skin stem cells. *Cell* 132, 299- 310.

Hynes, R. O. (2002). Integrins:bidirectional, allosteric signaling machines. *Cell* 110 (6), 673-87.

Hynes, R. O. (2009). The extracellular matrix: not just pretty fibrils. *Science* 326(5957), 1216-9.

Isogai, S., Lawson, N. D., Torrealday, S., Horiguchi, M., Weinstein, B. M. (2003). Angiogenic network formation in the developing vertebrate trunk. *Development* 130(21), 5281-90.

Ito, M., Kizawa, K., Hamada, K., Cotsarelis, G. (2004). Hair follicle stem cells in the lower bulge form the secondary germ, a biochemically distinct but functionally equivalent progenitor cell population, at the termination of catagen. *Differentiation* 72(9-10), 548-57.

Ito, M., Liu, Y., Yang, Z., Nguyen, J., Liang, F., Morris, R. J., Cotsarelis, G. (2005). Stem cells in the hair follicle bulge contribute to wound repair but not to homeostasis of the epidermis. *Nat Med* 11, 1351-4.

Jensen, K. B., Collins, C. A., Nascimento, E., Tan, D. W., Frye, M., Itami, S., Watt, F. M. (2009). Lrig1 expression defines a distinct multipotent stem cell population in mammalian epidermis. Cell Stem Cell 4, 427-39.

Kanzaki, T., Olofsson, A., Moren, A., Wernstedt, C., Hellman, U., Miyazono, K., Claesson-Welsh, L., Heldin, C. H. (1990). TGF-β1 binding protein, a component of the large latent complex of TGF-β1 with multiple repeat sequences. *Cell* 61,

1051-1061.

Kjellén, L., Lindahl, U. (1991). Proteoglycans: structures and interactions. *Annu Rev Biochem*. 60, 443-75.

Kobielak, K., Stokes, N., De la Cruz J., Polak, L., Fuchs, E. (2007). Loss of a quiescent niche but not follicle stem cells in the absence of bone morphogenetic protein signaling. *Proc Natl Acad Sci* USA 104, 10063-8.

Laird, P. W., A. Zijderveld, K. Linders, M. A. Rudnicki, R. Jaenisch, and A. Berns. (1991). Simplified mammalian DNA isolation procedure. *Nucleic Acids Res.* 19, 4293.

Lausen, M., Lynch, N., Schlosser, A., Tornoe, I., Sackmose, S. G., Teisner, B., Willis, A. C., Crouch, E., Schwaeble, W., Holmskov, U. (1999). Microfibril-associated protein 4 is pesent in lung washings and binds to the collagen region of lung surfactant protein D. *J Biol Chem.* 274, 32234-32240.

Lawson, N. D., Vogel, A. M., Weinstein, B. M. (2002). Sonic hedgehog and vascular endothelial growth factor act upstream of the Notch pathway during arterial endothelial differentiation. *Dev Cell* 3(1), 127-36.

Legate, K., Wickstrom, S. and Fassler, R. (2009). Genetic and cell biological analysis of integrin outside-in signaling. *Genes Dev.* 23(4), 397-418.

Legué, E., Nicolas, J. F. (2005). Hair follicle renewal: organization of stem cells in the matrix and the role of stereotyped lineages and behaviors. *Development* 132(18):4143-54.

Levy, V., Lindon, C., Zheng, Y., Harfe, B. D., Morgan, B. A. (2007). Epidermal stem cells arise from the hair follicle after wounding. *Faseb J* 21, 1358-66.

Liu, W. G., Faraco, J., Qian, C. P., Franche, U. (1997). The gene for microfibril-associated protein-1 (MFAP1) is located several megabases centrometric to FBN1 and is not mutated in Marfan syndrome. *Hum. Genet.* 99, 578-584.

Liu, Y., Lyle, S., Yang, Z., Cotsarelis, G. (2003). Keratin 15 promoter targets putative epithelial stem cells in the hair follicle bulge. *J Invest Dermatol* 121, 963-8.

Lohr, J. L., Danos, M. C., Yost, H. J. (1997). Left-right asymmetry of a nodal-related gene is regulated by dorsoanterior midline structures during Xenopus development. *Development* 124(8), 1465-72.

Lyle, S., Christofidou-Solomidou, M., Liu, Y., Elder, D. E., Albelda, S., Cotsarelis, G. (1999). Human hair follicle bulge cells are biochemically distinct and possess an epithelial stem cell phenotype. *J Investig Dermatol Symp Proc* 4, 296-301.

Mangos, S., Lam, P. Y., Zhao, A., Liu, Y., Mudumana, S., Vasilyev, A., Liu, A. and Drummond, I. A. (2010). The ADPKD genes pkd1a/b and pkd2 regulate extracellular matrix formation. *Dis. Model. Mech.* 3, 354-365.

Masunaga, T., Shimizu, H., Yee, C., Borradori, L., Lazarova, Z., Nishikawa, T., Yancey, K. B. (1997). The extracellular domain of BPAG2 localizes to an- choring filaments and its carboxyl terminus extends to the lamina densa of normal human epidermal basement membrane. *J Invest Dermatol*. 109, 200–206.

Mecham, R. P. and Devis, E. C. (1994). Elastic fiber structure and assembly. In *Extracellular Matrix Assembly and Structure.* pp. 281-314.

Milanetto, M., Tiso, N., Braghetta, P., Volpin, D., Argenton, F., Bonaldo, P. (2008). Emilin genes are duplicated and dynamically expressed during zebrafish embryonic development. *Dev Dyn.* 237(1), 222-32.

Mokkapati, S., Baranowsky, A., Mirancea, N., Smyth, N., Breitkreutz, D., Nischt, R. (2008). Basement membrane in skin are differently affected by lack of nidogen 1 and 2. *J Invest Dermatol.* 128(9), 2259-67

Mongiat M., Mungiguerra G., Bot S., Mucignat M. T., Giacomello E., Doliana R., Colombati A. (2000). Self-assembly and supramolecular organization of EMILIN. J Biol Chem. 275, 25471-25480.

Mongiat, M., Ligresti, G., Marastoni, S., Lorenzon, E., Doliana, R., Colombatti, A. (2007). Regulation of the extrinsic apoptotic pathway by the extracellula matrix glycoprotein EMILIN2. *Mol Cell Biol*. 27(20), 7176-87.

Mongiat, M., Marastoni, S., Ligresti, G., Lorenzon, E., Schiappacassi, M., Perris, R., Frustaci, S., Colombatti, A. (2010). The extracellular matrix glycoprotein elastin microfibril interface located protein 2: a dual role in the tumor microenvironment. *Neoplasia* 12(4), 294-304.

Montagna, W. (1974b) The structure and function of skin. *Academic press, New York*.

Morris, R. J., Liu, Y., Marles, L., Yang, Z., Trempus, C., Li, S., Lin, J. S., Sawicki, J. A., Cotsarelis, G. (2004). Capturing and profiling adult hair follicle stem cells. *Nat Biotechnol* 22, 411-7.

Muller-Rover, S., Handjiski, B., Van der Veen, C., Eichmuller, S., Foitzik, K., McKay, I. A., Stenn, K. S., Paus, R. (2001). A comprehensive guide for the accurate classification of murine hair follicles in distinct hair cycle stages. *J Invest Dermatol* 117, 3-15.

Naba, A., Clauser, K. R., Hoersch, S., Liu, H., Carr, S. A., Hynes, R. O. (2011). The matrisome: in silico definition and in vivo characterization by proteomics of normal and tumor extracellular matrices. *Mol Cell Proteomics* 11(4),

M111.014647.

Nakamura, T., Lozano, P. R., Ikeda, Y., Iwanaga, Y., Hinek, A., Minamisawa, S., Cheng, C. F., Kobule, K., Dalton, N., Takada, Y. (2002). Fibulin-5/DANCE is essential for elastogenesis in vivo. *Nature* 415, 171-175.

Nijhof, J. G., Braun, K. M., Giangreco, A., van Pelt, C., Kawamoto, H., Boyd, R. L., Willemze, R., Mullenders, L. H., Watt, F. M., de Gruijl, F. R., van Ewijk, W. (2006). The cell-surface marker MTS24 identifies a novel population of follicular keratinocytes with characteristics of progenitor cells. *Development* 133, 3027-37.

Ohyama, M., Terunuma, A., Tock, C. L., Radonovich, M. F., Pise-Masison, C. A., Hopping, S. B., Brady, J. N., Udey, M. C., and Vogel, J. C. (2006). Characteriza- tion and isolation of stem cell-enriched human hair follicle bulge cells. *J Clin Invest.* 116, 249–260.

Oshimori, N., Fuchs, E. (2012). Paracrine TGF-beta signaling counterbalances BMP-mediated repression in hair follicle stem cell activation. *Cell Stem Cell* 10, 63-75.

Pagnon-Minot, A., Malbouyres, M., Haftek-Terreau, Z., Kim, H. R., Sasaki, T., Thisse, C., Thisse, B., Ingham, P. W., Ruggiero, F. and Le Guellec, D. (2008). Collagen XV, a novel factor in zebrafish notochord differentiation and muscle development. *Dev. Biol.* 316, 21-35.

Panteleyev, A. A., Jahoda, C. A., Christiano, A. M. (2001). Hair follicle predetermination. *J Cell Sci* 114, 3419-31.

Parsons, M. J., Pollard, S. M., Saude, L., Feldman, B., Coutinho, P., Hirst, E. M. and Stemple, D. L. (2002). Zebrafish mutants identify an essential role for laminins in notochord formation. *Development* 129, 3137-3146.

Paus, R., Müller-Röver, S., Van Der Veen, C., Maurer, M., Eichmüller, S., Ling, G., Hofmann, U., Foitzik, K., Mecklenburg, L., Handjiski, B. (1999). A comprehensive guide for the recognition and classification of distinct stages of hair follicle morphogenesis. *J Invest Dermatol.* 1999 Oct;113(4):523-32.

Paus, R., Foitzik, K. (2004). In search of the "hair cycle clock": a guided tour. *Differentiation* 72, 489-511.

Placzek, M., Jessell, T.M., Dodd, J. (1993). Induction of floor plate differentiation by contact- dependent, homeogenetic signals. *Development* 117(1), 205-18.

Poole, A. R. (1986). Proteoglycans in health and disease: structures and functions. *Biochem J.* 236(1), 1-14.

Pourquié, O., Coltey, M., Teillet, M. A., Ordahl, C., Le Douarin, N. M. (1993). Control of dorsoventral patterning of somitic derivatives by notochord and floor plate. *Proc Natl Acad Sci USA.* 90(11), 5242-6.

Proksch, E., Brandner, J. M., Jensen, J. M. (2008). The skin: an indispensable barrier. *Exp Dermatol.* 17(12):1063-72.

Raughunath, M., Tschodrich-Rotter, M., Sasaki, T., Meuli, M., Chu, M. L., Timpl, R. (1999). Confocal laser scanning analysis of the association of fibulin-2 with fibrilin-1 and fibronectin define stages of skin regeneration. *J Invest Dermatol.* 112, 97-101.

Rendl, M., Polak, L., Fuchs, E. (2008). BMP signaling in dermal papilla cells is required for their hair follicle-inductive properties. *Genes Dev* 22, 543-57.

Ricard-Blum, S. (2011). The collagen family. *Cold Spring Harb Perspect Biol.* 3(1), a004978.

Roark, E. F., Keene, D. R., Haudenschild, C. C., Godyna, S., Little, C. D., Argraves, W. S. (1995). The association of human fibulin-1 with elastic fibers: an immunohistological, ultrastructural, and RNA study. *J Histochem Cytochem.* 43, 401-411.

Roy, S., Qiao, T., Wolff, C., Ingham, P. W. (2001). Hedgehog signalling pathway is essential for pancreas specification in the zebrafish embryo. *Curr Biol.* 11(17), 1358-63.

Ruoslahti, E. (1988). Structure and biology of proteoglycans. *Annu Rev Cell Biol*. 4, 229-55.

Sakai, L. Y., Keene, D. R., Engvall, E. (1986). Fibrillin, a new 350-kD glycoprotein, is a component of extracellular microfibrils*. J Cell Biol*. 103(6 Pt 1), 2499-509.

Saùde, L., Woolley, K., Martin, P., Driever, W., Stemple, D. L. (2000). Axis-inducing activities and cell fates of the zebrafish organizer. *Development* 127(16), 3407-17.

Schiavinato, A., Becker, A. K., Zanetti, M., Corallo, D., Milanetto, M., Bizzotto, D., Bressan, G., Guljelmovic, M., Paulsson, M., Wagener, R., Braghetta, P., Bonaldo, P. (2012). EMILIN-3, a peculiar member of elastin microfibril interface-located protein (EMILIN) family, has distinct expression pattern, forms oligomeric assemblies, and serves a s transforming growth factor β (TGF-β) antagonist. *J Biol Chem.* 287(14), 11498-515.

Schmidt-Ullrich, R., Paus, R. (2005). Molecular principles of hair follicle induction and morphogenesis. *Bioessays* 27, 247-61.

Schneider, M. R., Schmidt-Ullrich, R., Paus, R. (2009). The hair follicle as a dynamic miniorgan. Curr Biol. 19(3), R132-42.

Schwarzbauer, J. E., DeSimone, D. W. (2011). Fibronectins, their fibrillogenesis, and in vivo functions. *Cold Spring Harb Perspect Biol.* 3(7), pii: a005041.

Scott, J. E. (2001). Structure and function in extracellular matrices depend on interactions between anionic glycosaminoglycans. *Pathol Biol*. 49(4), 284-9.

Shih, J., Fraser, S. E. (1996). Characterizing the zebrafish organizer: microsurgical analysis at the early-shield stage. *Development* 122(4), 1313-22.

Silbert, J. E., Sugumaran, G. (1995). Intracellular membranes in the synthesis, transport and metabolism of proteoglycans. *Biochim Biophys Acta.* 1241(3), 371-84.

Simpson, C. L., Patel, D. M., Green, K. J. (2011) Deconstructing the skin: cytoarchitectural determinants of epidermal morphogenesis. Nat Rev Mol Cell Biol 12, 565-80.

Snippert, H. J., Haegebarth, A., Kasper, M., Jaks, V., van Es, J. H., Barker, N., van de Wetering, M., van den Born, M., Begthel, H., Vries, R. G., Stange, D. E., Toftgard, R., Clevers, H. (2010b). Lgr6 marks stem cells in the hair follicle that generate all cell lineages of the skin. *Science* 327, 1385-9.

Spessotto, P., Cervi, M., Mucignat, M. T., Mungiguerra, G., Sartoretto, I., Doliana, R., Colombatti, A. (2003). β1 integrin-dependent cell adhesion to EMILIN-1 is mediated by the gC1q domain. *J Biol Chem.* 278, 6160-6167.

Stenn, K. S., Paus, R. (2001). Controls of hair follicle cycling. *Physiol Rev* 81, 449-494.

St-Jacques, B., Dassule, H. R., Karavanova, I., Botchkarev, V. A., Li, J., Danielian, P. S., McMahon, J. A., Lewis, P. M., Paus, R., McMahon, A. P. (1998). Sonic hedgehog signaling is essential for hair development. *Curr Biol.* 8(19), 1058-68.

Taylor, G., Lehrer, M. S., Jensen, P. J., Sun, T. T., Lavker, R. M. (2000). Involvement of follicular stem cells in forming not only the follicle but also the epidermis. *Cell* 102, 451-61.

Timpl, R. (1996). Macromolecular organization of basement membranes. *Curr Opin Cell Biol.* 8, 618–624.

Tumbar, T., Guasch, G., Greco, V., Blanpain, C., Lowry, W. E., Rendl, M., Fuchs, E. (2004). Defining the epithelial stem cell niche in skin. *Science* 303, 359–363.

Whitbread, L. A., Powell, B. C. (1998). Expression of the intermediate filament keratin gene, K15, in the basal cell layers of epithelia and the hair follicle. Exp Cell Res. 244(2), 448-59.

Xie, J., Murone, M., Luoh, S. M., Ryan, A., Gu, Q., Zhang, C., Bonifas, J. M., Lam, C. W., Hynes, M., Goddard, A., Rosenthal, A., Epstein, E. H., de Sauvage, F. J. (1998). Activating Smoothened mutations in sporadic basal-cell carcinoma. *Nature* 391(6662), 90-2.

Yamada, T., Placzek, M., Tanaka, H., Dodd, J., Jessell, T. M. (1991). Control of cell pattern in the developing nervous system: polarizing activity of the floor plate and notochord. *Cell* 64(3), 635-47.

Yamamoto, M., Morita, R., Mizoguchi, T., Matsuo, H., Isoda, M., Ishitani, T., Chitnis, A. B., Matsumoto, K., Crump, J. G., Hozumi, K., Yonemura, S., Kawakami, K., Itoh, M. (2010). Mib-Jag1-Notch signalling regulates patterning and structural roles of the notochord by controlling cell-fate decisions. *Development* 137(15), 2527-37.

Yanagisawa, H., Davis, E. C., Starcher, B. C., Ouchi, T., Yanagisawa, M., Richardson, J. A., Olsen, E. N. (2002). Fibulin-5 is an elastin-binding protein essential for

elastic fiber development in vivo. *Nature* 415, 168-171.

Yurchenco, P. D. (2011). Basement menbranes: cell scaffoldings and signaling platforms. *Cold Spring Harb Perspect Biol.* 3(2), pii: a004911.

Zacchigna, L., Vecchione, C., Notte, A., Cordenonsi, M., Dupont, S., Maretto, S., Cifelli, G., Ferrari, A., Maffei, A., Fabbro, C., Braghetta, P., Marino, G., Selvetella, G., Aretini, A., Colonnese, C., Bettarini, U., Russo, G., Soligo, S., Adorno, M., Bonaldo, P., Volpin, D., Piccolo, S., Lembo, G., Bressan, G. M. (2006). Emilin1 links TGF-beta maturation to blood pressure homeostasis. *Cell* 124(5), 929-42.

Zanetti, M., Braghetta, P., Sabatelli, P., Mura, I., Doliana, R., Colombatti, A., Volpin, D., Bonaldo, P., Bressan, G. M. (2004). EMILIN-1 deficiency induces elastogenesis and vascular cell defects. *Mol Cell Biol.* 24, 638-650.

Zhang, H., Apfelroth, S. D., Hu, W., Davis, E. C., Sanguineti, C., Bonadio, J., Mecham, R. P., Ramirez, F. (1994). Structure and expression of fibrillin-2, a novel microfibrillar component preferentially located in elastic matrices. *J Cell Biol.* 124(5), 855-63.